U.PORTO

MESTRADO EM ONCOLOGIA

ESPECIALIZAÇÃO EM ONCOLOGIA LABORATORIAL

Establish biomimetic 3D tumor-immune spheroids as a model to address Triple-negative breast cancer radioresponse

Filipa Raquel Leal Trabuco

M

2021

U.PORTO

Filipa Raquel Leal Trabuco. Establish biomimetic 3D tumor-immune spheroids as a model to address Triple-negative breast cancer radioresponse

Establish biomimetic 3D tumor-immune spheroids as a model to address Triple-negative breast cancer radioresponse

Filipa Raquel Leal Trabuco

INSTITUTO DE CIÊNCIAS BIOMÉDICAS ABEL SALAZAR

M.ICBAS **2021**

Filipa Raquel Leal Trabuco

Establish biomimetic 3D tumor-immune spheroids as a model to address Triple-negative breast cancer radioresponse

Dissertação de Candidatura ao grau de **Mestre em Oncologia** – Especialização em Oncologia Laboratorial submetida ao Instituto de Ciências Biomédicas Abel Salazar da Universidade do Porto.

Orientador – Doutora Maria José Cardoso Oliveira
Investigadora principal e coordenadora do grupo *Tumour and Microenvironment Interactions* no i3S-Instituto de Investigação e Inovação em Saúde
Professora Afiliada na Faculdade de Medicina da Universidade do Porto
Professora Associada Convidada no Instituto de Ciências Biomédicas Abel Salazar da Universidade do Porto.

Co-orientador – Doutora Joana Cancela de Amorim Falcão Paredes
Investigadora principal e coordenadora do grupo *Cancer Metastasis* no i3S-Instituto de Investigação e Inovação em Saúde
Professora Afiliada na Faculdade de Medicina da Universidade do Porto

“There are no secrets to success. It is the result of preparation, hard work, and learning from failure.”

Colin Powell

AGRADECIMENTOS

Chegando ao fim desta etapa da minha vida, gostaria de agradecer a todos que me acompanharam ao longo deste percurso e que de alguma forma, científica ou pessoal, contribuíram para que alcançasse com sucesso o fim desta jornada.

Em primeiro lugar, o meu enorme agradecimento à minha orientadora, Professora Doutora Maria José Oliveira, pela disponibilidade de me aceitar no seu grupo, *Tumour and Microenvironment Interactions* (TMI), mesmo num ano atípico e cheio de incertezas. Obrigada pela partilha de conhecimento científico que me fez crescer profissionalmente, pelo suporte e incentivo que me deu ao longo destes meses e por sempre expressar o orgulho que sente no trabalho que desenvolvemos.

Gostaria também de agradecer à minha co-orientadora, Professora Doutora Joana Paredes, por todo o conhecimento, críticas e sugestões que partilhou comigo, essenciais para a realização deste projeto, e pela disponibilidade demonstrada.

À Professora Doutora Carmen Jerónimo, Diretora do Mestrado em Oncologia, por me aceitar neste mestrado, permitindo aprofundar o meu conhecimento nesta área, e pelos conselhos que me deu ao longo destes dois anos.

À Catarina, a pessoa que me acompanhou incansavelmente ao longo de toda esta jornada, do fundo do meu coração um enorme obrigada. Sem a tua ajuda, dedicação e motivação teria sido impossível realizar todo este trabalho em tão pouco tempo. Muito obrigada por todo o conhecimento que partilhaste comigo, obrigada por estares sempre disponível para me ouvir e ajudar, por me apoiares e acompanhares neste percurso com muitos obstáculos. Foram muitos os desafios que enfrentámos nos últimos meses, muitas as horas que passámos juntas a trabalhar, e nos momentos mais difíceis a tua presença e as tuas palavras de conforto e motivação deram-me a força necessária para continuar a trabalhar. Obrigada pela tua amizade, foste a melhor pessoa que podia ter ao meu lado durante esta etapa da minha vida.

Gostaria também de agradecer aos membros do Serviço de Radioterapia do Centro Hospitalar Universitário São João, especialmente às técnicas, por sempre me receberem tão bem e por me ajudarem a irradiar as células, permitindo a realização deste projeto.

Quero também agradecer à Cláudia Machado por ter realizado o processamento histológico e os cortes das amostras, à Flávia Castro pelas sugestões e partilha de conhecimento que permitiram a realização deste estudo, e à Claúdia Martins por me ensinar a trabalhar com os moldes de agarose e principalmente por estar sempre disponível para esclarecer todas as minhas dúvidas.

Aos elementos do meu grupo, TMI: Ângela Costa, Patrícia, Tânia, Ana, Andreia, Ângela Magalhães, Diogo, Flávia, Maria, Miguel, Rafaela, agradeço imenso pela forma como me acolheram no grupo e pela vossa disponibilidade para me ajudar. Obrigada pelo vosso apoio e por todos os momentos que passamos tanto a trabalhar no laboratório, como nos nossos divertidos convívios. A vossa presença tornou esta jornada mais especial e enriquecedora.

Aos meus amigos, especialmente à Mariana, ao Gonçalo, e à Xana, por estarem sempre ao meu lado em todas as etapas da minha vida. Obrigada pelo vosso apoio e incentivo, sou muito grata por vos ter na minha vida. Mais ainda, quero agradecer-vos profundamente por todos os momentos que passamos nestes últimos meses, apesar de serem menos frequentes do que o desejado, os nossos risos e momentos de descontração deram-me a energia necessária para concluir esta fase da minha vida académica.

Por último, quero agradecer à minha mãe, ao nelo e toda a minha família, tios, tias, primos e primas, por todo suporte, amor, carinho e por todos os momentos de descontração. Obrigada por sempre me ouvirem quando as coisas corriam menos bem, mesmo não percebendo nada do que estava a falar. Obrigada por me animarem nos maus momentos e por festejarem comigo cada conquista. Um especial agradecimento à minha mãe e ao nelo por sempre acreditarem em mim, por me incentivarem a seguir os meus sonhos e sobretudo obrigada pelas múltiplas vezes que me levaram e me foram buscar ao instituto fora de horas, sem a vosso apoio incondicional não seria possível concluir com sucesso e orgulho este percurso.

Esta dissertação é dedicada à minha mãe!

A todos o meu mais sincero obrigada!

RESUMO

O cancro da mama triplo-negativo (CMTR) é o subtipo mais agressivo, representando cerca de 10 a 20% de todos os cancros de mama diagnosticados. Sendo geralmente caracterizado pela ausência da expressão dos recetores de estrogénio e progesterona, e da amplificação do oncogene *HER2*, não tem, por este motivo, terapias dirigidas que sejam eficazes no seu tratamento. Além disso, é também mais resistente às terapias convencionais, como a radioterapia, o que contribui para um pior prognóstico.

Para estudarmos os mecanismos de resistência tumoral à radioterapia, e identificarmos novos alvos terapêuticos, não se pode ter em conta apenas as caraterísticas das células tumorais, uma vez que todo o microambiente tumoral pode ter um impacto na resposta a este tratamento. Por este motivo, devemos também dar importância ao papel dos macrófagos, a principal população imune presente no microambiente tumoral que pode, sobre determinados estímulos, promover a progressão do tumor.

O principal objetivo deste projeto foi desenvolver um modelo 3D para estudar o papel dos macrófagos na resposta à radioterapia do cancro da mama triplo-negativo. Para isso, otimizámos o estabelecimento de tumor-imuno esferoides com a linha celular MDA-MB-231 e macrófagos humanos. Concluiu-se que a utilização de micro-moldes de agarose é o modelo mais adequado, devido à homogeneidade e reprodutibilidade dos esferoides formados. Além disso, após várias otimizações, foram escolhidas, como condições ideais para a formação destes tumor-imuno esferoides, a utilização de 5000 células iniciais por esferoide, com um rácio inicial de 35:65 de MDA-MB231:monócitos e em meio de cultura DMEM/F12.

Após três dias de co-cultura, os tumor-imuno esferoides foram dissociados e o perfil inflamatório dos macrófagos (CD86, CD40, HLA-DR, CD163, CD206, PD-L1), e a imunogenicidade das células tumorais (PD-1, PD-L1, CD47, HLA-ABC, CD40) foram caracterizados por citometria de fluxo. Notavelmente, oss macrófagos presentes neste modelo apresentam um fenótipo intermédio expressando elevados níveis de CD40, um marcador pro-inflamatório, e de CD206, um marcador anti-inflamatório. Quanto às células tumorais, é visível que a presença de macrófagos altera o seu fenótipo imunogénico, com um aumento da expressão dos marcadores CD47, PD-1 e CD40.

Seguidamente, ao terceiro dia de co-cultura, os esferoides e tumor-imuno esferoides foram submetidos a dois esquemas de radioterapia utilizados na prática clínica: 2.67 e 5.2 Gy durante um ou cinco dias, representando um dia ou uma semana de tratamento dos pacientes. Vinte e quatro horas após a primeira ou a quinta fração, os esferoides foram dissociados para avaliar o perfil inflamatório dos macrófagos e o perfil das

células tumorais, como previamente descrito. O impacto da radioterapia na viabilidade celular e apoptose foi aferido através da marcação com anexina V e com iodeto de propídeo. Além disso, os sobrenadantes das culturas 3D foram recolhidos para análise da secreção de fatores solúveis (IL-6, IL-10, IL-12/IL-23 (p40), TNF-α, CCL18 e TGF-β), por ELISA.

Os resultados obtidos demonstraram que os macrófagos, após radioterapia, adquirem um fenótipo mais pro-inflamatório, com o aumento da expressão dos marcadores pro-inflamatórios CD86 e CD40, e a diminuição da expressão dos marcadores anti-inflamatórios CD163 e CD206. Contudo, apesar da aquisição deste fenótipo, os macrófagos demonstraram capacidade de proteger as células tumorais da morte causada pela irradiação. Após o tratamento de radioterapia, as células tumorais adquirem um fenótipo mais imunogénico com um aumento da expressão de HLA-ABC e diminuição da expressão de PD-L1. Porém, a presença dos macrófagos promove um aumento da expressão de PD-L1, o que sugere o escape imunológico das células tumorais. De um modo geral, não se verificaram diferenças entre os dois esquemas de radioterapia testados e apenas ao fim de cinco frações cumulativas de irradiação é que se observaram efeitos no microambiente tumoral.

Os resultados obtidos sugerem a importância de combinar a radioterapia com imunoterapia em pacientes com CMTR. Para além disso, neste projeto estabelecemos e caraterizamos detalhadamente culturas 3D que mimetizam, de forma mais precisa o microambiente tumoral do CMTR. Este modelo pode ser agora explorado, não só para o estudo dos mecanismos de radiorresistência, mas também para investigar a resistência do CMTR a outras terapias, e encontrar novos alvos farmacológicos para melhorar o tratamento destes tumores com mau prognóstico.

Palavras-chave:

Cancro da mama triplo-negativo; Macrófagos; Radioterapia; Tumor-imuno esferoides

ABSTRACT

Triple-negative breast cancer (TNBC) is the most aggressive subtype and accounts for 10 to 20% of all diagnosed breast tumors. Being characterized by the lack of expression of estrogen and progesterone receptors and the amplification of the oncogene *HER2*, this breast cancer subtype lacks efficient target therapies. Furthermore, TNBC is also more resistant than other subtypes, to conventional therapies, such as radiotherapy, which contributes to its worse prognosis.

As radioresistance cannot be fully explained only by tumor cells genetic characteristics, attention has also to be paid to the other elements of the tumor microenvironment, as macrophages. These immune cells are known to be modulated by cancer cells into an immunosuppressive phenotype, and have the ability to promote breast cancer progression.

Therefore, the main aim of this project was to develop a 3D model that closely mimics the breast tumor microenvironment, to study the role of macrophages in triple-negative breast cancer radioresponse. To achieve this aim, we first optimized the establishment of 3D tumor-immune spheroids with MDA-MB-231 TNBC cells and human macrophages. From the distinct methodologies tested, we concluded that agarose micro-molds were the most suitable model, given the high spheroids homogeneity and reproducibility. The optimal conditions have been achieved: i) a total of 5000 cells were initially seeded per spheroid, ii) an initial ratio of 35:65 of MDA-MB-231:monocytes was selected and iii) DMEM/F12 medium was considered ideal.

After three days of co-culture, tumor-immune spheroids were dissociated and the inflammatory profile of macrophages (CD86, CD40, HLA-DR, CD163, CD206, PD-L1) and the immunogenicity of cancer cells (PD-1, PD-L1, CD47, HLA-ABC, CD40) were characterized by flow cytometry into detail. Interestingly, macrophages showed an intermediate phenotype expressing high levels of CD40, a pro-inflammatory marker, and of CD206, an anti-inflammatory marker. On its turn, macrophages modulated cancer cell immunogenic phenotype, inducing an increased expression of CD47, PD-1 and CD40 markers.

On the third day of co-culture, tumor spheroids and tumor-immune spheroids were submitted to two radiotherapy schemes commonly used in the clinical practice: 2.67 Gy and 5.2 Gy, for one or five cumulative fractions, representing one day or one week of cancer patients treatment, respectively. Twenty-four hours after the first or fifth fraction, spheroids were dissociated to evaluate, as previously, the inflammatory profile of macrophages and the immunogenic profile of tumor cells, as well cell viability and apoptosis by annexin

V/propidium iodide staining. In addition, 3D cultures conditioned media were collected to analyze the secretion of soluble factors (IL-6, IL-10, IL-12/IL-23 (p40), TNF-α, CCL18 and TGF-β) by ELISA.

Our results demonstrated that after radiotherapy, macrophages acquire a more pro-inflammatory phenotype, with increased expression of the pro-inflammatory markers CD86 and CD40, and decreased expression of the anti-inflammatory markers CD163 and CD206. Despite the acquisition of this phenotype, macrophages have the ability to protect tumor cells from death caused by irradiation. Furthermore, after radiotherapy treatment, tumor cells also acquired a more immunogenic phenotype, with increased expression of HLA-ABC and decreased expression of PD-L1. Macrophages promoted an increase of cancer cells PD-L1 expression, which may favors the escape of tumor cells from the immune system. In general, there were no differences between the two radiotherapy schemes and only five fractions of ionizing irradiation had a significant impact on the tumor microenvironment.

Altogether, our findings highlighted the importance of combining radiotherapy with immunotherapy in TNBC patients. Remarkably, in this project, we were able to develop 3D cultures that mimic the TNBC microenvironment. This model can be now used, not only to study radioresistance mechanisms, but also to investigate the resistance of these tumors to other therapies and to unveil novel pharmacological targets to better treat TNBC patients.

KEYWORDS:

Triple-Negative Breast Cancer; Macrophages; Radiotherapy; Tumor-immune spheroids

TABLE OF CONTENTS

FIGURE INDEX

LIST OF ABBREVIATIONS

2D: Two-dimension

3D: Three-dimension

Akt: Protein kinase B

Bcl2: B-cell lymphoma 2

Bcl-xL: B-cell lymphoma-extra large

BC: Breast cancer

BRCA: Breast cancer gene

CAF: Cancer-associated fibroblast

CCL: CC chemokine ligand

CCR: CC chemokine receptor

CD: Cluster of differentiation

CD163: Hemoglobin receptor

CD206: Mannose receptor

CHUSJ: Centro Hospitalar Universitário São João

CT: Computed tomography

CXCL: CXC chemokine ligand

DMEM: Dulbecco's modified eagle medium

EGFR: Epidermal growth factor receptor

ELISA: Enzyme-linked immunosorbent assay

EMT: Epithelial-to-mesenchymal transition

ER: Estrogen receptor

FBS: Fetal bovine serum

FDA: Food and Drug Administration

G-CSF: Granulocyte colony-stimulating factor

HER2: Human epidermal growth factor receptor 2

HLA-DR: Human leukocytes antigen-D related

HNSCC: Head and neck squamous cell carcinoma

HPV: Human papillomavirus

IFN-γ: Interferon-gamma

IL: Interleukin

ISH: In-situ hybridization

Lcn2: Lipocalin-2

LPS: Lipopolysaccharide

MCP-1: Monocyte chemoattractant protein-1

M-CSF: Macrophage colony-stimulating factor

MDSCs: Myeloid-derived suppressor cells

MHC: Major histocompatibility complex

MMP: Matrix metalloproteinase

MRI: Magnetic resonance imaging

NF-κB: Nuclear factor kappa B

NO: Nitric oxide

PBS: Phosphate-buffered saline

PFA: Paraformaldehyde

PARP: Poly (ADP-ribose) polymerase

PD-1: Programmed cell death protein 1

PD-L1: Programmed cell death protein 1 ligand

PET: Positron emission tomography

PI: Propidium iodide

PI3K: Phosphatidylinositol 3-kinase

PolyHEMA: Poly(2-hydroxyethyl methacrylate)

PR: Progesterone receptor

PTGS2: Prostaglandin-endoperoxide synthase 2

RPMI: Roswell park memorial institute

ROS: Reactive oxygen species

RT: Radiotherapy

SD: Standard deviation

STAT6: Signal transducer and activator of transcription 6

TAMs: Tumor-associated macrophages

TCR: Toll-like receptor

TILs: Tumor-infiltrating lymphocytes

TGF-β: Transforming growth factor-beta

Th17: T helper type 17

TNBC: Triple-negative breast cancer

TNF: Tumor necrosis factor

TNM: Tumor lymph node metastasis

Tregs: Regulatory T cells

VEGFA: Vascular-endothelial growth factor A

I. INTRODUCTION

1. Breast cancer

Breast cancer (BC) is the most common incident malignancy worldwide, surpassing recently lung cancer with an estimated 2.3 million new cases in 2020, and constitutes the fifth leading cause of cancer-related deaths (**Figure 1A**) [1]. In women, this neoplasia is the most diagnosed and deadliest, representing 24.5% and 15.5% of the overall incidence and mortality, respectively (**Figure 1B**) [1]. The high incidence of this malignancy is a consequence of the longstanding higher prevalence of reproductive, hormonal and lifestyle risk factors [1]. Importantly, declining in mortality rates is a reflex of implemented screening programs favoring early detection, and development of more advanced effective treatments [2]. Notwithstanding, this neoplasia remains the leading cause of women cancer-related death worldwide, due to relapse and/or metastatic disease, as well as due to therapeutic resistance [1]. Thus, there is an urgent need to improve our understanding on breast cancer biology in order to ameliorate patients outcome.

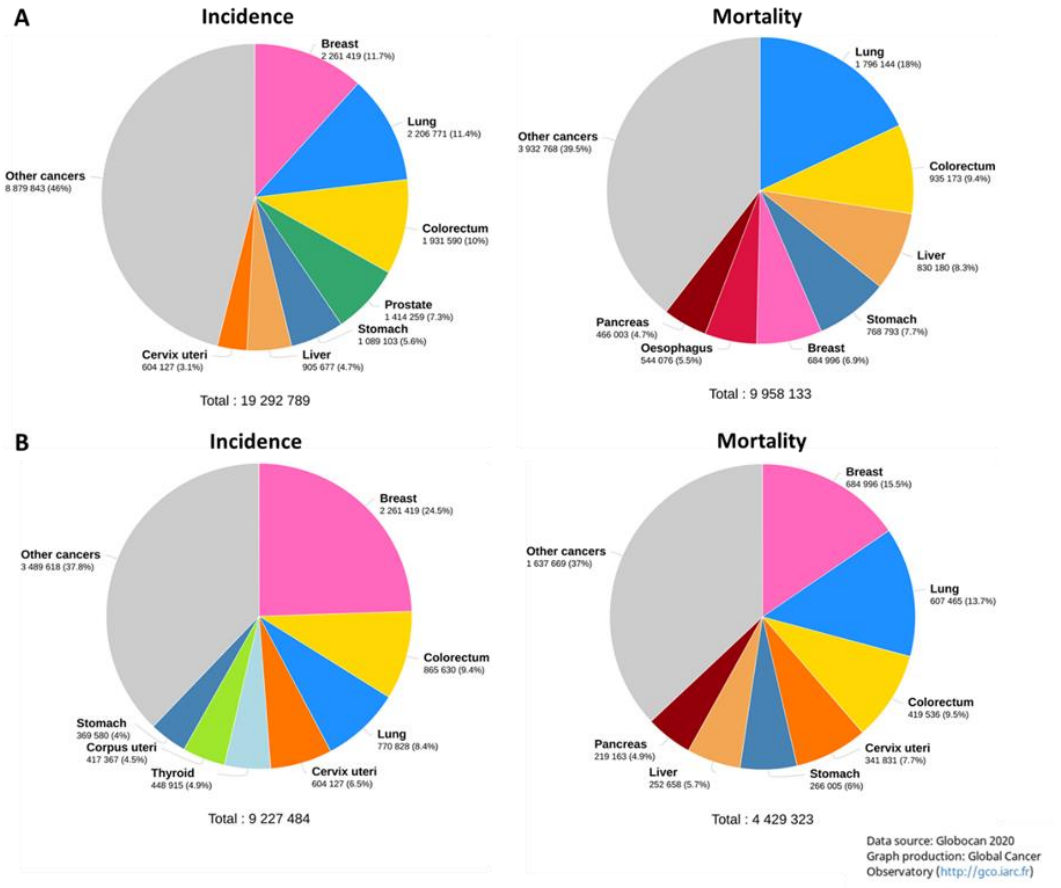

Figure 1- Breast cancer incidence and mortality A) in both sexes and **B)** in women, worldwide, in 2020. Breast cancer represents 24.5% of all cancers diagnosed in women and 15.5% of cancer-related death in women worldwide. Adapted from [1].

1.1 Pathogenesis and risk factors

Breast cancer development is a multi-step process which implicates the accumulation of genetic and/or epigenetic alterations leading to cancer cells transformation. These alterations are caused by the activation of proto-oncogenes or the inactivation of tumor suppressors in signaling pathways related to cell proliferation, differentiation and survival [3].

There are numerous factors associated with BC development. Some of the risk factors cannot be controlled since the risk of developing disease increases with age and it is far more common in women. The risk of developing this disease is also increased by genetic predisposition/family history, high breast density, use of hormone replacement therapy after menopause, the existence of atypical hyperplasia, exposure to estrogens and ionizing radiation, early menarche and later menopause. On the other hand, breastfeeding and parity are documented as protective factors [3, 4]. In addition, lifestyle conditions as obesity, high alcohol consumption and reduced physical activity also contribute to the increased incidence of breast cancer [3-5].

Furthermore, 5 to 10% of all diagnosed breast cancers are inherited, associated with an hereditary mutation. Hereditary breast cancer is mainly associated to mutations in breast cancer gene (*BRCA*) *1* and *BRCA2* [6], which increase in 70% the probability of women developing breast cancer [3]. Other familiar syndromes, such Li-Fraumeni (mutations on *TP53* gene), Cowden (mutations on *PTEN* gene) and ataxia telangiectasia (mutations on *ATM* gene) are also related to breast cancer development; however, the risk and prevalence are lower than in *BRCA1* and *BRCA2* mutations [3, 6].

1.2 Detection, diagnosis and therapy

Breast cancer can be detected before the appearance of a palpable tumor mass. Therefore, screening programs for early diagnosis were implemented in many countries, including Portugal. These programs recommend mammography for women with more than 40 years, normally every two years, and in some cases the addition of other complementary high-resolution imaging techniques, as magnetic resonance (MRI) or ultrasound imaging [4].

Imaging techniques in combination with biopsies are important tools for BC diagnosis and its classification. Indeed, BC is a highly heterogenous disease with several histologic subtypes identified. Breast carcinomas usually arise from luminal epithelial cells, which can then be divided in lobular or ductal carcinomas. The most common subtypes are

ductal or lobular carcinomas (*in situ* or invasive) [3]. Additionally, all breast cancers are classified as grade 1 to 3, depending on tumor cell histologic characteristics as tubular formation, nuclear pleomorphism and mitotic count [7].

To better evaluate the disease extension, all breast cancers can be classified for stage from 0 (better prognosis) to IV (worse prognosis), according to the Tumor Lymph Node Metastasis (TNM) system, which gives information about the primary tumor size (T), as well as about the disease extension to regional lymph nodes (N) or to distant metastatic sites (M) [4, 5]. Classification is essential for the multidisciplinary medical team to select the best treatment plan for each patient, which can include surgery, radiotherapy, chemotherapy, endocrine therapy or targeted therapy [5, 8]. Surgery is a frequent option of treatment of this disease, being applied as conservative breast surgery or, in advanced breast tumors, as mastectomy. Radiotherapy is recommended for all breast cancers as postoperative treatment. Chemotherapy is usually used as a neoadjuvant treatment (before surgery) to reduce tumor size or as adjuvant therapy (after surgery) to eliminate undetected tumor cells. The treatment with endocrine or target therapies depends on the molecular BC subtype [5].

1.3 Molecular subtypes

Regarding its molecular characteristics, breast cancer can be divided into four different subtypes: Luminal A, Luminal B, HER2 (human epidermal growth factor receptor 2) overexpression, or “Basal-like” (**Figure 2**). This stratification relies on estrogen (ER) and progesterone receptors (PR) expression of assessed by immunohistochemistry and the overexpression of HER2 evaluated using a combination of immunohistochemistry and *in situ* hybridization (ISH) [5, 9]. “Basal-like” subtype is commonly named “triple-negative breast cancer” (TNBC) because there is an 80% overlap between these two types of tumors. However, not all basal-like tumors have a triple-negative phenotype, and not all triple-negative breast cancers have a basal-like gene expression profile [9].

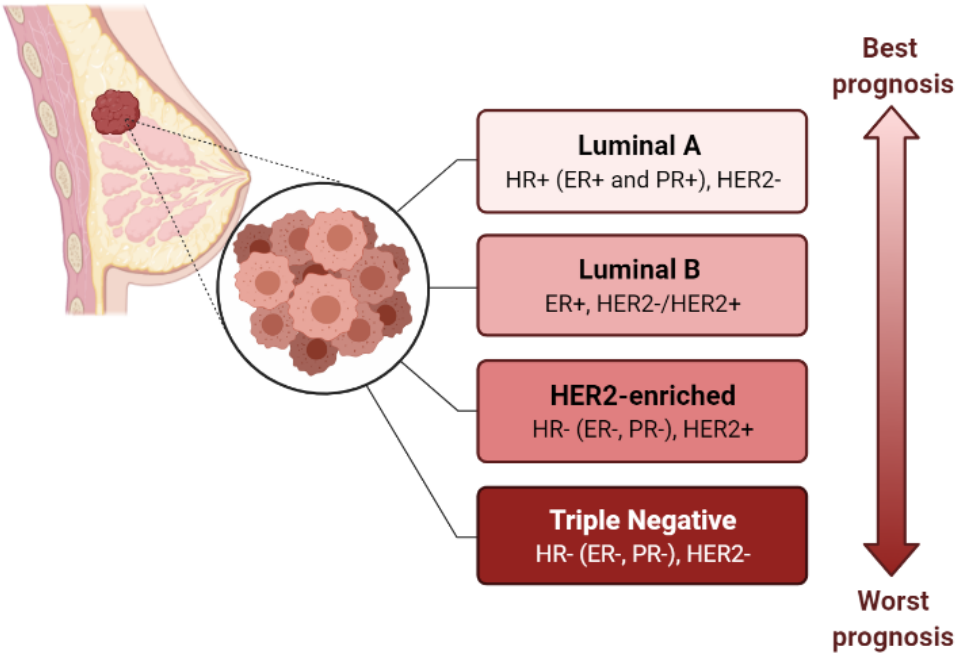

Figure 2- Breast cancer molecular subtypes. Breast cancer can be classified into four different molecular subtypes, which have an impact on treatment and prognosis. Figure created with Biorender.

Luminal A breast cancers represent about 40% of all breast cancer subtypes [3] being characterized by the expression of ER and PR, and the absence of HER2, exhibiting also a low (<14%) expression of Ki67, an indicator of proliferation. This BC subtype is recommended to be treated with endocrine therapy, such as Tamoxifen, a selective ER modulator, or with aromatase inhibitors, as Anastrozole. However, the best endocrine treatment is generally selected depending on patients menopausal status [5, 8, 10].

Luminal B accounts for approximately 20% of all breast cancers [3] and can be subdivided into two different subtypes. The first is characterized by the expression of ER, absence of HER2, and the presence of at least one of the following characteristics: high (>14%) expression of Ki67, negative or low (<20%) PR expression. This type of breast cancer is treated with endocrine therapy and chemotherapy. The second luminal B subtype is positive to ER and characterized by the amplification or overexpression of HER2 and, for that reason, this subtype should also be treated with anti-HER2 therapy (e.g. Trastuzumab) [8, 10].

HER2 overexpression breast cancer subtype corresponds to 10-15% of all BC [3], being characterized by the amplification or overexpression of HER2 and the absence of ER and PR expression, being treated with anti-HER2 target therapy and chemotherapy.

Lastly, triple-negative breast cancer (TNBC) is negative regarding the expression of the three receptors and no target therapy is known, being chemotherapy the only therapy

available to treat this low prognostic tumors [10]. In addition to these treatments, surgery and radiotherapy must be considered for all breast cancer subtypes [5].

1.3.1 Triple-negative breast cancer

Triple-negative breast cancer (TNBC) represents 10-20% of all diagnosed breast tumors [7, 11] and is characterized by the lack of ER and PR and HER2 overexpression, being the most aggressive BC subtype [12]. This BC subtype is more common in African women or in women with African ancestry, as well as in pre-menopausal females, affecting younger women (age <40) [7, 13]. About 20% of these cancers show a BRCA mutation, mainly *BRCA1* [9, 14].

The majority of TNBC are of high histological grade (grade 3 or poorly differentiated) [13, 14], exhibiting high mitotic activity, atypical mitosis, high proliferation, and cellular pleomorphism [9], and at diagnosis, present larger size and greater lymph node involvement [7]. Within the TNBC, some histological subtypes, such as invasive ductal or lobular, high-grade metaplastic, and high-grade neuroendocrine carcinomas, have a very unfavorable prognosis [7]. Comparing to other BC, TNBC patients have a higher risk of recurrence in the first 5 years after diagnosis [9], and the 5-year survival rate decreases from 90% to 77% when only TNBC is considered, instead of all breast cancers [15, 16]. For these patients the overall and breast cancer-specific survival are also lower in all disease stages [7, 14].

At diagnosis, about 10% of TNBC patients already present metastatic dissemination. In this tumor, metastasis involves more visceral sites, such as lung, liver, and brain [7], which might explain its aggressiveness [7], with a lower probability of axillary and bone lymph node metastases [11]. Indeed, when compared to other breast cancer subtypes, TNBC patients have also lower survival rates after metastasis had occurred [13]. The worse prognosis is not only associated with the more aggressive form, but also with the lack of current efficient target therapies.

Currently, the therapeutic options for TNBC patients are surgery, radiotherapy, and chemotherapy [9]. For this form of breast cancer, chemotherapy, particularly taxanes or anthracyclines, is used as primary systemic approach, while surgery and radiotherapy are selected for patients with locoregional disease [17]. The treatment of metastatic TNBC also includes sequential chemotherapy, however, it is not known which is the most effective drug and the best therapeutic sequence [7]. Although not all patients will respond to the standard care treatments, there are no predictive biomarkers to determine which patients will benefit from each treatment [13].

2. Radiotherapy

Radiotherapy (RT) is one of the most frequent treatment modalities used in clinical practice and it is estimated that approximately 50% of all tumors will be, at least once, submitted to ionizing radiation, either as monotherapy or in combination with surgery, chemotherapy or immunotherapy [18]. RT can be used before surgery to reduce tumor size (neoadjuvant), or after surgery (adjuvant), to eliminate undetected tumor cells that can be left behind and lead to locoregional recurrence or distant metastasis formation [18, 19].

Radiotherapy uses ionizing radiation to cause DNA damage in cancer cells. Radiation has direct and indirect effects on DNA, because can directly cause double strand DNA breaks or form free radicals, by interacting with water, which in turn cause DNA damage (**Figure 3**), genomic instability and cell death. The most frequent mechanisms of cell death induced by radiation are apoptosis and mitotic cell death, involving the activation of ataxia telangiectasia mutated (ATM), a central regulator of cellular responses to DNA damage, and subsequent activation of downstream effectors, as the p53 signaling pathway. Upon p53 phosphorylation, other downstream effectors may be activated, as p21 and Bax, leading to cell cycle arrest and apoptosis, respectively. Furthermore, irradiation can also induce cell necrosis, dependent on the tumor necrosis factor (TNF)-α pathway, senescence, involving the cellular homologue of the viral oncogene *myc* (c-MYC) cascade and autophagy, activated by the phosphatidylinositol 3-kinase (PI3K) signaling pathway [18]. Despite normal cells may also be affected by radiation, these can repair DNA damage faster and more efficiently than cancer cells [18, 20].

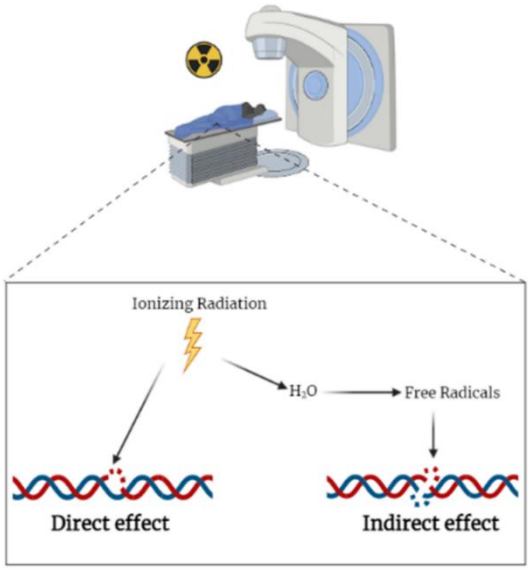

Figure 3- Ionizing irradiation direct and indirect effects on DNA. Ionizing irradiation can cause double strand breaks and damage DNA through direct interaction (Direct effect), or can interact with water forming free radicals by, which in turn cause DNA damage (Indirect effect). Figure created with Biorender.

The effects of radiation do not only depend on the specific organ, but also on the type of radiation, namely its intensity, energy, and exposure time. Thus, the total dose, the dose per fraction, and the total exposure time are crucial parameters for the treatment [7]. Radiotherapy aims to maximize tumor cell damage while protecting the surrounding normal cells [18]. For that, the total dose is usually divided into several fractions. The fractionation effects can be summarized in the five Rs of radiobiology: Repair (healthy cells are able to repair their DNA damage, but cancer cells should not recover due to defects in DNA repair pathways), Redistribution (multiple fractions allow cells to progress through mitosis, a more radiosensitive phase of the cell cycle), Repopulation (cell proliferation between fractions), Reoxygenation (hypoxic regions are less radiosensitive) and Radiosensitivity (different cells have different radiosensitivity) [21, 22].

2.1 Radiotherapy in breast cancer

In radiotherapy services, about a third of whole treatments are dedicated to breast cancer, because of the prevalence of this disease and of the importance of radiotherapy in its treatment [7].

In breast cancer, RT must be considered for all patients as a local adjuvant treatment [5, 19]. Indeed, it has been shown that adjuvant radiotherapy can reduce three times the annual probability of local recurrence, and decrease distant metastasis rate [23]. As for metastatic breast cancer, about 50-60% of patients are submitted to RT as a form of treatment, but also for symptoms relief [7].

Specifically in BC, treatment involves breast irradiation in a conventional regimen (50 Gy divided into 25 fractions, at 2 Gy/fraction) [7] or using an hypofractionated scheme with 15 fractions at 2.67 Gy per fraction, totalizing 40 Gy. Nevertheless, in recent years, an hypofractionated regimen of 26 Gy in one week (5.2 Gy/fraction) was also implemented, since this regimen revealed to be efficient for tumor control and safer for normal tissue preservation. Indeed, when compared to the conventional hypofractionated scheme, the treatment with 26 Gy in 5 fractions reduced patient breast cancer relapse from 2.1% to 1.4%, in the five years after radiotherapy. Furthermore, the early effects on normal tissues, namely breast erythema, were less severe in the 5.2 Gy/fraction scheme and there were no differences in the late side effects when comparing the two radiotherapy regimens. Additionally, the implementation of one-week radiotherapy treatment is more convenient for patients, particularly in older patients with other comorbidities, and it is less expensive for radiotherapy services [24, 25].

Regardless of the benefits of this treatment, RT can cause some acute effects, namely skin erythema and fatigue in patients. Late side effects are less frequent and include telangiectasia, impaired cosmesis with fibrosis, arm lymphoedema, shoulder stiffness, radiation-induced pneumonitis, pulmonary fibrosis, heart endothelial cell damage, atherosclerosis, myocardial ischemia, heart fibrosis, acute pericarditis, pericardial effusion, and arrhythmias [19]. In the last decades, in order to reduce side effects, technological improvement had emerged, allowing to reduce the damage caused in normal cells by the introduction of image-guided radiotherapy using computed tomography (CT), positron emission tomography (PET), and MRI [18, 19, 26].

Although radiotherapy has largely improved locoregional control of breast cancer, TNBCs are still considered more radioresistant than the other BC subtypes and have been significantly associated with a higher locoregional recurrence risk and a higher distant metastases rate following RT [19, 23], being estimated that about 10% of irradiated TNBC will locally relapse, and the majority will develop systemic disease [27].

The lack of efficient therapeutic approaches urges the need to unveil the mechanisms underlying TNBC radioresistance, envisaging the disclosure of alternative therapies to radiosensitise cancer cells and improve TNBC management [17, 19].

2.2 Mechanisms of radioresistance

In the last decades, advances in radioresistance mechanisms have been partially elucidated. It is well known that radiotherapy induces double-strand breaks that impair cell-cycle progression and that, if not repaired, will ultimately lead to apoptosis [18]. Nevertheless, it has been described that cancer cells can acquire resistance to ionizing radiation through several mechanisms.

Firstly, tumor cells are able to repair radio-induced DNA damage since DNA double-strand breaks can activate damage sensors that will recruit DNA repair complexes, such as ATM and BRCA1 to repair DNA damage [26]. In BC, it is described that radioresistant cells increased ATM expression, which improves DNA repair efficiency [28, 29]. Additionally, the presence of radioresistant cancer stem cells can also lead to cancer radioresistance, since these cells are capable to generate heterogeneous lineages if they are not totally eliminated with anti-cancer treatment [26].

Furthermore, the upregulation of the PI3K/Protein kinase B (AKT) signaling pathway, and the presence of hypoxic events could increase HIF-1α signaling and angiogenesis, which allows tumor revascularization and leads to tumor cell radioresistance [26]. In fact, it is well established that hypoxic areas are the most radioresistant zones within a tumor mass

[30]. In addition, the PI3K/AKT signaling pathway activation may also increase cell proliferation, DNA damage repair and reduce apoptosis [26, 31]. The upregulation of this signaling pathway could be caused by epidermal growth factor receptor (EGFR) gene overexpression or its amplification, an alteration identified in approximately 45-70% of the breast tumors [31].

Further, radioresistance mechanisms may consist of: i) apoptotic machinery deficiency, such as p53 mutations [32]; ii) mutagenesis with the acquisition of a more resistant phenotype; iii) epigenetic modifications and iv) micro-RNAs deregulation [26]. Regarding this last mechanism, it has been reported in BC that the miR-95 overexpression induces S1P signaling, activating PI3K/AKT signaling pathway, contributing to cancer radioresistance [33].

In addition to these mechanisms of radioresistance, it is also important to pay attention to the acquisition of a radioprotective immunosuppressive microenvironment [34]. Indeed, Boustani *et al*. suggest the addition of the "anti-tumor immune response Reactivation" as the "6th R" of radiobiology [21]. Although radiotherapy causes an immune response within the tumor microenvironment, it also contributes to potentiate hypoxia, to modulate the cancer-associated fibroblasts (CAF) activity, and to recruit immune cells, such as tumor-associated macrophages (TAMs) that, in the tumor microenvironment, can acquire a more immunosuppressive phenotype. For this reason, some studies try to combine known drugs targeting the tumor microenvironment (hypoxia, fibrosis and CAF, and immune cells) to increase tumor radiosensitivity [34]. However few studies try to improve radiosensitivity by targeting TAMs, which may be important due to their significant role in the tumor microenvironment.

3. The tumor microenvironment

The tumor microenvironment comprises not only cancer cells, but also other cellular populations that surround and communicate with them, such as immune (e.g. neutrophils, macrophages, lymphocytes) and endothelial cells, fibroblasts, adipocytes, but also extracellular matrix components (**Figure 4**). Given the large diversity of cell populations, tumor progression is not only influenced by cancer cell intrinsic characteristics, but also by their interactions with neighbor elements, which can exert anti- or pro-tumor functions [35].

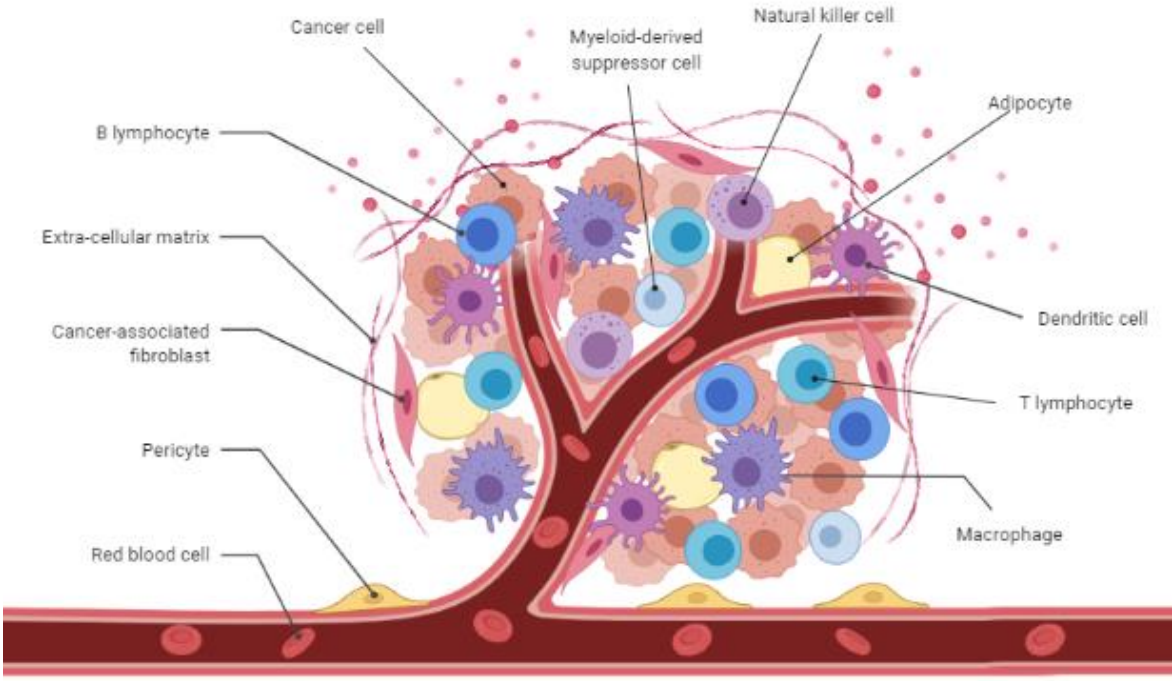

Figure 4- Tumor microenvironment. Cancer cells are surrounded by different cell populations, namely immune cells as macrophages, and extracellular matrix that have an impact on cancer progression. Figure created with Biorender.

Radioresistance cannot be fully explained by cancer cell genetic instability or clonal diversity, thus the role of other elements of the tumor microenvironment, as immune cells have been studied on radiotherapy response. We now know that radiation treatment causes tumor cell death, promoting cytokines and chemokines release, which will in turn recruit additional immune cells to the tumor microenvironment [36]. However, depending on the stimuli, these cells can acquire a pro-inflammatory phenotype, leading to tumor elimination, or be converted into immunosuppressive populations that will promote tumor escape and radioresistance (**Figure 5**). Thereby, immune cells can modulate cancer cell response and tumor progression [34, 35, 37].

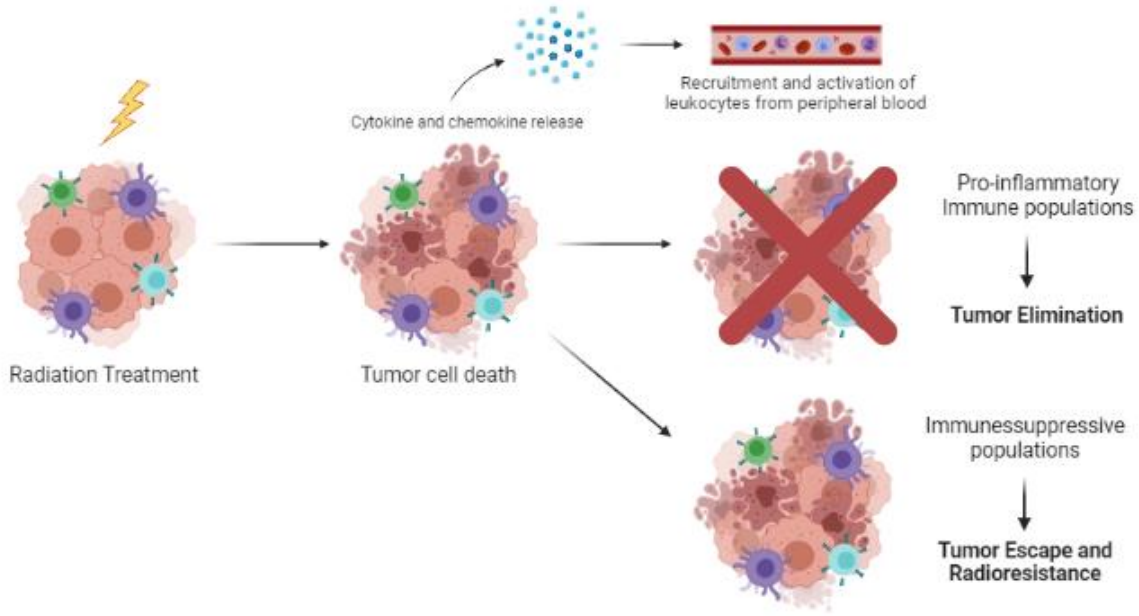

Figure 5- Radiotherapy affects the tumor microenvironment. Irradiation causes tumor cell death promoting cytokines and chemokines release, recruiting immune cells to the tumor microenvironment. These cells can turn pro-inflammatory, leading to tumor elimination, or anti-inflammatory, inducing tumor escape and radioresistance. Adapted from [37]. Figure created with Biorender.

Cancer cells and immune system interaction is a very complex and dynamic process characterized by three stages: elimination, equilibrium and escape (**Figure 6**). In the elimination phase, immune cells can suppress cancer cells through their anti-tumor activities, preventing their progression. However, tumor cells are able to accumulate genetic alterations and, if immune cells are not able to eliminate the tumor, some mutated variants may be generated and escape to immune surveillance [38].

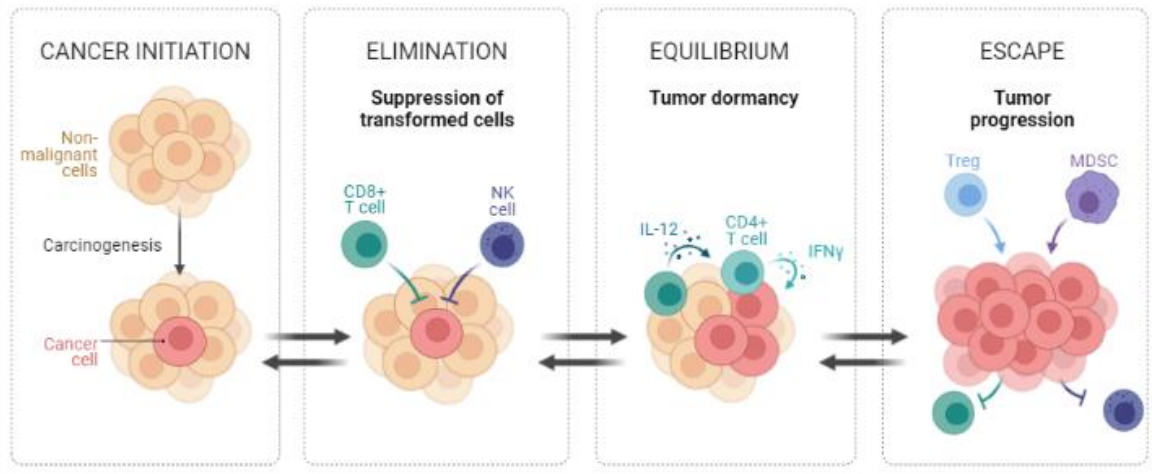

Figure 6- Stages of immunoediting in cancer: Elimination, Equilibrium and Escape. After cancer initiation immune cells could be able to suppress cancer cells (Elimination). If the immune system is unable to eliminate all cancer cells, a phase of tumor dormancy could prevail (Equilibrium), or tumor cells can escape to immunosurveillance, by decreasing in their immunogenicity (Escape). Figure created with Biorender.

Indeed, the immune system relevance on cancer cell progression was recognized in 2011, when Hanahan and Weinberg recognized the ability of cells to avoid immune destruction and tumor-promoting inflammation as two news Hallmarks of Cancer [39].

3.1 Mechanisms of tumor immune escape

Tumor-infiltrating lymphocytes (TILs) are one of the most common and studied elements of the tumor microenvironment and are considered as biomarkers of immunotherapy response. In breast cancer, and specifically in TNBC, the presence of these cells is associated with a better prognosis, a decrease of local and distant recurrence, and an increase in patients overall survival [13].

Although BC is not a very immunogenic cancer, as melanoma [40], TNBC has a higher number of T cell infiltrated when compared to other subtypes and, consequently, is the more promising candidate to immunotherapy [7].

Although, the presence of TILs in the tumor microenvironment is considered a marker of good prognosis, tumor cells can still escape immune surveillance in several ways: i) by decreasing the expression of major histocompatibility complex (MHC) class I molecules, reducing antigen presentation; ii) inducing apoptosis of immune cells through expression of death signals (e.g. FAS ligand); iii) secreting immunosuppressive molecules, such as interleukin (IL)-10 and transforming growth factor-beta (TGF-β); iv) releasing prostaglandins that inhibit dendritic cell maturation, affecting antigen presentation and recognition by T cells; v) expressing immune checkpoints, such as the programmed cell death protein 1 (PD-1) and its ligand (PD-L1) that provide inhibitory signals to T cells [41]; vi) expressing the cluster of differentiation (CD)47, a marker recognized as "*don't eat me*" signal, which prevents phagocytosis of tumor cells by macrophages [42]. Furthermore, tumor cells can still express CD40. The interaction of this marker with CD40 ligand present on T cells increases the TGF-β production and enhances the differentiation of T cells into T helper (Th)17 and this binding promotes tumor cells proliferation [43] (**Figure 7**).

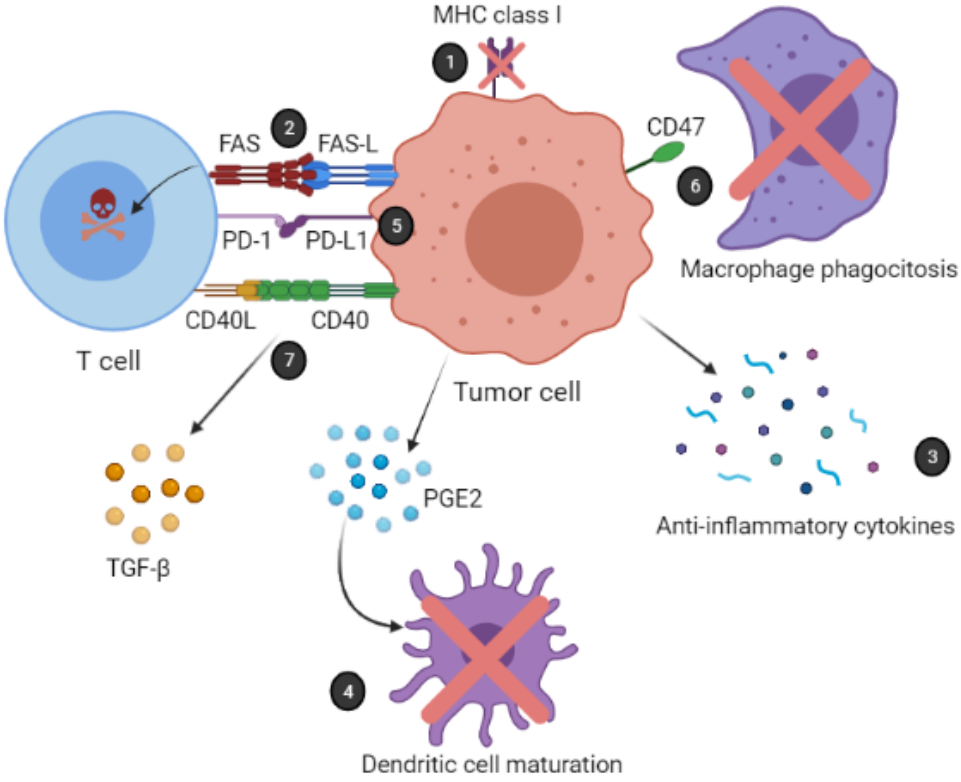

Figure 7- Mechanisms of immune escape in the tumor microenvironment. 1) Decrease MHC-I expression. 2) Induce apoptosis of immune cells through death signals expression (e.g. FASL). 3) Secretion of immunosuppressive cytokines. 4) Release of prostaglandins that inhibit dendritic cell maturation. 5) Express of immune checkpoints, such as PD-1 and PD-L1 that provide inhibitory signals to T cells. 6) Expression of CD47 prevents the tumor cell phagocytosis by macrophages. 7) CD40-CD40L ligation increases TGF-β production. Adapted from [41]. Figure created with Biorender.

Considering these characteristics of cancer cells, several treatments have been suggested to inhibit some of these molecules (e.g. PD-1, PD-L1 and CTLA4) and enable a better response of the immune system to the tumor. Thus, immunotherapy is currently an anti-cancer therapy for many cancer types [44].

In 2019, the Food and Drug Administration (FDA) approved Atezolizumab, an anti-PD-L1 antibody and, more recently, in 2020, Pembrolizumab, an anti-PD-1 antibody, for treatment of TNBC patients with PD-L1 expressing tumors, and to be used in combination with chemotherapy. However, due to conflicting results from different clinical trials, the Atezolizumab approval for TNBC treatment was withdrawn in the United States [45].

Despite the efforts in breast cancer treatment improvements, TNBC remains as a BC subtype with a worse prognosis. Therefore, it is essential to study the other cell populations present in the tumor microenvironment, such as macrophages, that can affect breast cancer progression [35].

3.2 Tumor-associated macrophages (TAMs)

Tumor-associated macrophages are a heterogeneous myeloid population that originates from tissue resident macrophages, differentiated from the embryo fetal liver, or on its majority, from bone marrow-derived circulating monocytes, recruited from the blood to the tissues [46]. Macrophages are pivotal regulators of tissue homeostasis, specifically engaged on host defense, wound healing and immune regulation [47]. Furthermore, macrophages link innate and adaptive immune systems, as they can phagocytose bacteria, viruses, tumor cells or cellular debris, but also carry out antigen presentation functions, activating T lymphocytes [46].

Depending on the microenvironment and on its functional requirements, macrophages can acquire different phenotypes that are described as a continuum of functional states [48]. In the extremes of their spectrum, macrophages are classified into pro-inflammatory (M1-like) or anti-inflammatory (M2-like) [35, 46] (**Figure 8**).

Pro-inflammatory, also known as “classically activated” macrophages, activated by interferon-gamma (IFN-γ) or bacterial lipopolysaccharide (LPS) [35, 46, 48], express toll-like receptors (TCR), the co-stimulatory receptors CD80/CD86, CD40 and MHC class II (such as human leukocytes antigen-D related, HLA-DR), crucial for antigen presentation and T cell activation [49]. These macrophages produce also pro-inflammatory cytokines, such as TNF-α, IL-1β, IL-6, and IL-12/IL-23, but also reactive oxygen species (ROS) and nitric oxide (NO). The production of these immune mediators allows them to attack tumor cells and eliminate phagocytosed products, and to attract other pro-inflammatory cells as neutrophils, CD4 T helper cells or CD8 cytotoxic T cells [35, 46, 48].

On the other hand, the differentiation towards an anti-inflammatory phenotype is driven by cytokines, such as IL-4, IL-10, IL-13, and TGF-β. The anti-inflammatory macrophages also produce regulatory and anti-inflammatory cytokines, such as IL-10 and TGF-β, being more associated with wound healing and tissue repair functions. In the tumor microenvironment, these macrophages are also associated with an immunosuppressive environment, promoting angiogenesis, cancer cell migration, invasion, tumor growth and metastasis formation [35, 46, 48]. Among other markers, anti-inflammatory macrophages generally express two scavenger receptors: the hemoglobin receptor CD163 and the mannose receptor CD206 [49]. Macrophages can also express the immune checkpoint PD-L1 and PD-L2, modulating T cell activation status [50].

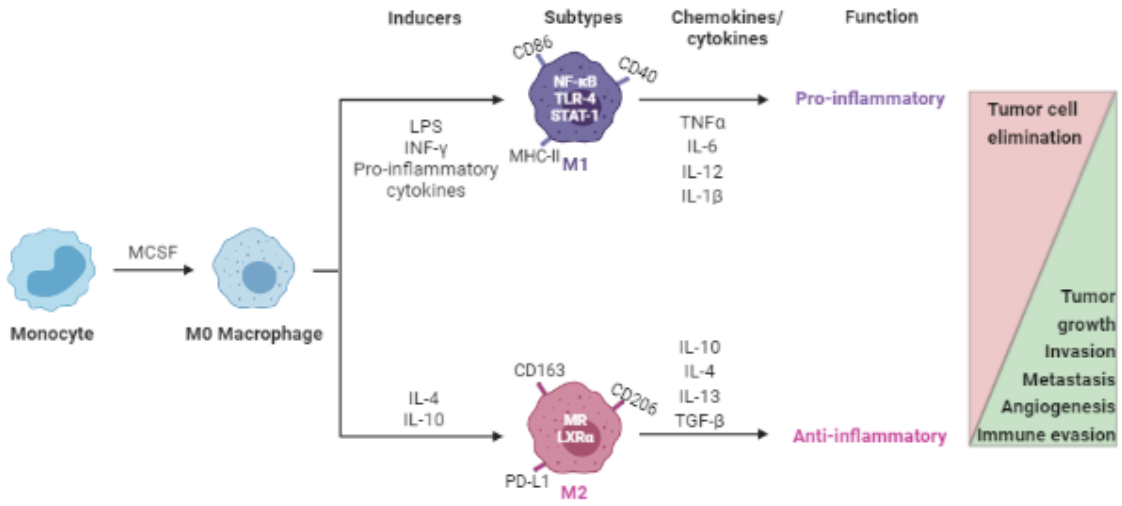

Figure 8- Macrophage phenotypes. Macrophages are classified as having a more pro-inflammatory phenotype, called "classically activated" or M1-like and a phenotype with more immunosuppressive characteristics, called "alternatively activated" or M2-like. While pro-inflammatory macrophages are associated with tumor cell elimination, the anti-inflammatory macrophages can promote tumor progression and immune escape. Adapted from [46]. Figure created with Biorender.

Within the tumor microenvironment, macrophages, known as tumor-associated macrophages (TAMs), may account for up to 50% of the whole tumor mass [38, 46]. Depending on the local stimuli driving macrophages polarization, TAMs can inhibit or promote tumor growth, influencing tumor progression [51]. In advanced tumors, TAMs may generally exhibit anti-inflammatory characteristics [48, 51], exerting immunosuppressive functions, promoting angiogenesis, tissue repair and production of matrix metalloproteinases (MMPs), which might contribute to tumor growth, survival, invasion and metastasis formation [35, 51].

In breast cancer, the presence of anti-inflammatory macrophages, expressing the CD163 marker, was associated with aggressive features, such as high proliferation and poor differentiation [52]. TAMs abundance was also related to a worse prognosis, since its presence on tumor stroma was associated with high invasion and metastatic rates, reduced relapse-free and overall survival [53]. Specifically, in TNBC, the TAMs presence is generally associated to promote tumor growth and progression [52].

In agreement with these results, Meng *et al.* demonstrated that the TAMs depletion in mouse models, just before radiotherapy, increased radiation anti-tumor effects [54]. Furthermore, after local tumor irradiation, TAMs and other suppressive cell types, such as myeloid-derived suppressor cells (MDSCs) and regulatory T cells (Tregs), are highly recruited to the tumor microenvironment [34, 36]. As these cells are less radiosensitive [34], it is important to dissect the mechanisms through which macrophages modulate TNBC cells radioresistance and immune escape to design novel therapeutic approaches.

4. Effect of macrophages-cancer cell interaction on radioresponse

4.1 Effects of radiotherapy on human macrophages

In the last years, our group has demonstrated that, after cumulative ionizing radiation (5x2 Gy, total 10 Gy), irradiated macrophages continued viable and metabolically active, impairing apoptosis and cell death, through the activation of the pro-survival nuclear factor kappa B (NF-κB) signaling pathway. Furthermore, we demonstrated that ionizing radiation modulates human macrophages into a pro-inflammatory profile, with an increase of pro-inflammatory (*CD80*, CD86, and HLA-DR) surface receptors, and a decrease of anti-inflammatory markers, such as IL-10. However, these irradiated macrophages still supported the ability to promote cancer cell invasion and angiogenesis, when colorectal cancer cells were present. These results suggest that TAMs exposed to ionizing radiation do not show a pro- or anti-inflammatory phenotype, but an intermediated phenotype [20].

Further studies demonstrated that the response of macrophages to ionizing radiation is dependent on its intensity. Moderate doses of radiotherapy (1-10 Gy) are described to induce a pro-inflammatory phenotype, with increased secretion of TNF-α, IFN-γ, IL-6, increased expression of HLA-DR and of CD86, and a decreased expression of CD163. Instead, low (<1 Gy) and high doses (>10 Gy) of ionizing radiation are associated with the acquisition of an anti-inflammatory phenotype. Low irradiation exposure promotes TNF-α and IL-1β decrease and an increase of TGF-β production. In opposition, high irradiation doses were related to an increment of CD206 and PD-L1 expression and IL-10 secretion, suggesting the generation of a more immunosuppressive microenvironment [55].

4.2 Macrophages modulate cancer cell radioresistance

Irradiated macrophages can modulate tumor cell response to radiation, however cancer cells can also modulate the macrophages response to ionizing radiation. Indeed, our group demonstrated that irradiated macrophages induce apoptosis by promoting poly (ADP-ribose) polymerase (PARP) and caspase-3 cleavage in radiosensitive colorectal cancer cells, while protecting radioresistant cancer cell cells from death, by inhibiting apoptosis and upregulating the expression of glucose transporters [56]. Additionally, irradiated cancer cells were also able to modulate the macrophage phenotype. Radiosensitive and radioresistant cancer cell types were able to increase mRNA expression levels of the macrophage pro-inflammatory markers (*TNF-α*, *IL-6*, CC chemokine ligand (*CCL*)*2*, and CC chemokine receptor (*CCR*)*7*) and *CCL18*, an anti-inflammatory marker.

But only radiosensitive cancer cells evidenced an increased expression of IL-1β, a macrophage pro-inflammatory marker, and only radioresistant cancer cells enhanced the expression of two pro-inflammatory markers (CXC chemokine ligand (CXCL)8 and CD80), and the extracellular matrix proteoglycan versican (VCAN) and IL-10, anti-inflammatory markers [56].

In head and neck squamous cell carcinoma (HNSCC), it was also demonstrated that macrophages can modulate tumor radioresponse. The presence of human papillomavirus (HPV) infection is described to increase IL-6 secretion, which promotes macrophages polarization towards a pro-inflammatory phenotype, and stimulates radiation-induced DNA damage, contributing to HNSCC cells radiosensitivity. Thus, high levels of pro-inflammatory infiltrating macrophages were associated with the higher radiosensitivity of this tumor [57].

4.3 Macrophages modulate breast cancer radioresistance

In breast cancer, macrophages also interact with cancer cells modulating their response to radiotherapy. Depending on macrophage polarization, they can have a dual role on cancer cell radioresponse. While M1-polarized THP-1 macrophages promote radiosensitivity in BC cells, macrophages polarized towards an M2-like phenotype promote breast cancer cells resistance to ionizing irradiation [58]. This modulation can be useful for BC treatment, since the combination of radiotherapy with compounds that promote the macrophages polarization into a pro-inflammatory phenotype can increase cancer cell elimination. For example, it was already demonstrated that macrophages treatment with signal transducer and activator of transcription 6 (STAT6) inhibitor can reduce the expression of anti-inflammatory macrophage markers, reducing radioresistance of breast cancer cells [58].

Another potential target for immunotherapy in BC is the CD47 receptor. The expression of this marker in tumor cells inhibits their phagocytosis by macrophages. However, the treatment of radioresistant breast cancer cells with anti-CD47 antibody increases their phagocytosis by macrophages [42]. Therefore, CD47 could be an efficient immune target in breast cancer in combination with radiotherapy.

Radiotherapy can also increase the cell fusion between breast cancer cells and TAMs. The macrophage:breast cancer cells hybrids subject to irradiation have less DNA damage than maternal breast cancer cells, which demonstrates that hybrid cells have a better DNA-repair capacity and are more radioresistant than maternal cancer cells, showing that macrophage and tumor cell fusion could be an important factor in tumor heterogeneity and one cause of resistance to radiotherapy [59].

5. Three-Dimension models relevance on macrophages-cancer interaction

Due to the importance of macrophages in the tumor microenvironment, the role of these immune cells in BC has been widely studied. However, most studies are performed in two-dimension (2D) culture systems. In a 2D model, cells grow in monolayer adherent in plastic tissue culture plates. The main advantages of this model are simplicity, convenience, and reduced cost. Nevertheless, the complexity of the tumor architecture and of the interactions established between cancer cells and the tumor microenvironment elements are lost in such two-dimension models [60].

Otherwise, three-dimension (3D) culture systems can represent the architecture and the time-spatial organization of the different cellular populations and non-cellular elements within the tumor microenvironment. Thereby, 3D models are more realistic representations that better mimic the tumor elements found *in vivo* and allow to deduce the effectiveness of new therapies more precisely [60, 61]. Actually, there are several 3D models, as spheroids, hydrogel embedding, and scaffolds, that have different advantages, being used for distinct purposes. Spheroids are cancer cell aggregates that can be formed with liquid overlay technique, a simple method that uses low adherence surface systems to potentiate cancer cell aggregation, or by a hanging drop method. Importantly, nutrients, growth factors and oxygen availability in spheroids are not equal in all cells, creating proliferative, hypoxic and necrotic zones, which better illustrates the *in vivo* tumor characteristics. Moreover, the addition of different cell types present in the tumor microenvironment, such as macrophages, T cells and fibroblasts to spheroids will allow mimicking an *in vivo* tumor more closely [60, 61].

In 3D culture systems, the behavior of tumor cells, but also of immune cells, can change. Macrophages are very plastic cells and, depending on the microenvironment, can vary from a rounded cell shape to a prolonged protrusion morphology, rather than the characteristic 2D rounded and flat morphology [62]. In spheroids, the MDA-MB-231 TNBC cell line, express higher levels of proteins associated with epithelial-to-mesenchymal transition (EMT), explaining their increased ability to form metastasis, despite the lower growth rate. In 3D conditions, these cells are also more resistant to anti-tumor therapies [63], indicating that 3D models are more accurate to study breast cancer resistance to cancer treatments.

Interestingly, in an indirect 3D co-culture of BC cells with macrophages that uses Matrigel as a cell substrate, there was increased production of IL-1β and IL-8, cytokines, associated with tumor progression, and also of MMP-1, MMP-2 and MMP-10, related with tumor aggressiveness and metastasis. The microenvironment created in this model also

promotes monocytes chemoattraction, once monocyte chemoattractant protein-1 (MCP-1) and granulocyte colony-stimulating factor (G-CSF) were found in high levels in tumor monocultures and support breast cancer cell invasion [64, 65].

Furthermore, in a collagen system, the direct co-culture of these cells showed that macrophages displayed an intermediate phenotype with the overexpression of pro-inflammatory markers, such as IL-1β and TNF-α, but also of anti-inflammatory markers, such as CCL22, vascular-endothelial growth factor A (VEGFA), and prostaglandin-endoperoxide synthase 2 (PTGS2) [66]. Usually, in 3D systems, the co-culture of BC cells with macrophages induces an M2-like macrophage phenotype [67, 68], characterized by increased IL-10 secretion [67], which improves the development of tumor spheroids [67, 68].

In a 3D collagen model, macrophages conditioned media can also promote breast cancer cell invasion by increasing the tunneling nanotubes formation [69], or through lipocalin-2 (Lcn2) secretion, a molecule related to cancer poor prognosis, since it can promote tumor proliferation, survival and migration in BC [70]. On the other hand, breast cancer cells secrete soluble chemoattractant factors promoting macrophages the infiltration in the tumor microenvironment [71]. For instance, the production of CCL2 by TNBC cells promotes macrophage recruitment and its polarization towards an anti-inflammatory phenotype, leading to TNBC progression in an indirect co-culture collagen-based model [72].

3D models are also an important tool to evaluate therapeutic efficacy of new anti-tumor therapies, since the 3D organization can better mimic drug resistance compared to a monolayer culture. Indeed, in Matrigel cultures, the interaction of macrophages with breast cancer cells turns them more resistant to paclitaxel [67]. However, the treatment of these co-cultures, in a magnetic levitation model, with MSV-nAb-PTX (albumin-bound paclitaxel loaded into porous silicon multistage nanovectors) stimulates the switch of anti-inflammatory macrophages into a pro-inflammatory phenotype, enhancing macrophage motility. This effect induced tumor cell death, which in turn increases the release of pro-inflammatory cytokines that, further, increases the polarization of M1-like macrophages [73].

Furthermore, in a Matrigel model, the presence of macrophages in TNBC spheroids also confers drug resistance to doxorubicin and increases cell viability. However, the treatment with cetuximab-targeted gold nanorods (CTX-AuNR), plus near-infrared (NIR) irradiation, increases ROS production, decreasing tumor hypoxia that promotes the acquisition of a pro-inflammatory macrophage phenotype [74].

In recent years, the role of radiotherapy in the tumor microenvironment also began to be investigated in 3D culture systems. For example, Chan *et al.* used the hanging drop method to form spheroids with lung cancer cells, fibroblasts, endothelial cells and lung cancer stem cells under hypoxia conditions, to study the effect of cancer stem cells in radioresistance. With this model, they concluded that the treatment of this tumor with 5 Gy not only was unable to inhibit tumor growth when cancer stem cells were present, but also increased the expression of cytokines and factors associated with tumor aggressiveness, such as TGF-β, CCL5, vimentin and MMPs. Nevertheless, this behavior was changed when combined treatment of radiotherapy and cisplatin was applied [75].

Moreover, in a Matrigel 3D model, direct interaction between fibroblasts, an important component of the tumor microenvironment, and breast or prostate cancer cells, promoted tumor survival after irradiation, showing that fibroblasts can promote tumor radioresistance [76].

Considering all available data, three-dimension models are essential to better understand how the tumor microenvironment can modulate tumor response to anti-cancer treatments, especially in tumors with a worse prognosis. Therefore, it is essential to establish 3D biomimetic tumor-immune spheroids to highlight the role of TAMs in TNBC radioresponse.

II. AIM OF THE STUDY

Triple-negative breast cancer is the subtype with a worse prognosis, partially due to its aggressiveness, but mainly due to the lack of efficient target therapies. Furthermore, TNBC is one of the more resistant tumors to radiotherapy, urging the need to unveil the mechanisms underlying TNBC radioresistance. This strategy envisages the disclosure of alternative therapies to radiosensitise cancer cells and improve disease management of this poor prognostic tumor.

Macrophages are the most common immune cell population present in the breast cancer microenvironment and could promote the progression of cancer cells even after radiotherapy. For this reason, it is essential to design a 3D model to highlight the immune-mediated radioresistance mechanisms to identify possible targets for the development of more efficient therapeutic strategies that, in combination with radiotherapy, could improve TNBC patients outcome.

Therefore, the main aim of this project was to develop a biomimetic 3D model that gathers TNBC cells and human macrophages to mimic the tumor microenvironment response to radiotherapy in a closer way. Specifically, to achieve this general goal, this project intends to:

1) Establish tumor-immune spheroids with triple-negative breast cancer cells and human macrophages;

2) Characterize the tumor-immune spheroids regarding macrophages inflammatory profile and cancer cells immunogenicity;

3) Evaluate the impact of two radiotherapy schemes (2.67 Gy and 5.2 Gy) on tumor-immune spheroids morphology, diameter and apoptosis, and macrophages inflammatory profile and breast cancer cells immunogenicity.

III. MATERIALS AND METHODS

1. Cell Culture

The human MDA-MB-231 (ATCC-HTB26) TNBC cell line was purchased from the American Type Culture Collection - ATCC (USA) and genotyped to confirm cell authenticity. Cells, derived from a 51 years old Caucasian female, were routinely maintained in 25 cm^2 culture flasks at 37°C in a humidified incubator with 5% CO_2 and cultured in Dulbecco's Modified Eagle Medium (DMEM) with GlutaMax (Invitrogen) supplemented with 100 U/mL penicillin, 100 mg/mL streptomycin (Invitrogen) and 10% of heat inactivated fetal bovine serum (FBS) (Biowest).

2. Human monocytes isolation

Human monocytes were isolated from buffy coats from healthy blood donors, as previously described [77], kindly provided by the Immunohemotherapy Service, Centro Hospitalar Universitário São João (CHUSJ), Porto-Portugal. The use of these buffy coats was approved by CHUSJ Ethics Committee for Health (protocol 90/19), in agreement with the Helsinki declaration. Before blood donation, all subjects provided informed written consent.

Briefly, buffy coats were centrifuged at 1200g, without brake, during 30 min at room temperature (RT). The whitish peripheral blood mononuclear layer was then collected and incubated with RosetteSep-Human Monocyte Enrichment Cocktail (StemCell) for 20 min under rotation at RT, using a negative isolation procedure. Then, this mixture was diluted (1:1) in phosphate-buffered saline (PBS) 1X solution with 2% FBS, added over an equal volume of Histopaque-1077 (Sigma-Aldrich), and centrifuged at 1200g, without brake, during 30 min at RT. The monocyte enriched layer was then collected, washed and centrifuged 3 times at 1300rpm for 6 min at RT.

3. Macrophage differentiation and polarization

Isolated monocytes were resuspended in Roswell Park Memorial Institute (RPMI) 1640 (Invitrogen) or DMEM/F12 (Invitrogen) (1:1), supplemented with 10% FBS, 100 U/mL penicillin and 100 mg/mL streptomycin. Then, $1x10^6$ of monocytes per mL were seeded in 6-well plates and differentiated using 50 ng/mL of macrophage colony-stimulating factor (M-CSF) (Immunotools) for seven days. The plates were then maintained at 37°C in a humidified incubator with 5% CO_2. After seven days, the medium (1.2 mL/well) was replaced by fresh medium without M-CSF, allowing cell resting. Ten days after isolation,

macrophages were stimulated for 72 hours, with 10 ng/mL of LPS (Sigma-Aldrich) and 50 ng/mL of IFN-γ (Immunotools) for the acquisition of a pro-inflammatory phenotype, or with 10 ng/mL of IL-10 (Immunotools) for an anti-inflammatory phenotype.

4. Flow cytometry

Differentiated macrophages were detached with accutase (GRiSP) for 40 min at 37°C and harvested by gentle scraping. Macrophages were then washed with PBS 1X and resuspended in FACS buffer (PBS 1X, 2% FBS, 0.01% sodium azide), containing the appropriated conjugated antibodies, and stained in the dark for 40 min at 4°C. Macrophages were immunostained with the following antibodies: anti-human CD14-APC (Clone MEM-15), CD86-FITC (clone BU63) and CD40-FITC (clone HI40a) (Immunotools), CD163-PE (clone GHI/61) (BD Pharmingen), CD206-PE (clone 15-2) (Biolegend) and HLA-DR-Pacific Blue (clone L243) (Invitrogen). Following primary antibodies incubation, macrophages were washed with FACS buffer and centrifuged at 1500 rpm for 5 min. Then, these were stained with live/dead antibody (APC-Cy7) (eBioscience™ Fixable Viability Dye), in the dark at 4°C for 30 min to select live cells. Next, cells were washed and fixed with 2% paraformaldehyde (PFA) (VWR Chemicals BDH). Cell fluorescence was acquired on a FACS Canto Flow Cytometer (BD Biosciences) using FACS Diva Software. Data analysis was performed with FlowJo software (v10.7.2).

An example of gating strategy is shown (**Figure 9**). The percentage of cells expressing CD86, HLA-DR, CD163, CD206 and CD40 markers and their expression levels (mean fluorescence intensity, MFI) were evaluated in gated live cells. The negative population was superimposed with the unstained controls, and the MFI of stained samples was normalized to the MFI of unstaining controls, to minimize sample auto-fluorescence and the voltages of flow cytometer between different experiments.

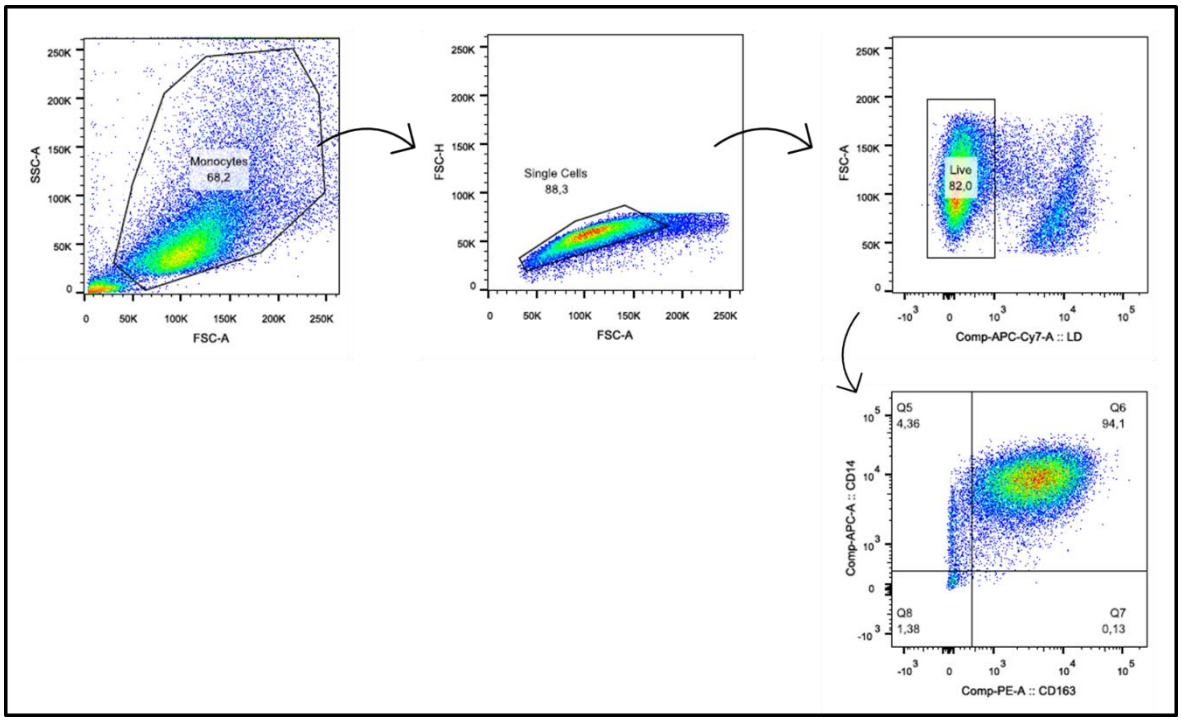

Figure 9- Example of the gating strategy used to select the different macrophage populations.

5. Tumor spheroids and tumor-immune spheroids formation

5.1. PolyHEMA coated plates

PolyHEMA solution was prepared by dissolving 3g of Poly(2-hydroxyethyl methacrylate) (Sigma-Aldrich) into 250 mL of 95% ethanol. The solution was left to dissolve in a hot plate (not above 50°C) for three days. Then, 50 µL of PolyHEMA solution was added into each well of a 96-well plate and 250 µL of the PolyHEMA solution was added into each well of a 24-well plate, as illustrated (**Figure 10A**). The plates were then incubated at 54°C in a non-CO_2 incubator until complete evaporation of the solvent. Next, MDA-MB-231 cells were seeded in the PolyHEMA coated plates at four different densities: 500, 1000, 1500, or 2000 cells/cm^2 in the presence of DMEM with high glucose (ATCC) medium, supplemented with 10% of FBS and 100 U/mL penicillin, 100 mg/mL streptomycin. Then, the plates were or not centrifugated at 180g for 5 min, to study the impact of centrifugation on spheroids formation. Plates were maintained at 37°C in a humidified incubator with 5% CO_2.

5.2. Agarose coated plates

MDA-MB-231 spheroids were formed with agarose coated plates, as previously described [78] and as illustrated (**Figure 10B**). Briefly, each flat bottom well of a 96-well plate was coated with 50 µL 1.5% (v/w) agarose (Lonza) dissolved in dH_2O. Then, MDA-MB-231 cells were seeded in agarose-coated plates at three different densities: 500, 1000, or 2500 cells/well and using two different media: DMEM and DMEM with high glucose. The plates were then maintained at 37°C in a humidified incubator with 5% CO_2. On day 1 and day 3, 50% of the medium was replaced.

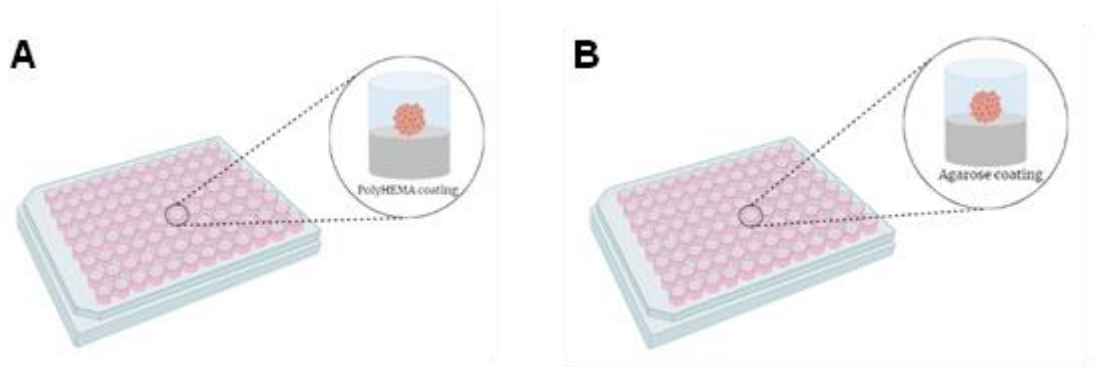

Figure 10- MDA-MB-231 cells seed in 96-well plates coated with A) PolyHEMA or B) 1.5% (w/v) agarose in dH_2O. Figure created with Biorender.

5.3. Agarose micro-molds

5.3.1. Tumor spheroid formation

MDA-MB-231 spheroids were formed with agarose micro-molds, as previously described [79] and as illustrated (**Figure 11**). Briefly, agarose micro-molds were formed by filling a 3D Petri Dish (MicroTissues Inc.) with 2% (w/v) agarose dissolved in 0.9% (w/v) chloride sodium (NaCl). Then, agarose micro-molds were placed in 12-well plates and 2 mL of DMEM/F12 (1:1) or DMEM with high glucose was added to each well, for at least 2 hours before cell seeding. Next, 190 µL of cell suspension containing 1000, 2500, or 5000 MDA-MB-231 cells was added to micro-mold/well. After 30 min, 2 mL of medium was added to each well. Culture plates were maintained at 37°C in a humidified incubator with 5% CO_2, monitored daily, and the medium was replaced every 2 days.

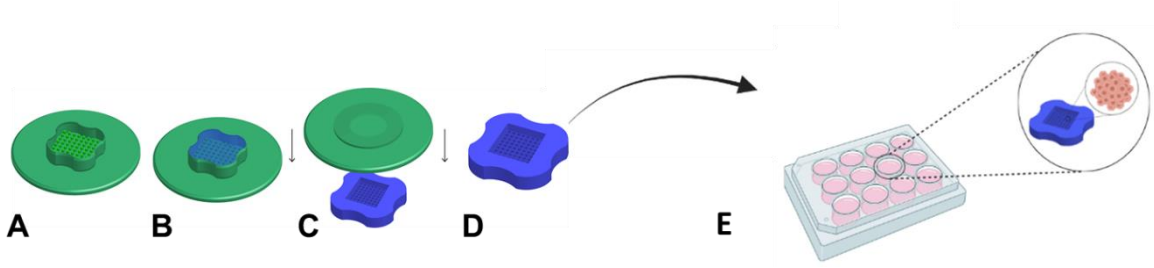

Figure 11- Agarose micro-molds and spheroids formation. A) 3D Petri Dish® micro-molds. **B)** Fill micro-mold with 2% (w/v) agarose in 0,9% (w/v) NaCl. **C)** Separate the gelled agarose from 3D Petri Dish® micro-mold. **D)** Agarose micro-mold is ready to use. **E)** Tumor cells seeded inside of the agarose micro-molds in a 12-well plate. Figure created with Adobe Illustrator and Biorender.

5.3.2. Tumor-immune spheroid formation

Tumor-immune spheroids were formed with agarose micro-molds as aforementioned. MDA-MB-231 cells were co-cultured with isolated human monocytes at four different ratios (MDA-MB-231:monocytes at 100:0, 50:50, 35:65, 25:75), and seeded in the micro-molds in a total of 5000 cells/well in 190 µL. After 30 min, 2 mL of DMEM/F12 supplemented with 50 ng/mL of M-CSF was added to each well to allow macrophage differentiation (**Supplementary Figure 1**). Culture plates were maintained at 37°C in a humidified incubator with 5% CO_2 and monitored daily.

6. Ionizing radiation exposure

The dosimetry plan was established, as previously described [20]. After three days of MDA-MB-231 spheroids (only cancer cells) and MDA-MB-231 tumor-immune spheroids (with cancer cells and monocytes), culture medium was replaced and spheroids were exposed to two different ionizing radiation schemes. A scheme of 2.67 Gy/fraction/day for one or five days (1 or 5 x 2.67 Gy), totalizing 13.35 Gy; or a scheme of 5.2 Gy/fraction/day for one or five days (1 or 5 x 5.2 Gy), totalizing 26 Gy. Control spheroids were not exposed to ionizing radiation, but were transported to the Radiotherapy Service of CHUSJ to avoid differences between irradiated and non-irradiated spheroids. Photon beam was produced by a PRIMUS (Siemens, Malvern, PA, USA) linear particle accelerator, used for human radiotherapy, operated at 18 MV at the Radiotherapy Service (**Figure 12**). To guarantee a uniform dose and avoid the build-up region of the 18 MV photon beam, 5 water plates were placed above and below the 12-well plates during irradiation. Following experiments were carried out 24 hours after the first fraction and 24 hours after the fifth fraction of ionizing radiation (**Figure 13**).

Figure 12- MDA-MB-231 spheroids and tumor-immune spheroids irradiation on PRIMUS linear particle accelerator at the Radiotherapy Service of CHUSJ.

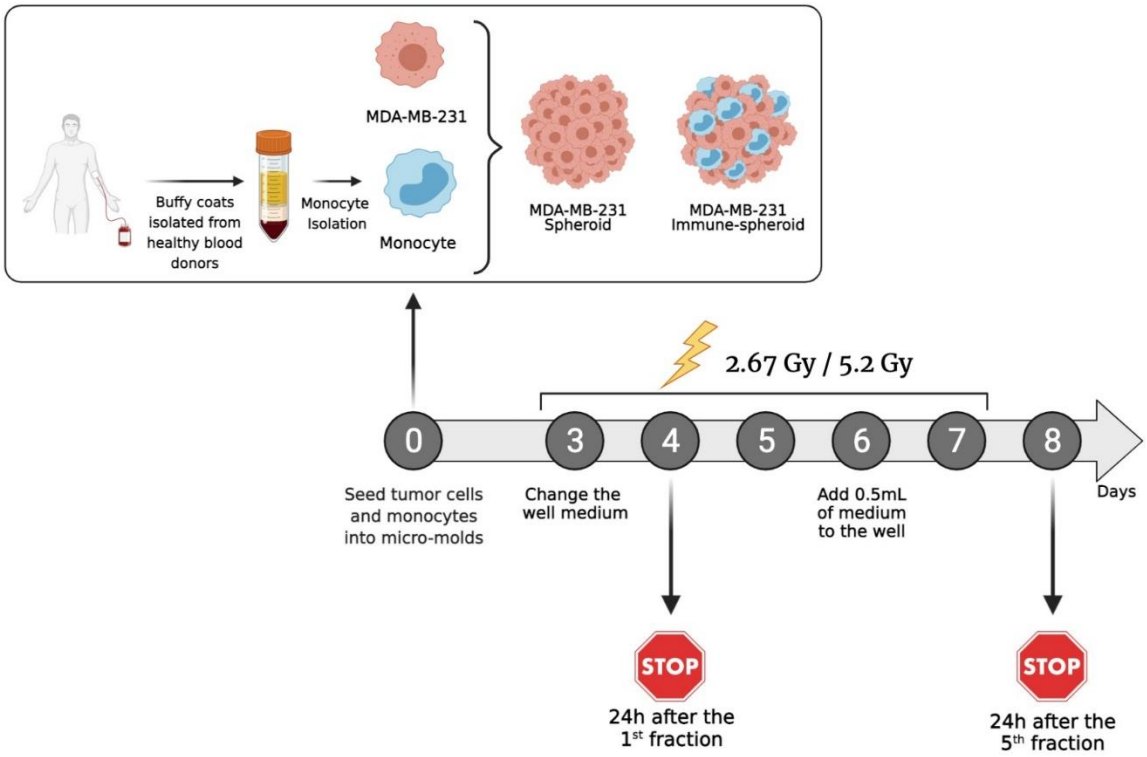

Figure 13- Schematic overview of the methodology used in this project. On day 0, MDA-MB-231 cancer cells were co-cultured or not with human monocytes isolated from healthy blood donors buffy coats to form MDA-MB-231 spheroids and tumor-immune spheroids. After 3 days, spheroids and tumor-immune spheroids were submitted to 2.67 Gy or 5.2 Gy during one or five consecutive five days. Spheroids and tumor-immune spheroids not irradiated were used as control. The characterization of tumor spheroids and tumor-immune spheroids was performed 24 hours after the first fraction, and 24 hours after the fifth fraction of ionizing radiation. Figure created with Biorender.

7. Tumor spheroids and tumor-immune spheroids characterization

7.1. Size measurement

At days 3, 4, and 8, images of tumor spheroids and tumor-immune spheroids were taken using a brightfield microscope (Leica DMi1 Inverted Microscopes, Leica Microsystems) and the size was determined by measuring the diameter using the ImageJ software. The size of each tumor spheroid and tumor-immune spheroid was measured by performing the two diameters mean and, for each condition, the diameter was measured in twelve different tumor spheroids and tumor-immune spheroids.

7.2. Immunophenotyping

The macrophages profile and the MDA-MB-231 immunogenicity in tumor spheroids and tumor-immune spheroids were assessed by flow cytometry. Briefly, tumor spheroids and tumor-immune spheroids were collected from the agarose micro-molds and dissociated into a single cell suspension with accutase. After 20 min at 37°C of incubation with accutase, cells were resuspended in FACS buffer. After one wash step, cells were resuspended in FACS buffer containing the appropriated conjugated antibodies and the staining was performed in the dark at 4°C for 40 min. Followed by a wash step with FACS buffer, and centrifugation at 1500 rpm for 5 min, the cells were stained with live/dead antibody (APC-Cy7) in the dark at 4°C for 30 min. Then, cells were washed and fixed with 2% PFA. Cell fluorescence was acquired on a FACS Canto Flow Cytometer using FACS Diva Software. Data analysis was performed with FlowJo software (v10.7.2).

The antibodies used were: anti-human CD14-APC (Clone MEM-15), CD86-FITC (clone BU63), HLA-DR-FITC (clone HI43) (Immunotools), CD163-PE (clone GHI/61) (BD Pharmingen), CD206-PE (clone 15-2), CD14-Pacific Blue (Clone 65D3) (Biolegend), HLA-ABC-PE (clone W6/32), CD47-FITC (clone MEM-122) (Immunotools), PD-1-PerCP-Cy5.5 antibody (clone EH12.1) (BD Pharmingen), PD-L1-FITC (clone MIH1) (BD Pharmingen) and CD40-PE (clone HI40a) (Immunotools).

An example of gating strategy is shown (**Figure 14**). Macrophages were selected as $CD14^+$, while MDA-MB-231 as $CD14^-$ cells. Live cells were selected inside of each single population. The percentage of cells expressing CD86, HLA-DR, CD163, CD206, CD40 and PD-L1 markers, and their expression levels (MFI), were evaluated in live/$CD14^+$ cells. Accordingly, the percentage of cells expressing CD47, HLA-ABC, CD40, PD-1 and PD-L1 markers, and their MFI, were assessed in live/$CD14^-$ cells. Specifically, the negative population was superimposed with the unstained controls, and the MFI of staining samples

was normalized to MFI of unstaining control, to minimize the auto-fluorescence of the samples and the voltages of flow cytometer between different experiments.

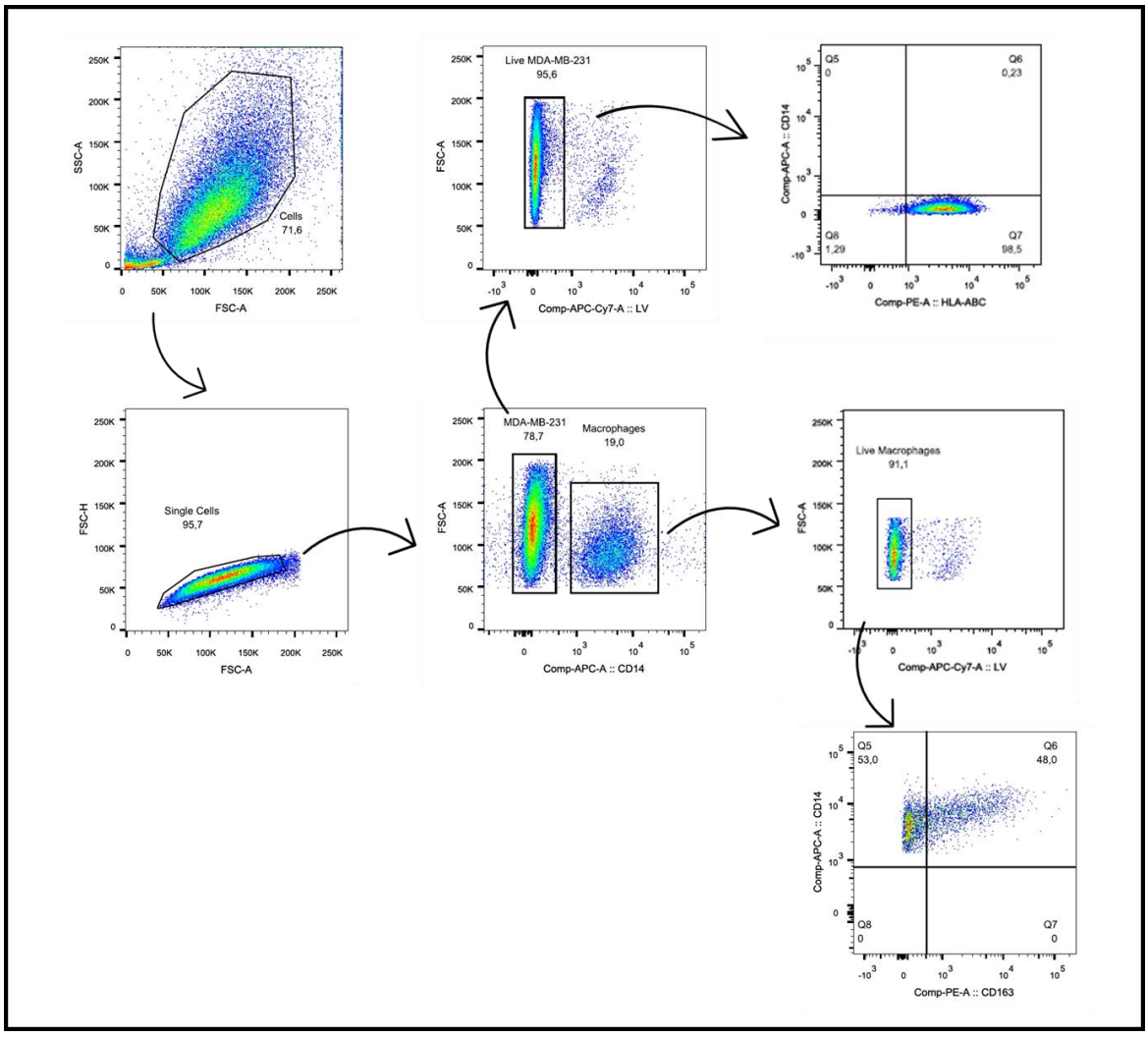

Figure 14- Example of gating strategy used to select the cell populations.

7.3. Apoptosis

The effect of radiotherapy on cell apoptosis was evaluated with the Annexin V/ Propidium Iodide (PI) staining. After tumor spheroid and tumor-immune spheroid dissociation, cells were washed twice with PBS 1X and then with Annexin V Binding Buffer (1X). Cells were incubated with 2 µL of Annexin V-FITC (Immunotools) and 5 µL of Propidium iodide (PI) (BD Biosciences) for 15 min at 4˚C in dark. The cell fluorescence was acquired on a FACS Canto Flow Cytometer using FACS Diva Software. Data analysis was performed with FlowJo software (v10.7.2).

An example of a gating strategy is shown (**Figure 15**). Unstained cells and single staining with antibodies were used as controls, and cells treated with H_2O_2 were used as a positive control to define the percentage of cells in early (Annexin V^+) and late apoptosis (Annexin V^+/PI^+).

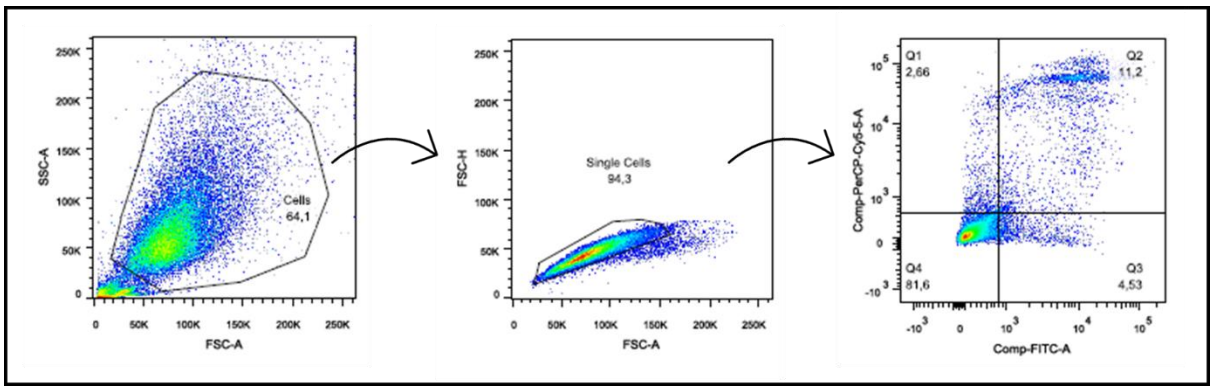

Figure 15- Example of gating strategy used to identify apoptotic cells.

7.4. Secretory profile

Cytokine levels, namely of IL-6, IL-10, IL12/IL-23(p40), TNF-α, TGF-β1 free active (BioLegend), and CCL18 (Abcam), were determined by enzyme-linked immunosorbent assay (ELISA) in the conditioned media of irradiated or non-irradiated MDA-MB-231 spheroids and tumor-immune spheroids, according to manufacturer's instructions. Briefly, for IL-6, IL-10, IL12/IL-23(p40), and TNF-α, 96-well plates were coated with the respective capture antibody and incubated overnight at 4°C. Then the plate was blocked with Assay Diluent A (1X) for 1 hour and 100 µL of conditioned media was added to the wells and incubated for 2 hours. Soluble proteins bound to the capture antibody were detected using a detection antibody for 1 hour, followed by an avidin-HRP conjugated solution for 30 min. Finally, plates were incubated with TMB substrate solution for 15 min, resulting in color change, being the intensity proportional to the amount of antigen captured. Absorbance was read at 450 and 570 nm. Cytokine levels were determined by plotting values on a standard curve.

To evaluate the secreted CCL18 protein levels, 100 µL of the conditioned media and the capture and detector antibodies were added to a pre-coated 96-well plate and incubated for 1 hour. Then, plates were incubated with TMB Substrate solution for 10 min and the absorbance was read at 450 nm. CCL18 levels were determined by plotting values on a standard curve.

TGF-β1 free active levels were also assessed. Briefly, 50 µL of the conditioned were added to 96-well plates pre-coated with anti-TGF-β1 antibody and incubated for 2 hours.

Soluble proteins bound to the capture antibody were detected using a detection antibody for 1 hour, followed by an avidin-HRP conjugated solution for 30 min. Finally, the addition of substrate F and absorbance was read at 450 and 570 nm. TGF-β1 levels were determined by plotting values on a standard curve.

8. Statistical analysis

Results are expressed as means ± standard deviation (SD). Data was analyzed with Shapiro-Wilk normality test. To compare between three or more groups samples were analyzed with two-way ANOVA, followed by Tukey multiple comparisons test, or with Friedman test. The comparations that involve only two groups were analyzed with unpaired t-test or with Mann-Whitney test. P-values lower than 0.05 were considered to indicate significant differences. Statistical analyses were performed using GraphPad Prism Software v9 (San Diego, CA) and with IBM SPSS software (Version 27, Chicago, IL). All graphs were performed with GraphPad Prism Software v9.

IV. RESULTS

1. Optimization of tumor spheroids formation

To establish a 3D TNBC model that more accurately represents the tumor microenvironment, we have selected the MDA-MB-231, a human TNBC cell line, and different experimental approaches.

Initially, cell culture plates were coated with a non-adherent component, PolyHEMA, which favors cell-cell interaction in detriment of cell-matrix adhesion, promoting the spontaneous formation of 3D structures, and tested different cellular densities. However, no tumor spheroids were formed using coated PolyHEMA plates (data not shown).

Alternatively, we decided to use agarose coated plates, another non-adherent component, as previously described by Saraiva *et al.* [78], seeding the cells at three different densities (500, 1000 and 2500 cells/well). Since the culture media can have a great impact on cell survival in 3D structures, we also tested two different media (DMEM and DMEM high glucose). Using this strategy, the MDA-MB-231 spheroids formation was successful in all conditions. However, these tumor spheroids were very heterogeneous and, at day 5, the spheroid dispersion regarding size and compactness was clearly visible (**Figure 16**).

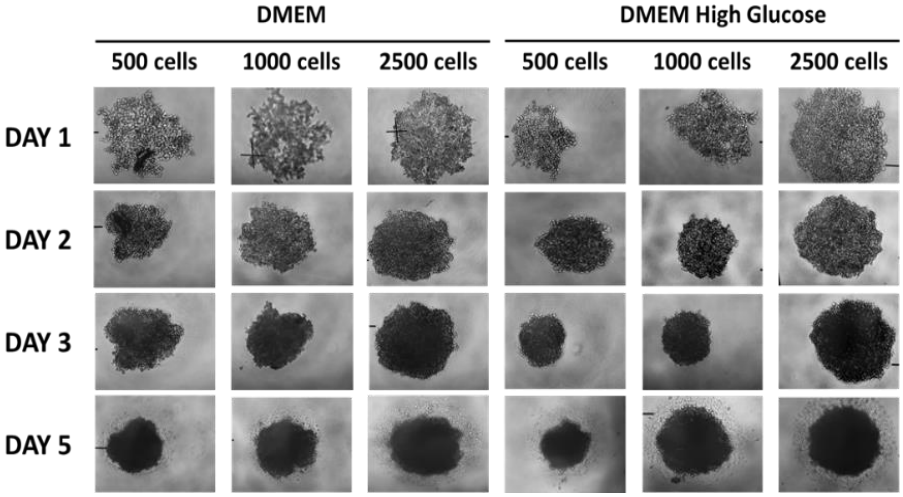

Figure 16- MDA-MB-231 spheroids formation on agarose coated plates. Tumor spheroids formation and culture morphology were monitored along 5 days in DMEM media with distinct glucose concentrations (DMEM and DMEM high glucose).

To overcome the heterogeneity observed in spheroids formed in agarose coated plates, TNBC spheroids were then formed using agarose micro-molds for scaffolds preparation, as previously described by our collaborators (Bauleth-Ramos T and Sarmento B) [21]. Three different cellular densities were tested: 1000, 2500 and 5000 cells per spheroid, using DMEM/F12 and DMEM high glucose media, since our previous data (Peirsman *et al*, in press) suggested DMEM/F12 as optimal media for tumor spheroid

formation as compared to DMEM. Using this strategy, MDA-MB-231 spheroids were already formed after 3 days of culture (**Figure 17**). This methodology allowed us to create, with a very high reproducibility, 81 homogenous spheroids from a single micro-mold.

Since we were planning to perform our irradiation experiments in the period of one week, the cells viability was evaluated at day 7. High cell viability (85.6-94.5%) was observed in all conditions (**Figure 18**), leading us to select the condition of 5000 cells per spheroid in DMEM/F12 for further experiments, since both media had similar effects. Considering that, in subsequent experiments, high glucose can mask radiotherapy induced death, we decided to use DMEM/F12 in all subsequent experiments.

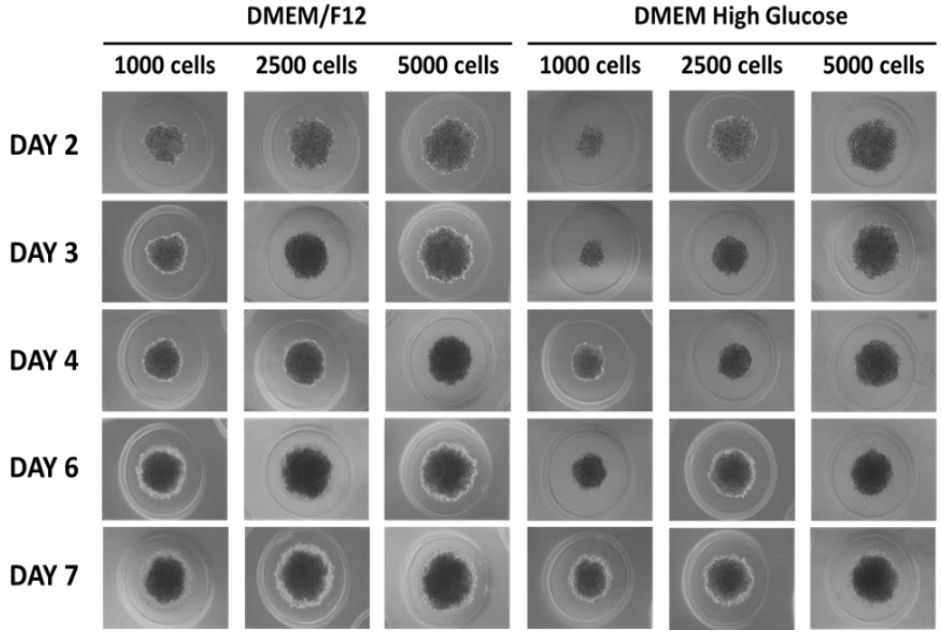

Figure 17- Tumor spheroids formation on agarose micro-molds. Tumor spheroids formation and culture morphology were monitored along 7 days in two distinct media (DMEM/F12 and DMEM high glucose) and using initial different cell densities (1000, 2500 and 5000 cells).

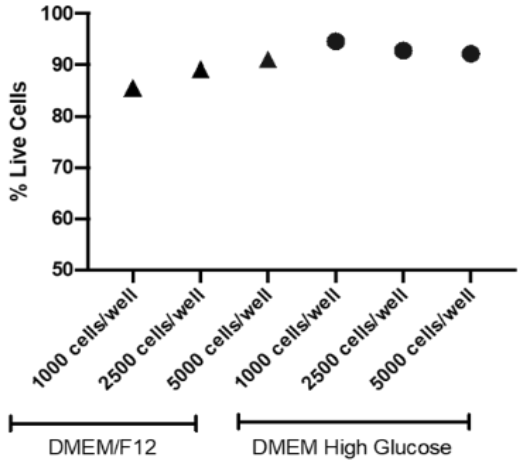

Figure 18- Percentage of MDA-MB-231 live cells at day 7, as evaluated by live/dead staining through flow cytometry on MDA-MB-231 spheroids formed at distinct cell densities (1000, 2500 and 5000 cells/well) in distinct media (DMEM/F12 and DMEM high glucose).

2. The effect of medium on macrophage polarization

It is well established that macrophages may polarize towards a pro- or an anti-inflammatory phenotype, depending on the external stimuli that they are exposed to [35, 46]. Therefore, before establishing tumor-immune spheroids, we evaluated whether DMEM/F12 medium composition, chosen in previous experiments, would have an impact on macrophage polarization upon proper exogenous stimulation. For that, the polarization of macrophages cultured in DMEM/F12 media was compared with the polarization of macrophages cultured in RPMI1640 medium, the most frequently medium used on macrophage cultures. Polarization profile was evaluated upon 72 hours of stimuli exposure through flow cytometry to assess the expression of specific macrophage cell surface receptors.

In DMEM/F12, macrophages stimulated for 72h with LPS (10 ng/mL) and IFN-γ (50 ng/mL), pro-inflammatory stimuli, displayed higher levels of the pro-inflammatory markers CD86, a T-cell co-stimulatory receptor, CD40, another co-stimulatory receptor sign of macrophage activation, and HLA-DR, an major histocompatibility complex (MHC)-II engaged of antigen presentation (**Figure 19**). In contrast, macrophages stimulated with IL-10 (10 ng/mL), an anti-inflammatory stimulus, expressed higher levels of the anti-inflammatory markers the scavenger receptor CD163 and the mannose receptor CD206 (**Figure 20**). Results with RPMI1640 were similarly observed, which allowed us to conclude that DMEM/F12 medium has no major impact on macrophage polarization and was, therefore, selected for further experiments.

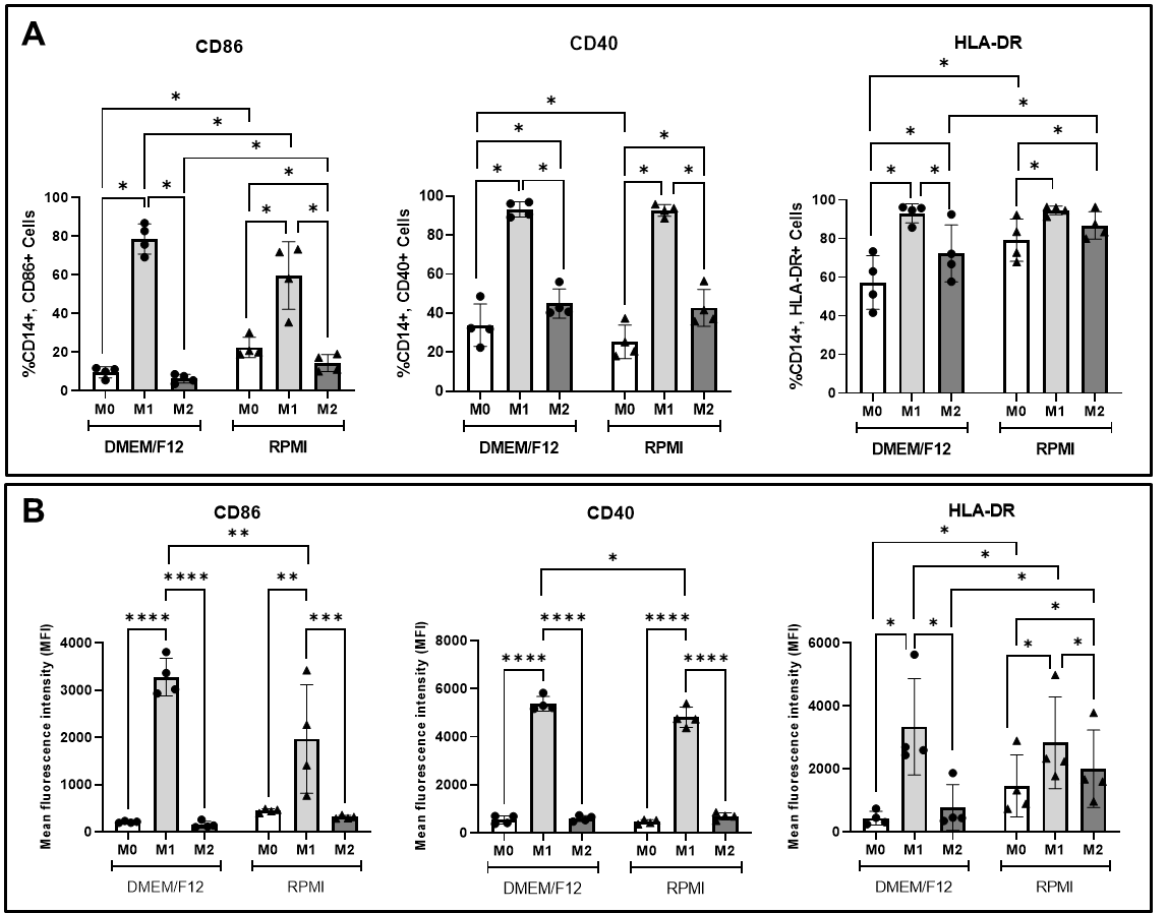

Figure 19- The impact of the media on macrophage polarization: pro-inflammatory markers. Human monocytes were differentiated into macrophages during 7 days. Ten days after isolation, macrophages were stimulated for 72 hours, with 10 ng/mL of LPS and 50 ng/mL of IFN-γ for a pro-inflammatory phenotype (M1), or with 10 ng/mL of IL-10 for an anti-inflammatory phenotype (M2). Unstimulated macrophages were used as control (M0). The results of DMEM/F12 were compared to those of RPMI1640 medium. **A)** Percentage of pro-inflammatory markers (CD86, CD40, and HLA-DR) in live $CD14^+$ cells, evaluated by flow cytometry. **B)** Mean fluorescence intensity of pro-inflammatory markers (CD86, CD40, and HLA-DR) in live $CD14^+$ cells, assessed by flow cytometry. The results represent the mean ± SD of analysis performed with macrophages derived from 4 distinct health blood donors (n=4). Each dot represents a different donor (n). Samples were analyzed with two-way ANOVA, followed by Tukey multiple comparisons test or with Friedman test. Statistical significance indicated with *p<0.05, **p<0.01, ****p<0.0001.

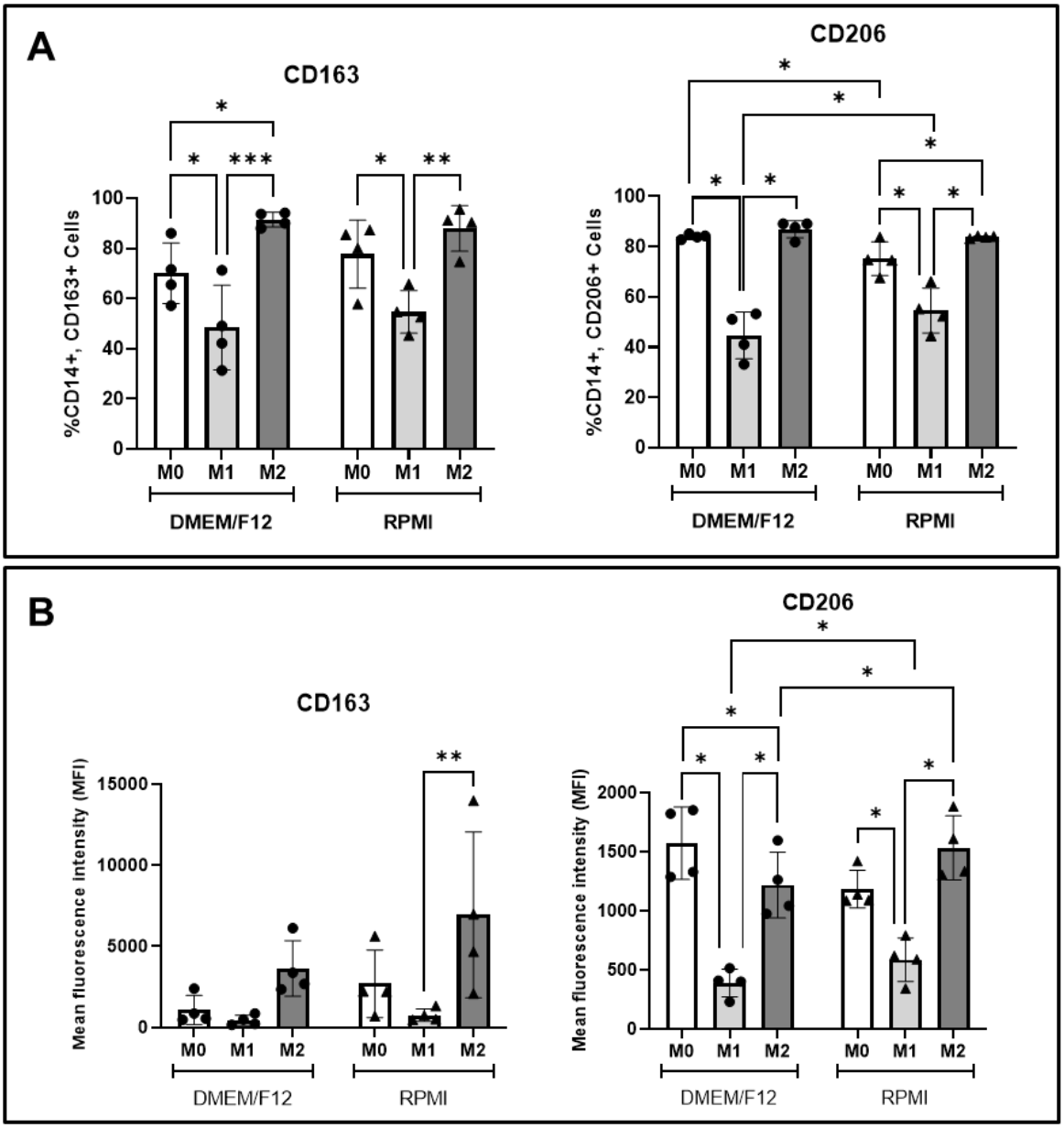

Figure 20- The impact of the media on macrophage polarization: anti-inflammatory markers. Human monocytes were differentiated into macrophages during 7 days. Ten days after isolation, macrophages were stimulated for 72 hours, with 10 ng/mL of LPS and 50 ng/mL of IFN-γ for a pro-inflammatory phenotype (M1), or with 10 ng/mL of IL-10 for an anti-inflammatory phenotype (M2). Unstimulated macrophages were used as control (M0). The results of DMEM/F12 were compared to those of RPMI1640 medium. **A)** Percentage of anti-inflammatory markers (CD163 and CD206) in live $CD14^+$ cells, evaluated by flow cytometry. **B)** Mean fluorescence intensity of anti-inflammatory markers (CD163 and CD206) in live $CD14^+$ cells, determined by flow cytometry. The results represent the mean ± SD of analysis performed with macrophages derived from 4 distinct health blood donors (n=4). Each dot represents a different donor (n). Samples were analyzed with two-way ANOVA, followed by Tukey multiple comparisons test or with Friedman test. Statistical significance indicated with *p<0.05, **p<0.01, ***p<0.001.

3. Tumor-immune spheroids formation

In both primary and metastatic niches, macrophages may represent up to 50% of all components within the tumor mass [38, 46] and, therefore, its inclusion in this 3D model is essential to mimic more closely the breast cancer microenvironment.

Considering our previous optimization results, tumor-immune spheroids were established co-culturing MDA-MB-231 cells and human monocytes, isolated from healthy blood donors buffy coats, in a total of 5000 cells per spheroid, in DMEM/F12 medium. Therefore, human monocytes and tumor cells were co-cultured at four different MDA-MB-231:monocyte ratios (100:0, 50:50, 35:65, and 25:75), since cancer cells replicate very fast, while monocytes do not proliferate so much *in vitro*.

At day 3, as expected, tumor-immune spheroids formation was already observed. However, these spheroids seem less homogeneous than tumor spheroids, since not all monocytes adhered to the spheroid structure (**Figure 21**).

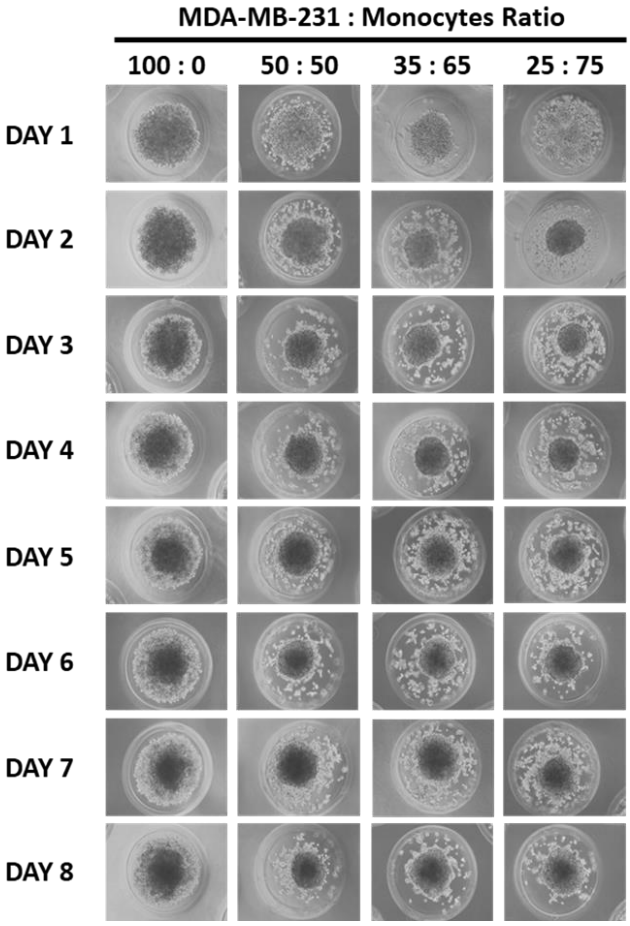

Figure 21- Tumor-immune spheroids formation on agarose micro-molds. Spheroids formation and morphology were monitored along 8 days, exploring distinct breast cancer cells:monocytes ratio (100:0; 50:50; 35:65 and 25:75).

Considering the morphology of the different tumor-immune spheroids, the initial ratio of 35:65 (MDA-MB-231:monocyte) was chosen to carry out all future experiments (**Supplementary Figure 2**). Moreover, the day 3 was selected as the starting point of irradiation, since both tumor spheroids (100:0) and tumor-immune spheroids (35:65) are already formed at this timepoint.

4. Tumor spheroids and tumor-immune spheroids characterization

Prior irradiation exposure, tumor spheroids and tumor-immune spheroids were characterized regarding their morphology, diameter and cellular components composition. In addition, characterization of macrophage inflammatory profile in the tumor-immune spheroid and the cancer cell immunogenicity in MDA-MB-231 spheroids and in tumor-immune spheroids were also performed on day 3.

As depicted in **Figure 22A**, tumor-immune spheroids are more compact than tumor spheroids at day 3. Additionally, tumor-immune spheroids are significantly smaller than tumor spheroids as the diameter decreases from 492.1 ± 43.75 µm to 328.8 ± 24.55 µm in the presence of macrophages (**Figure 22B**).

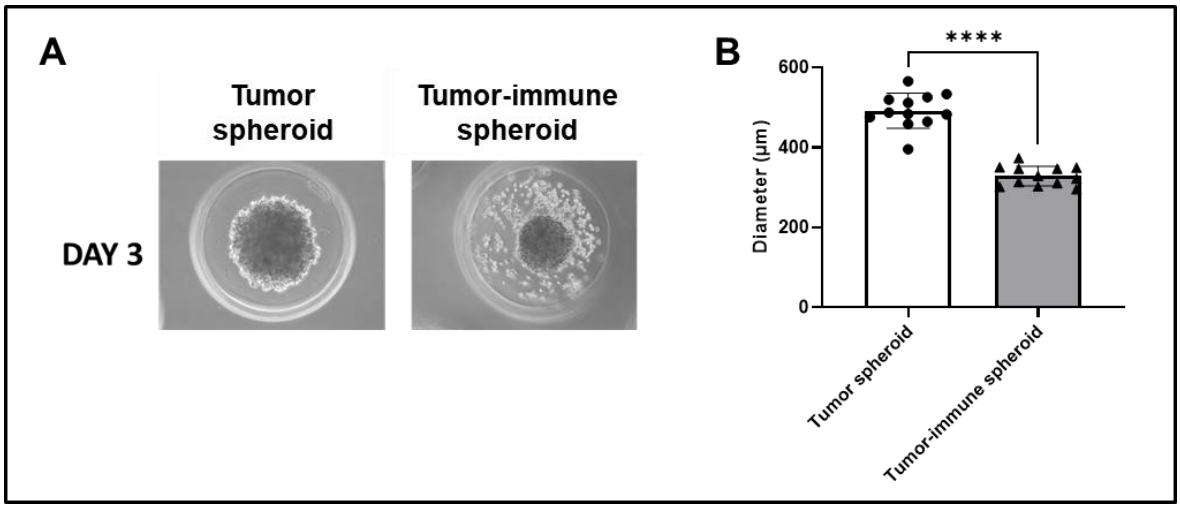

Figure 22- Tumor spheroid and tumor-immune spheroid characterization at day 3 of co-culture. A) MDA-MB-231 tumor spheroid and tumor-immune spheroid (MDA-MB-231 cells and human macrophages) morphology, as illustrated by brightfield microscopy. **B)** Tumor spheroid and tumor-immune spheroid diameter (n=12) determined with ImageJ Software. The results represent the mean ± SD. Each dot represents a different independent experiment (n). Samples were analyzed with unpaired t-test. Statistical significance indicated with ****p<0.0001.

To assess, prior irradiation, the tumor-immune spheroids composition regarding the distinct cellular components, spheroids were dissociated, and the percentage of each cell population was analyzed by flow cytometry. Macrophages were identified as $CD14^+$ cells, while MDA-MB-231 cells as $CD14^-$ cells, since these cells do not express this macrophage lineage marker. On day 3, macrophages represent approximately 20.15% of the whole tumor-immune spheroid cell population (**Figure 23A**), and approximately 84.55% of these macrophages remained alive (**Figure 23B**). Notably, no significant differences on TNBC cells ($CD14^-$ population) viability was found between tumor spheroid and tumor-immune spheroids, with approximately 91% of live cells in both conditions (**Figure 23C**). These results suggest that short-time 3D cultures of MDA-MB-231 with macrophages do not affect cancer cell viability.

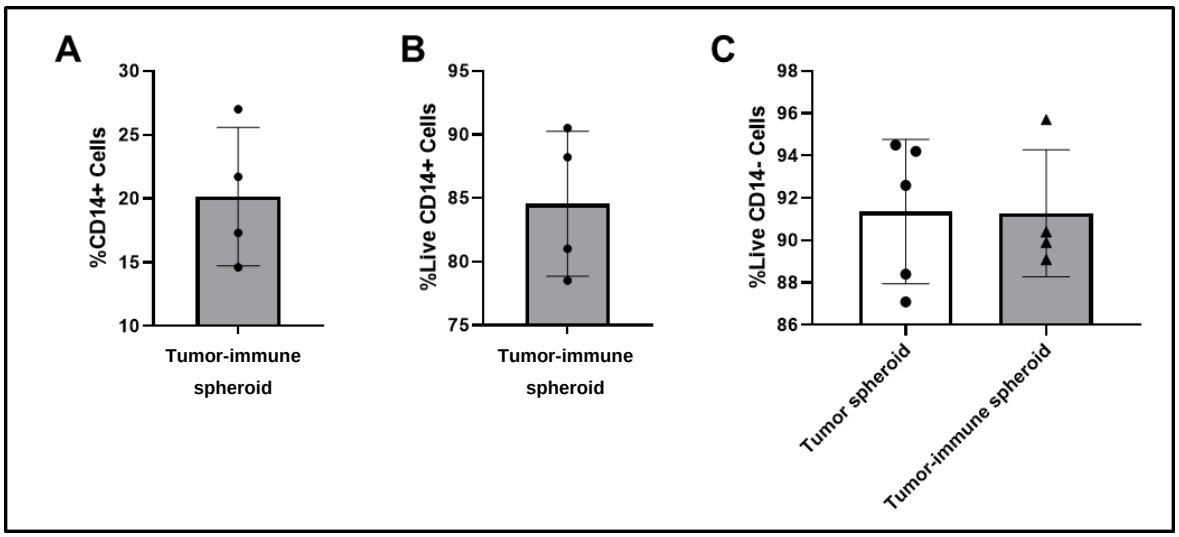

Figure 23- MDA-MB-231 and macrophages characterization at day 3. A) Percentage of $CD14^+$ cells in tumor-immune spheroid evaluated by flow cytometry (n=4). **B)** Percentage of live $CD14^+$ cells in tumor-immune spheroid (n=4) measured by live/dead staining through flow cytometry. **C)** Percentage of live $CD14^-$ cells in tumor spheroids (n=5) and tumor-immune spheroids (n=4) assessed by live/dead staining through flow cytometry. The results represent the mean ± SD. Each dot represents a different independent experiment (n). Samples were analyzed with unpaired t-test.

4.1 In tumor-immune spheroids, macrophages have an intermediate phenotype

It is well known that cancer cells can modulate macrophages towards an immunosuppressive phenotype. Thus, to characterize the macrophage inflammatory profile on tumor-immune spheroids, pro-inflammatory markers, such as CD86, HLA-DR (MHC-II) and CD40, and the anti-inflammatory markers, namely CD163 and CD206, as well as the immune checkpoint PD-L1 marker, were evaluated by flow cytometry on day 3, prior ionizing radiation exposure.

In tumor-immune spheroids, a high percentage of macrophages expressing the pro-inflammatory marker CD40 (99.35% ± 0.35) and the anti-inflammatory marker CD206 (86.85% ± 4.12) was found (**Figure 24**), suggesting that macrophages have an intermediate phenotype. The mean fluorescence intensity (MFI) for both markers was higher than for the other macrophage surface receptors. A considerable percentage of macrophages expressing CD86 (29.03% ± 10.77), HLA-DR (57.80% ± 17.62), and CD163 (39.53% ± 13.53) were also found (**Figure 24**). Furthermore, at this time point, the expression of PD-L1 by macrophages was very low (1.42% ± 0.63) (**Figure 24**).

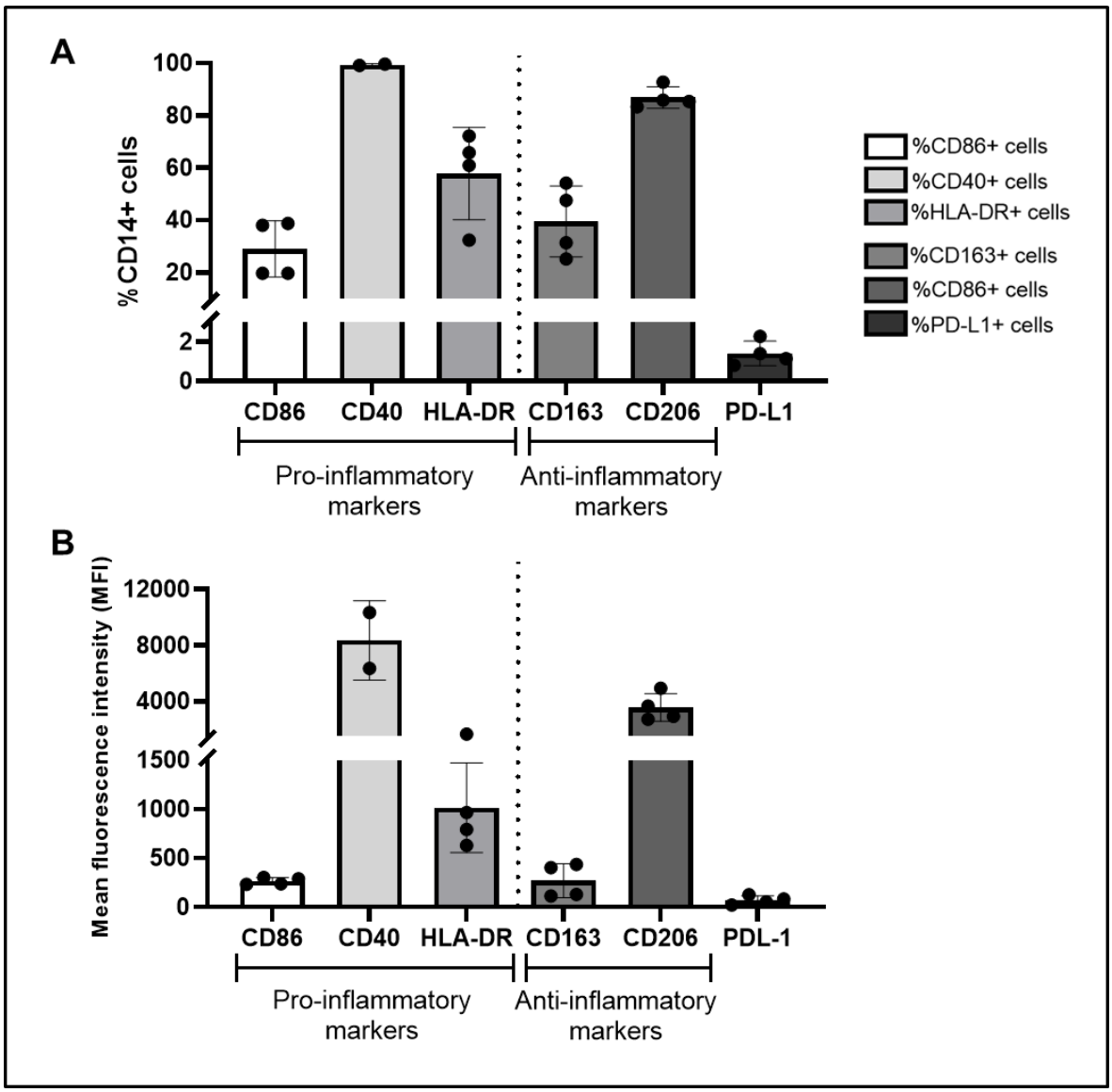

Figure 24- Macrophages inflammatory profile in tumor-immune spheroids: pro- and anti-inflammatory markers. **A)** Percentage and **B)** Mean fluorescence intensity of pro-inflammatory (CD86, CD40 and HLA-DR), anti-inflammatory markers (CD163 and CD206) and PD-L1 in live $CD14^+$ cells determined by flow cytometry. The results represent the mean ± SD (n≥2). Each dot represents a different independent experiment (n).

4.2 Macrophages modulate cancer cells immunogenic phenotype

To infer the impact of macrophages on cancer cell immunogenic profile, tumor spheroids and tumor-immune spheroids were dissociated, and the expression of specific cell surface receptors was investigated by flow cytometry on day 3, prior ionizing irradiation exposure.

Interestingly, we observed that at both tumor spheroids and tumor-immune spheroids MDA-MB-231 cancer cells expressed a high percentage of HLA-ABC, a molecule involved in direct antigen presentation (87.72% ± 21.00 in tumor spheroids and 97.43% ± 1.56 in tumor-immune spheroids), and CD40, a member of the tumor necrosis factor receptor family (96.13% ± 0.42 in tumor spheroids and 97.60% ± 0.00 in tumor-immune spheroids), with a tendency to increase their expression levels in co-culture with macrophages (**Figure 25**). While few MDA-MB-231 cells express the CD47 receptor, a molecule involved in *"don't eat me"* signals impairing phagocytosis by macrophages, the number of cells expressing CD47 and the intensity of expression per cell increased slightly in tumor-immune spheroids. These results suggest that in co-culture with macrophages, cancer cells may try to impair their recognition and digestion by the phagocytes.

The expression of PD-1 and PD-L1, immune checkpoint molecules, was also evaluated. Interestingly, MDA-MB-231 cells tend to express higher PD-1 levels and lower PD-L1 levels when in contact with macrophages, however the number of cells expressing PD-1 and PD-L1 is still very low to make robust considerations (**Figure 25**).

Altogether, these results suggested that, at this short time of 3D co-cultures with macrophages, cancer cells have the tendency to change their immunogenic phenotype, in particularly, regarding CD40 expression.

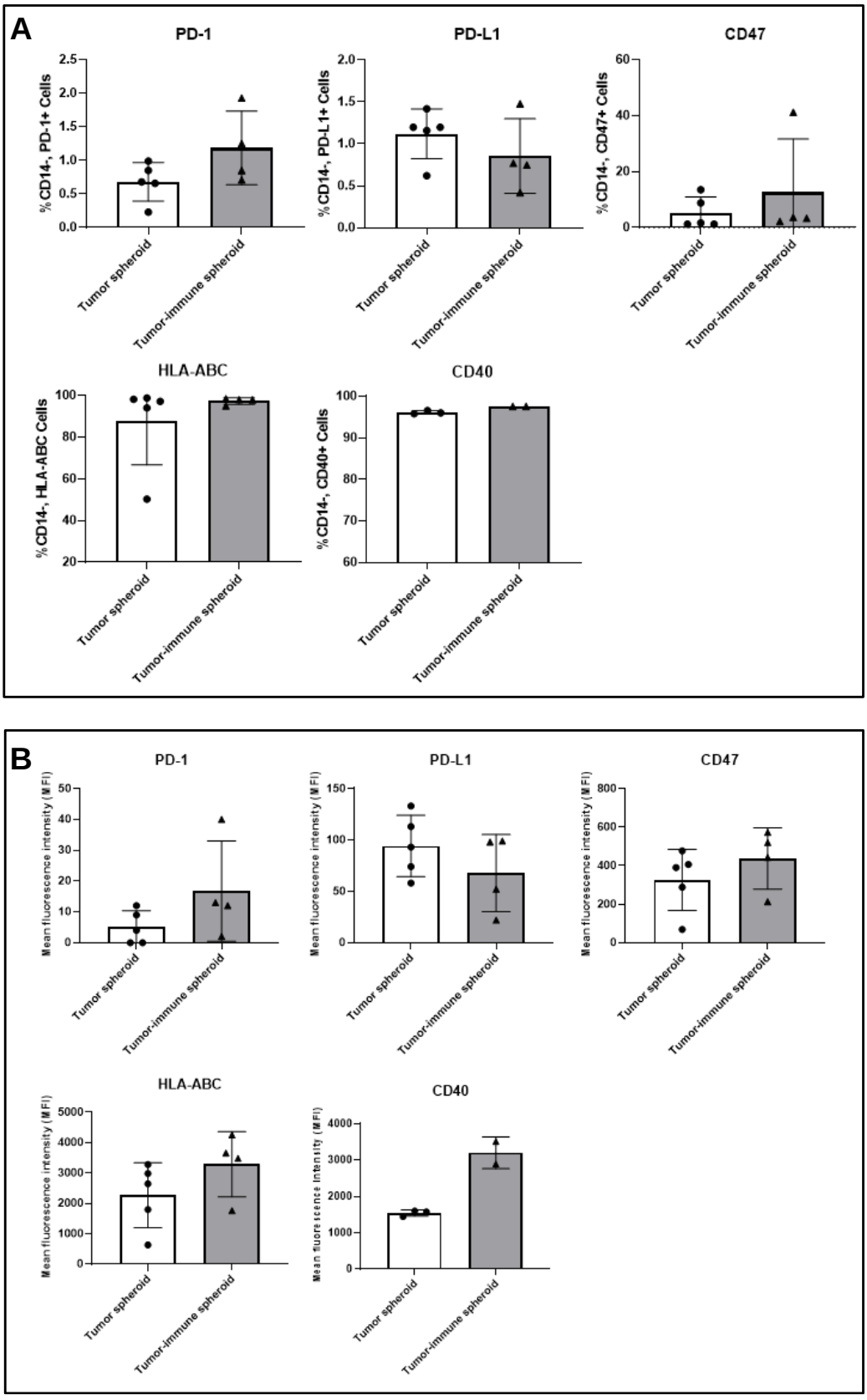

Figure 25- MDA-MB-231 immunogenicity in both tumor spheroid and tumor-immune spheroid. **A)** Percentage and **B)** Mean fluorescence intensity of PD-1, PD-L1, CD47, HLA-ABC, and CD40 in live $CD14^-$ cells, determined by flow cytometry. The results represent the mean ± SD (n≥3). Each dot represents a different independent experiment (n). Samples were analyzed with unpaired t-test or with Mann-Whitney test.

5. The effect of ionizing irradiation on tumor spheroids and tumor-immune spheroids

Since TNBC has no approved target therapy, radiotherapy is one of the standard treatments. However, not all patients with TNBC respond to this specific treatment and several patients may still relapse [9, 13]. It is known that immune cells, including macrophages, play an important role on cancer cell response to radiotherapy [56]. Therefore, to highlight this effect on 3D cultures, and to further dissect the underlying molecular mechanisms, established tumor spheroids and tumor-immune spheroids were exposed to two different radiotherapy schemes, routinely used in the clinical practice [24, 25].

Therefore, on day 3 of spheroid formation, MDA-MB-231 spheroids and tumor-immune spheroids were submitted to 2.67 Gy (mimicking long radiotherapy scheme) or to 5.2 Gy (mimicking short radiotherapy scheme) for one or five days. Non-irradiated tumor spheroids and tumor-immune spheroids were used as control. Spheroids diameter measurement, macrophage inflammatory profile and immunogenicity of cancer cell characterization were performed 24 hours after the first and the fifth fraction of radiotherapy.

The **Figure 26A** depicts the morphology of tumor spheroids and tumor-immune spheroids upon one and five fractions of ionizing radiation exposure, as well as of non-irradiated tumor spheroids and tumor-immune spheroids, at the same time points. After the first irradiation, tumor-immune spheroids diameter was significantly smaller than tumor spheroids in non or irradiated conditions, independently of the radiotherapy dose (2.67 Gy or 5.2 Gy) (**Figure 26B**). Conversely, after five radiotherapy fractions, the 2.67 Gy-irradiated (total of 13.35 Gy) and the 5.2 Gy-irradiated (total of 26 Gy) tumor spheroids and tumor-immune spheroids displayed very similar diameters. Further, upon five irradiation fractions, tumor and tumor-immune spheroids size significantly decrease compared to non-irradiated, contrarily to observed after a single fraction. As expected, the size of non-irradiated tumor spheroids and tumor-immune spheroids increased over time, while significantly decreased in irradiated tumor spheroids. Over time, no differences were observed in tumor-immune spheroids diameter upon radiotherapy. Remarkably, there were also no differences regarding spheroids diameter between the two radiotherapy schemes.

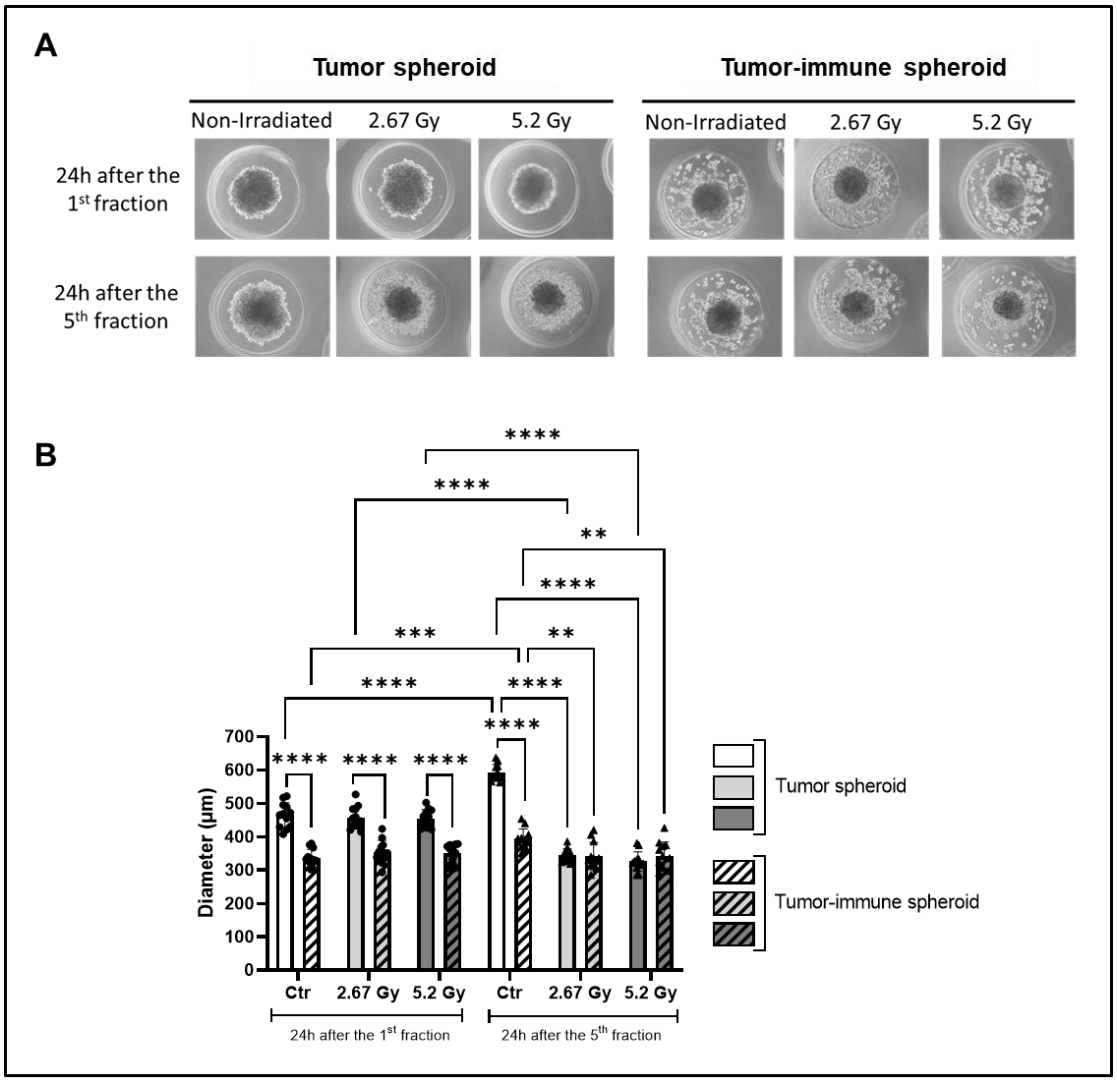

Figure 26- Tumor spheroids and tumor-immune spheroids characterization 24 hours after one or five fractions of two different radiotherapy schemes (2.67 Gy and 5.2 Gy). A) Tumor spheroids and tumor-immune spheroids morphology. **B)** Tumor spheroids and tumor-immune spheroids diameter (n=12). The results represent the mean ± SD. Each dot represents a different independent experiment (n). Samples were analyzed with two-way ANOVA, followed by Tukey multiple comparisons test. Statistical significance indicated with **p<0.01, ***p<0.001, ****p<0.0001.

Furthermore, the effect of irradiation on tumor-immune spheroids cellular composition, particularly on the percentage of macrophages and cancer cells, was assessed by flow cytometry. The macrophages percentage, $CD14^+$ cells, tended to increase in irradiated tumor-immune spheroids, being statistically significant after five doses of ionizing radiation. Moreover, in 5.2 Gy-irradiated tumor-immune spheroids, the percentage of macrophages was higher than in 2.67 Gy-irradiated tumor-immune spheroids (**Figure 27A**). These findings led us to assume that MDA-MB-231 cells could die more or proliferate less with a higher dose of ionizing radiation. Thus, cell viability was assessed by live/dead staining through flow cytometry analysis, but no significant differences on $CD14^+$ cell viability was observed in any condition (**Figure 27B**).

On the other hand, cancer cell viability in tumor spheroids upon five fractions of irradiation in 2.67 Gy and 5.2 Gy was significantly reduced towards 53.6% ± 16.03 and 30.9% ± 21.06, respectively, highlighting the anti-tumor effect of radiotherapy. Interestingly, in tumor-immune spheroids, MDA-MB-231 cell viability remained high (90.8% ± 1.19 in 2.67 Gy and 84.1% ± 5.35 in 5.2 Gy) (**Figure 27C**), strongly suggesting that macrophages confer resistance to cancer cell death under irradiation exposure.

In concordance with previous findings, no differences in cell death were observed in irradiated tumor-immune spheroids. However, the percentage of apoptotic cells was significantly higher upon five fractions in irradiated tumor spheroids, especially in the 5.2 Gy irradiation dose (**Figure 28**).

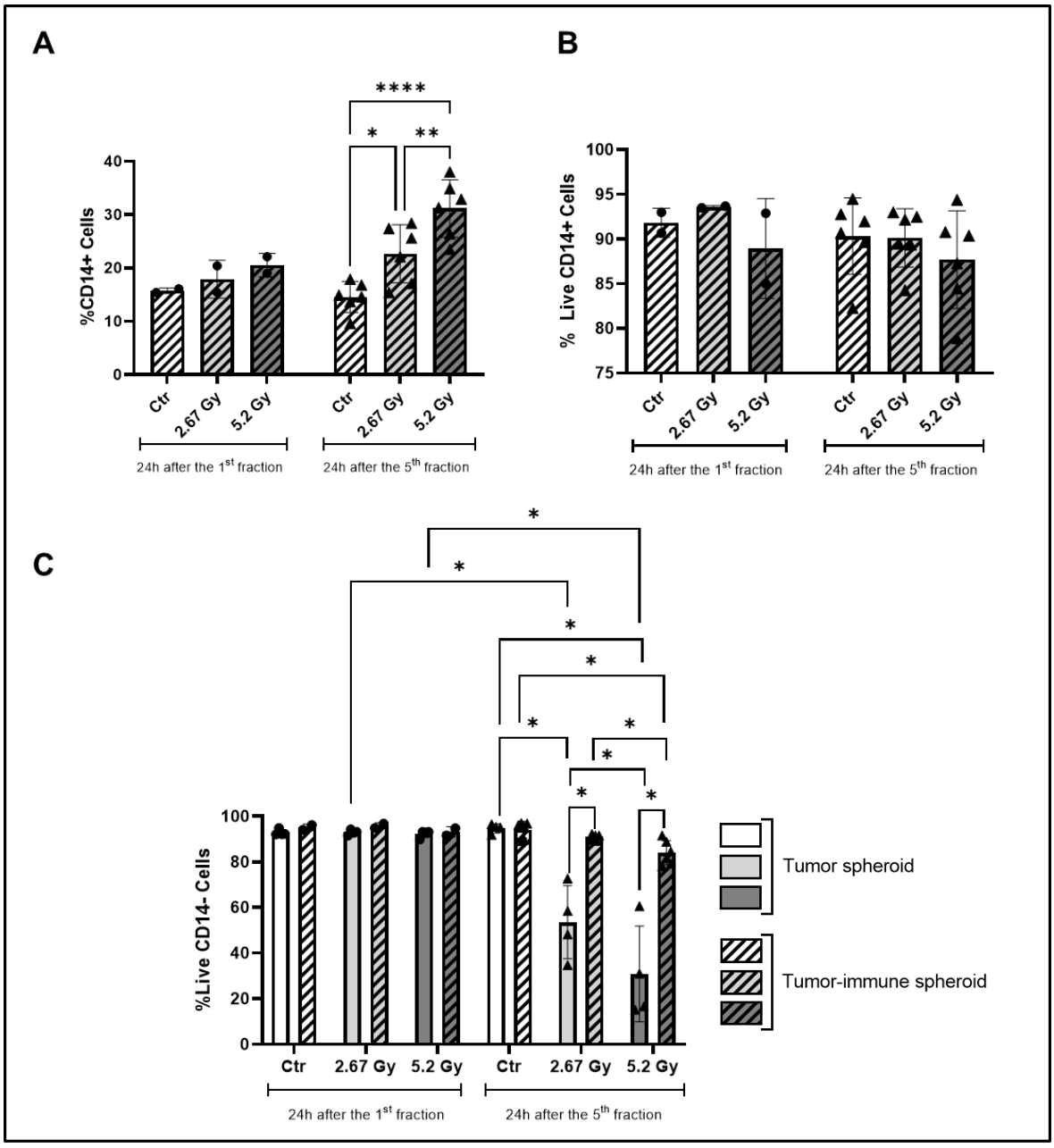

Figure 27- MDA-MB-231 and macrophages characterization 24 hours after one or five fractions of two different radiotherapy schemes (2.67 Gy and 5.2 Gy). A) Percentage of $CD14^+$ cells in tumor-immune spheroid evaluated by flow cytometry (n≥2). **B)** Percentage of live $CD14^+$ cells in tumor-immune spheroid (n≥2) measured by live/dead staining through flow cytometry. **C)** Percentage of live $CD14^-$ cells in tumor spheroids and tumor-immune spheroids (n≥2) assessed by live/dead staining through flow cytometry. The results represent the mean ± SD. Each dot represents a different independent experiment (n). Samples were analyzed with two-way ANOVA, followed by Tukey multiple comparisons test or with Friedman test. Statistical significance indicated with *p<0.05, **p<0.01, ***p<0.001.

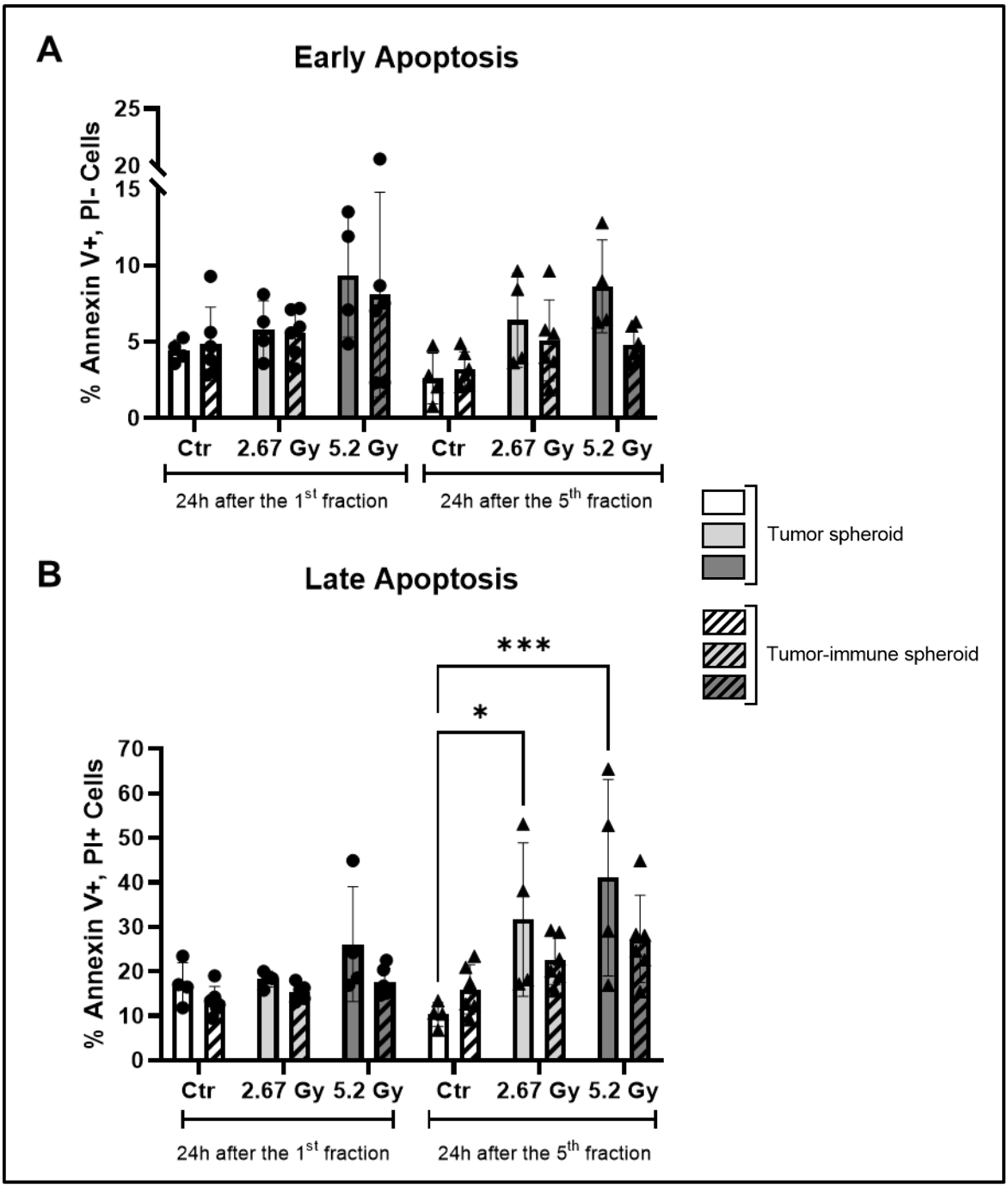

Figure 28- Tumor spheroids and tumor-immune spheroids apoptosis evaluated by Annexin V/ PI staining by flow cytometry. A) Early apoptosis is determined by the percentage of annexin V+ and PI- cells. **B)** Late apoptosis is defined by the percentage of annexin V+ and PI+ cells. The results represent the mean ± SD (n≥4). Each dot represents a different independent experiment (n). Samples were analyzed with two-way ANOVA, followed by Tukey multiple comparisons test. Statistical significance indicated with *p<0.05, ***p<0.001.

5.1 Ionizing radiation directs macrophages towards a pro-inflammatory phenotype

It is already known that macrophages are a key player on BC resistance to anti-cancer therapies, including radiotherapy [58]. Therefore, we investigated the impact of two radiotherapy schemes (2.67 Gy and 5.2 Gy/fraction) on macrophages polarization profile co-cultured with MDA-MB-231 cells in 3D tumor-immune spheroids, by analyzing a panel of pro- (**Figure 29**) and of anti-inflammatory (**Figure 30**) markers, by flow cytometry.

Our results evidenced that ionizing radiation induced a significant increase in the MFI of CD86 and CD40 on macrophages upon five fractions of radiotherapy (**Figure 29B**), albeit the total percentage of macrophages expressing these surface receptors tended to decrease in irradiated tumor-immune spheroids (**Figure 29A**). For HLA-DR marker, no significant differences were observed and there were no clear differences between the two radiotherapy schemes. Regarding to anti-inflammatory markers, the percentage of macrophages expressing CD163 and CD206 significantly decreased (**Figure 30A**), as well as the intensity of CD163 per each cell (MFI) after five 2.67 Gy or 5.2 Gy irradiation fractions. More interesting, in 2.67 Gy- and 5.2 Gy-irradiated macrophages an increase on PD-L1 expression levels were observed (**Figure 30B**).

Altogether, these results demonstrate that ionizing radiation directs macrophages towards a pro-inflammatory phenotype, and this effect is significantly evidenced upon five fractions of irradiation.

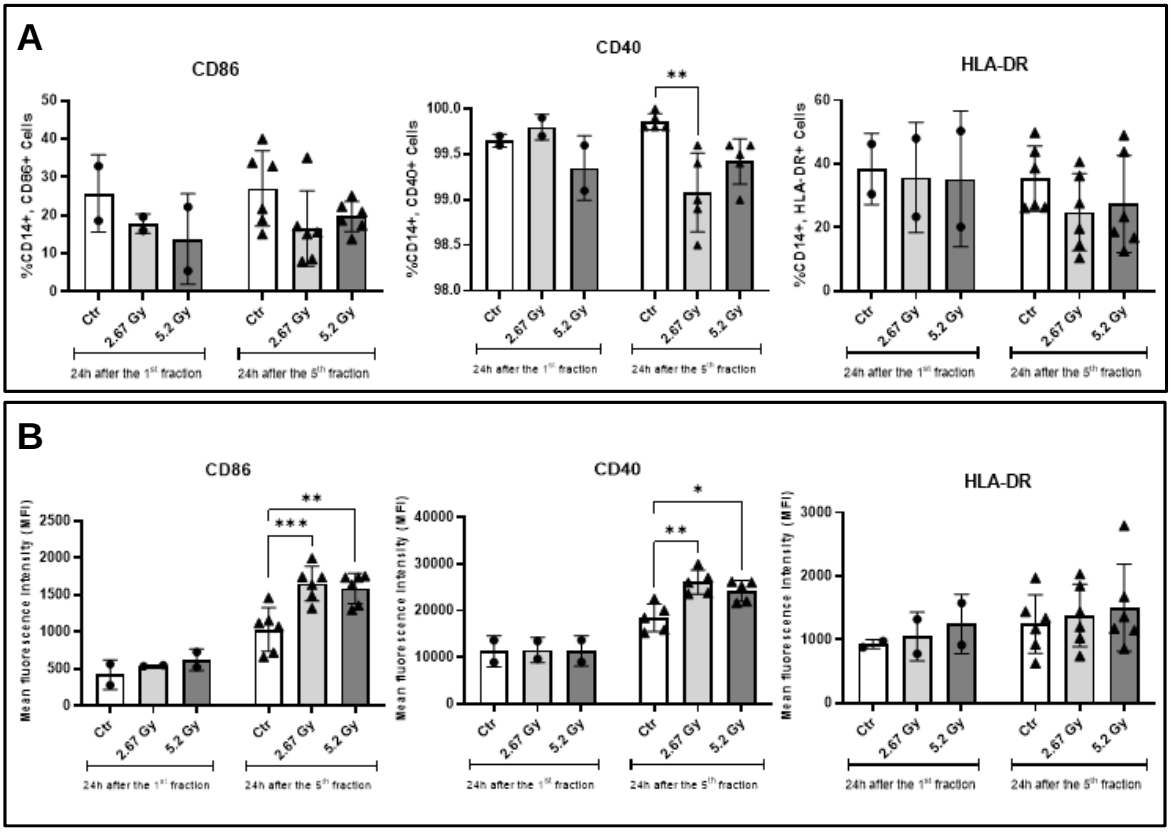

Figure 29- Macrophages pro-inflammatory markers expression in tumor-immune spheroid 24 hours after one of five fractions of two different radiotherapy schemes (2.67 Gy and 5.2 Gy). A) Percentage of pro-inflammatory markers (CD86, CD40, and HLA-DR) in live $CD14^+$ cells determined by flow cytometry. **B)** Mean fluorescence intensity of pro-inflammatory markers (CD86, CD40, and HLA-DR) in live $CD14^+$ cells, evaluated by flow cytometry. The results represent the mean ± SD (n≥2). Each dot represents a different independent experiment (n). Samples were analyzed with two-way ANOVA, followed by Tukey multiple comparisons test or with Friedman test. Statistical significance indicated with *p<0.05, **p<0.01, ***p<0.001, ****p<0.0001.

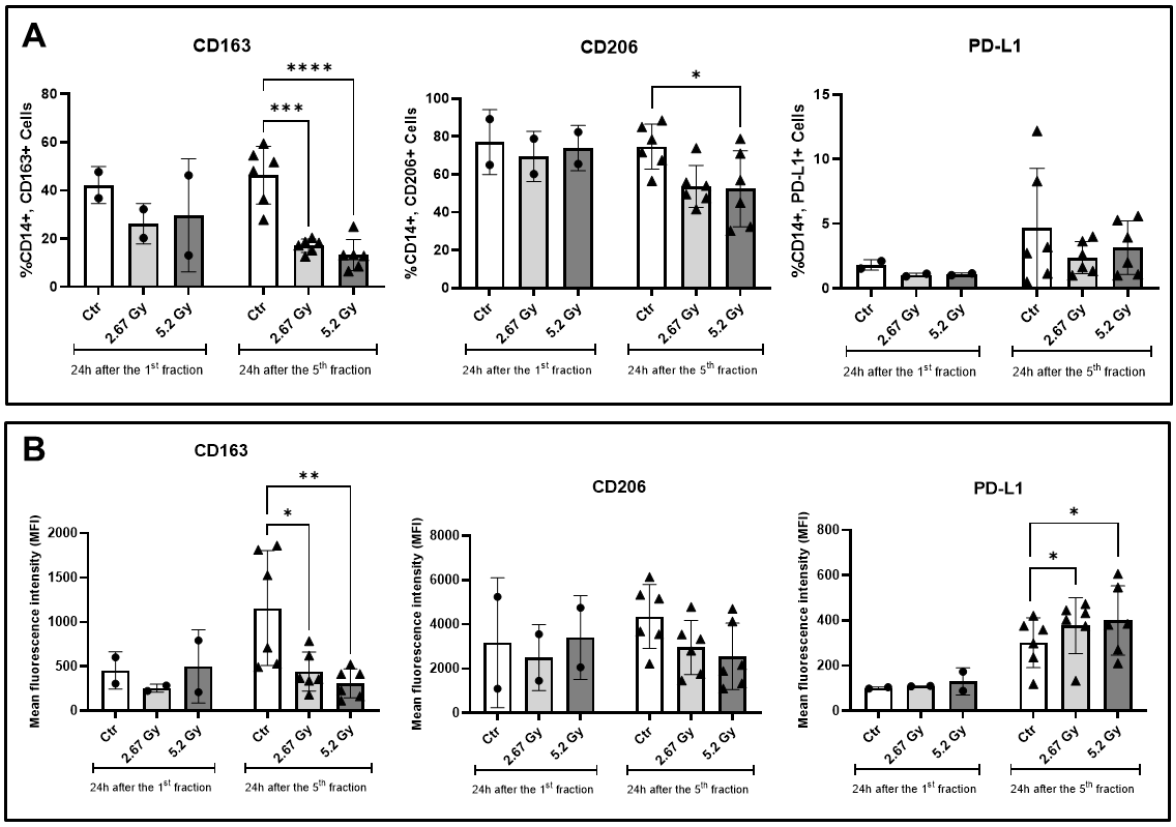

Figure 30- Macrophages anti-inflammatory markers expression in tumor-immune spheroid 24 hours after one of five fractions of two different radiotherapy schemes (2.67 Gy and 5.2 Gy). A) Percentage of anti-inflammatory markers (CD163 and CD206) and PD-L1 in live $CD14^+$ cells determined by flow cytometry. **B)** Mean fluorescence intensity of anti-inflammatory markers (CD163 and CD206) and PD-L1 in live $CD14^+$ cells, evaluated by flow cytometry. The results represent the mean ± SD (n≥2). Each dot represents a different independent experiment (n). Samples were analyzed with two-way ANOVA, followed by Tukey multiple comparisons test or with Friedman test. Statistical significance indicated with *p<0.05, **p<0.01, ***p<0.001, ****p<0.0001.

To better evaluate the inflammatory profile of the tumor-immune spheroids, the levels of several cytokines was measured. Twenty-four hours after the first and fifth radiotherapy fractions, the conditioned media of tumor spheroids and of tumor-immune spheroids were collected to quantify different cytokines secretory levels by ELISA.

Accordingly, the levels of IL-10, an anti-inflammatory cytokine, and the levels of IL-12/IL-23 and TNF-α, two pro-inflammatory cytokines, were assessed. However, using this method, it was not possible to detect the concentration of these cytokines in the media.

As shown in **Figure 31A**, at the beginning of the culture, tumor spheroids did not secrete IL-6, a pro-inflammatory cytokine; however, on the eighth day upon culture, this secretion was evident, being independent of radiotherapy (control of 24h after the 5th fraction). On the other hand, the production of this cytokine in the tumor-immune spheroid is visible since the beginning and increasing over time. Also, in tumor-immune spheroids, IL-6 secretion seems to be independent of irradiation, being always more accentuated in the tumor-immune spheroid in comparison to the tumor spheroid of the same condition. It remains, however, to be elucidated if the secretion is strictly performed by macrophages or by cancer cells upon macrophage stimulation. For that, the cytokine mRNA expression levels of this cytokine should be performed in both cancer cells and macrophages, upon tumor-immune spheroid dissociation, at the end of the experiment.

As for the anti-inflammatory cytokine CCL18, its expression in the tumor-immune spheroid increases slightly after five fractions of ionizing radiation when compared to the respective control, although this result is not statistically significant (**Figure 31B**). In the tumor spheroid, no measurable levels of CCL18 were detected (results not shown).

Furthermore, no differences were detected on TGF-β production, another anti-inflammatory cytokine, after one or five fractions of 2.67 Gy and 5.2 Gy (**Figure 31C**). Again, further transcriptomic analysis will be required to clarify which population is contributing to the expression of these cytokines.

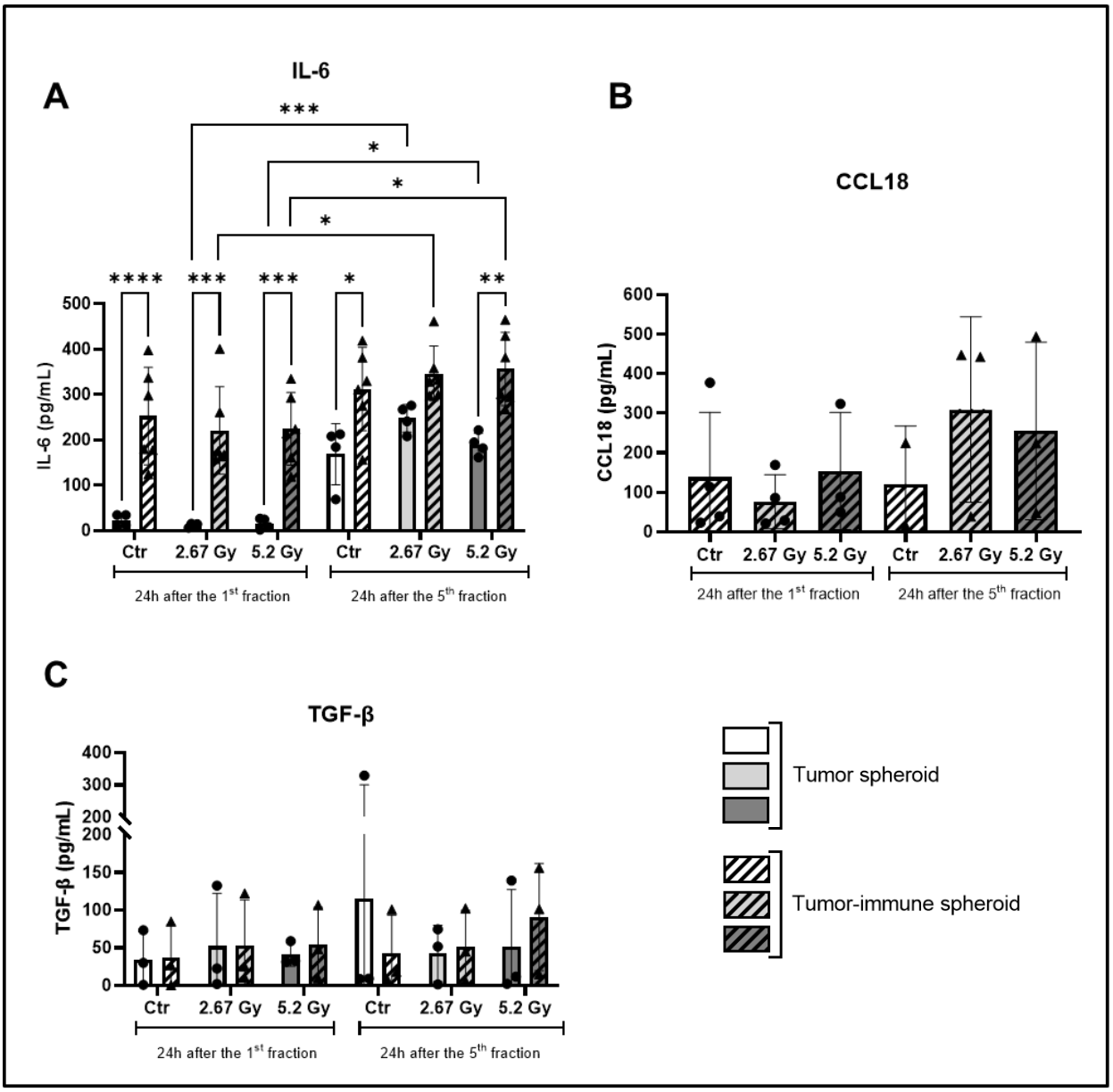

Figure 31- Secreted cytokines levels in MDA-MB-231 spheroids and tumor-immune spheroids, 24 hours after one or five fractions of two different radiotherapy schemes (2.67 Gy and 5.2 Gy). A) IL-6 (n=6) and **B)** CCL18 (n≥2) **C)** TGF-β (n=3) expression analyzed by ELISA. The results represent the mean ± SD (n≥2). Each dot represents a different independent experiment (n). Samples were analyzed with two-way ANOVA, followed by Tukey multiple comparisons test (IL-6) or with Kruskal-Wallis test (CCL18). Statistical significance indicated with *p<0.05, **p<0.01, ***p<0.001, ****p<0.0001.

5.2 Macrophages induce a less immunogenic phenotype on irradiated cancer cells

In order to understand if ionizing radiation can have an impact on tumor cells immunogenicity, we evaluated the effect of distinct radiotherapy fractions and doses on MDA-MB-231 cancer cells immunogenicity, by flow cytometry.

In this low immunogenic breast cancer cell model, the percentage of cells endogenously expressing the immune checkpoint molecules, PD-1 and PD-L1 were very low (bellow 4%). In the presence of macrophages and absence of radiotherapy, the expression levels of these receptors remained very low. However, the percentage of $CD14^-$ cells expressing PD-L1, and its intensity, was significantly higher in 5.2 Gy-irradiated tumor-immune spheroids than in tumor spheroids (**Figure 32** and **Figure 33**), suggesting a macrophage-mediated effect in response to ionizing radiation exposure.

Similarly, the percentage of non-irradiated MDA-MB-231 spheroid cells expressing CD47 marker was very low (bellow 5%) (**Figure 32**); however after five fractions of 5.2 Gy exposure, its expression levels significantly increased in tumor spheroids (**Figure 33**). Further, in tumor spheroids, the CD47 intensity increased over time in both 2.67 Gy and 5.2 Gy, after five fractions, in an ionizing radiation dependent manner (**Figure 33**). Interestingly, no significant differences regarding the percentage or intensity of CD47 expression was observed in cancer cells in tumor-immune spheroids, except for those of non-irradiated or of a single 2.67 Gy exposure (**Figure 32**).

Conversely, the percentage of cancer cells expressing the HLA-ABC complex was around 90% in all conditions (**Figure 32**). Upon five fractions, 2.67 Gy-irradiated tumor spheroid cells expressing HLA-ABC was significantly low in comparison to cells in direct contact with macrophages (**Figure 32**). The 5.2 Gy-irradiated tumor spheroids showed an increase in HLA-ABC per each cell compared to non-irradiated spheroids, after five fractions of radiotherapy (**Figure 33**), but no differences on these cells were induced by the co-culture with macrophages.

Additionally, the percentage of cancer cells expressing CD40 tend to decrease in tumor spheroids and in tumor-immune spheroids over time (even in controls, in absence of radiotherapy exposure). Furthermore, after five fractions, in 2.67 Gy- and 5.2 Gy-irradiated tumor-immune spheroids, the percentage of MDA-MB-231 cells expressing the CD40 receptor significantly decreased compared to non-irradiated (**Figure 32**). The opposite tendency was observed in CD40 MFI in 5.2 Gy-irradiated tumor-immune spheroids, being the increase statistically significant (**Figure 33**).

Overall, these findings suggest that ionizing irradiation induces a more immunogenic phenotype, increasing HLA-ABC and decreasing PD-L1 on cancer cells, and, interestingly, in the presence of macrophages, irradiated cancer cells became less immunogenic.

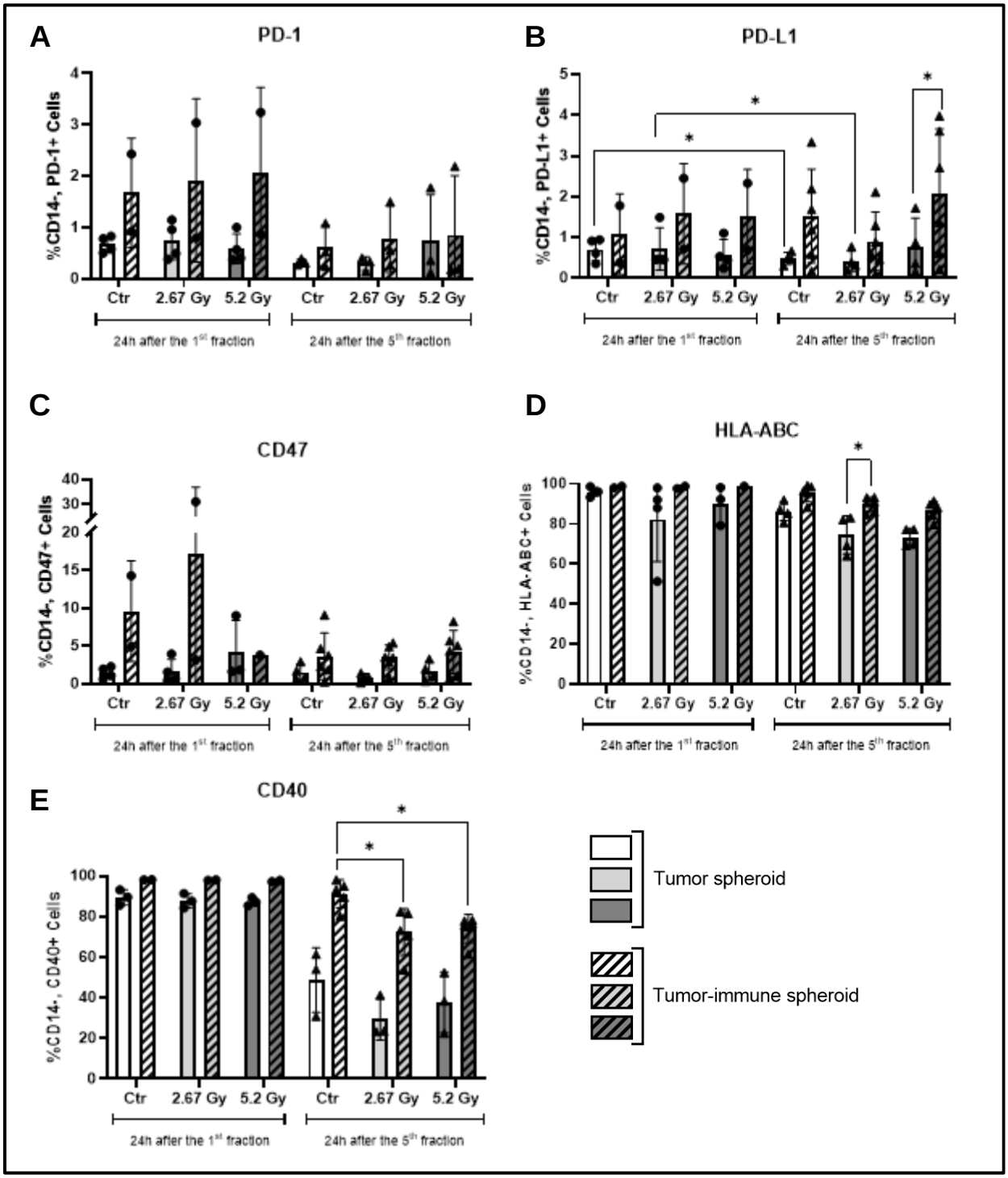

Figure 32- MDA-MB-231 cells immunogenicity in tumor spheroids and tumor-immune spheroids 24 hours after one or five fractions of two different radiotherapy schemes (2.67 Gy and 5.2 Gy): Percentage of **A)** PD-1, **B)** PD-L1, **C)** CD47, **D)** HLA-ABC, and **E)** CD40 in live $CD14^-$ cells, determined by flow cytometry. The results represent the mean ± SD (n≥2). Each dot represents a different independent experiment (n). Samples were analyzed with two-way ANOVA, followed by Tukey multiple comparisons test or with Friedman test. Statistical significance indicated with *p<0.05, **p<0.01, ***p<0.001.

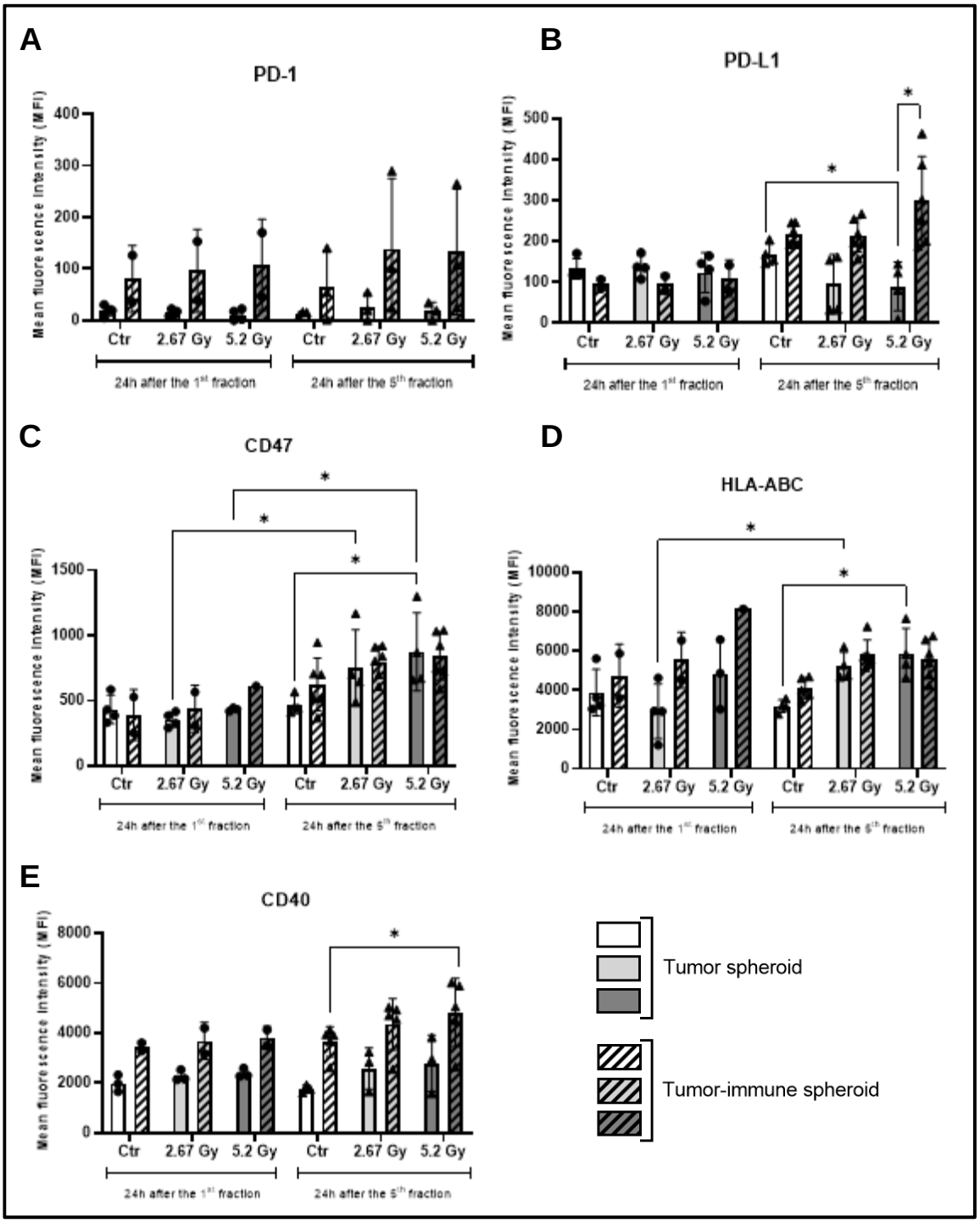

Figure 33- MDA-MB-231 cells immunogenicity in tumor spheroids and tumor-immune spheroids 24 hours after one or five fractions of two different radiotherapy schemes (2.67 Gy and 5.2 Gy): Mean fluorescence intensity of **A)** PD-1, **B)** PD-L1, **C)** CD47, **D)** HLA-ABC, and **E)** CD40 in live $CD14^-$ cells, determined by flow cytometry. The results represent the mean ± SD (n≥2). Each dot represents a different independent experiment (n). Samples were analyzed with two-way ANOVA, followed by Tukey multiple comparisons test or with Friedman test. Statistical significance indicated with *p<0.05, **p<0.01, ***p<0.001.

V. DISCUSSION

TNBC is the most aggressive and poor prognostic breast cancer subtype. This worse prognosis is due to the lack of efficient target therapies and its resistance to standard treatments, namely to radiotherapy [12, 19, 23]. Highlighting the mechanisms underlying cancer resistance to ionizing radiation will improve our understanding in breast cancer biology and unveil novel targets to develop more efficient target therapies.

To achieve this goal, attention has also to be focused on other elements of the tumor microenvironment that are irradiated with the tumor mass and may contribute to radioresistance. TAMs are frequently appointed as the most abundant immune populations at the BC microenvironment, representing up to 50% of the total tumor mass [38, 46]. Furthermore, their presence in TNBC stroma has been associated with tumor growth, enhanced locoregional invasion and distant metastasis formation [52, 53]. In addition, radiotherapy, one of the most common treatment modalities used, through the generation of novel antigens and damaged tissue stress signals release, may promote the recruitment of additional macrophages to the irradiated tumor site, where they might polarize into a pro-tumor phenotype [34, 36]. Several studies have been devoted to understanding the role of TAMs in breast cancer radioresponse. However, most of these were performed in monolayer cultures (2D), which do not consider the complexity of the tumor architecture and organization. Recently, various reports highlighted the 3D models importance to study, with more accuracy and efficacy, the response to different cancer target therapies.

Therefore, this study aimed to develop a 3D co-culture system, gathering MDA-MB-231 TNBC cell line and human macrophages, to understand their role in TNBC radioresponse. Thus, to develop a 3D spheroid with MDA-MB-231 and macrophages and choose the optimal culture conditions for their establishment, we firstly tested different protocols to form MDA-MB-231 spheroids. First, we used a protocol that consists in coating the plates with PolyHEMA, a non-adherent component that favors cell-cell interactions instead of cell-cell adhesion, allowing the spontaneous formation of 3D spheroids. However, using this component, we were not able to achieve this purpose, probably because this model is normally used to form mammospheres by enriching for anoikis-resistant breast cancer stem cells.

Alternatively, we used the protocol described by Saraiva *et al*, which consisted in seeding cancer cells in a plate pre-coated with agarose, another non-adherent component [78]. Although we were able to, through this methodology, establish 3D spheroids, they were very heterogeneous. This variability led us to use instead other protocol, previously described by Bauleth-Ramos *et al* [79]. In this protocol, MDA-MB-231 spheroid formation was performed using a microwell array technology, which allow us to form multiple spheroids in a high-throughput manner. The cells were seeded in agarose micro-molds and cultured for 7 days. Interestingly, tumor spheroids were successfully formed in three cell

densities and in two different media. Surprisingly, at the third day, a 3D structure was already formed. Taking into consideration that there were no differences on cell viability, 5000 initial cells per each spheroid was chosen to perform further experiments.

As we intend to develop the 3D co-culture with MDA-MB-231 and macrophages, and it is known that media composition can influence the inflammatory macrophage phenotype, the effect of distinct media on macrophages polarization was also tested. Since our results demonstrated that macrophages polarized to pro- or anti-inflammatory phenotype upon stimulation with LPS and IFN-y or IL-10, respectively, we considered that DMEM/F12 was an optimal condition to use in all subsequent studies.

Thus, the following step was dedicated to optimizing the TNBC co-culture with peripheral blood-derived human monocytes, to closely mimic the tumor microenvironment. Initially, three different ratios of MDA-MB-231 cells to monocytes (50:50, 35:65 and 25:75) were tested in DMEM/F12 medium supplemented with M-CSF, which promote the differentiation of monocytes to macrophages. Importantly, we observed that the M-CSF addition had not an effect on tumor cell surface markers expression (**Supplementary Figure 1**). Similarly to MDA-MB-231 spheroids at day 3, tumor-immune spheroids were already formed. However, these displayed a more compact structure, with a small cell aggregate on the vicinity, which likely correspond to monocytes that did not penetrate the spheroid. Considering the morphology, the initial 35:65 ratio was chosen, and at day 3 of co-culture, the macrophage percentage in the tumor-immune spheroid was about 20%. This was probably due to the high proliferative rate of the tumor cells, since macrophages do not proliferate *in vitro*. Considering these results, day 3 was chosen as a starting point to radiotherapy. However, before radiotherapy initiation, we characterized macrophage phenotype and the cancer immunogenicity.

Several studies using 3D models have shown that macrophages, in direct contact with breast cancer cells, exhibit a more anti-inflammatory phenotype [67, 68]. Conversely, in this work, after the third day of co-culture, macrophages displayed an intermediate phenotype, with high expression of CD40, a pro-inflammatory marker, and of CD206, an anti-inflammatory marker. This result agrees with another study that also demonstrated the existence of an intermediate phenotype in macrophages cultured in 3D with breast cancer cells [66]. Surprisingly, PD-L1 and CD47 expression in MDA-MB-231 cells was very low, although these two markers had been previously reported in 3D studies [78, 80]. These unexpected results can be due to differences in cell media composition, since we cultured cancer cells and macrophages in DMEM/F12 medium instead of DMEM or RPMI. However, to confirm this statement, it will be necessary to compare the expression of these two markers in tumor cells seeded in agarose micro-molds with the different media.

Furthermore, the high expression of MHC class I (HLA-ABC) and CD40 was found in MDA-MB-231 cells, as described [81]. Remarkably, cancer cells expressed low PD-1 levels, in comparison to another study, where the percentage of MDA-MB-231 expressing this immune checkpoint was approximately 20% [82].

Interestingly, our results also demonstrated that macrophages can modulate the immunogenic phenotype of tumor cells. Indeed, MDA-MB-231 cells tend to increase the levels of CD47, PD-1 and CD40 expression, suggesting that cancer cells acquire a less immunogenic phenotype in the presence of macrophages. Despite this, macrophage presence also seems to increase the HLA-ABC expression, which turn cells more vulnerable to immune cells recognition, by macrophages or by cytotoxic CD8 T lymphocytes. Despite the scarcity of studies demonstrating the direct impact of macrophages on the expression of these markers (CD47, PD-1 and CD40), it is recognized that macrophages have the ability to modulate the immunogenicity of tumor cells indirectly, through the production of anti-inflammatory cytokines, such as TGF-β and IL-10, essential for the maintenance of regulatory T cells, and the inhibition of cytotoxic T cells through PD-1/PD-L1 binding [83].

Radiotherapy is widely used as an anti-tumor treatment [18]. Since TNBC has no efficient target therapy, we strongly believe that radiotherapy could be an important tool to treat this BC subtype. However, TNBC is described to be more radioresistant, contributing to its poor prognosis [10, 17, 23]. Therefore, in this project, we evaluate the effect of tumor cell-macrophages communication on radio immune response. For that purpose, both MDA-MB-231 spheroids and tumor-immune spheroids were submitted to two different radiotherapy regimens, commonly used in breast cancer clinical practice (2.67 and 5.2 Gy/fraction) [24, 25]. Additionally, the effect of one or five fractions of each radiotherapy scheme was evaluated, to understand the effect of a single fraction or five fractions, simulating one week of patients treatment on the interaction with immune cells.

As already observed on the third day, 24 hours after the first fraction of radiotherapy, tumor-immune spheroids exhibited a smaller diameter than non-irradiated tumor spheroids, and therefore, a unique fraction of radiotherapy had no impact on spheroids size. The evaluation of spheroid size is essential to understand if the selected anti-cancer treatments can effectively reduce tumor mass. As expected, five fractions of ionizing irradiation significantly decreased the diameter of MDA-MB-231 spheroids, and a larger cell dissociation was also observed. Interestingly, this was not observed in tumor-immune spheroids, where the percentage of macrophages significantly increased upon five fractions of ionizing radiation. These findings led us to propose that MDA-MB-231 cells could die or have less proliferative ability after high doses of ionizing radiation. However, no differences between non-irradiated and irradiated tumor-immune spheroids were observed regarding

cell viability or apoptosis. These results suggested that cumulative irradiation could mainly affect tumor cells proliferation, which needs to be confirmed through Ki67 staining, for instance. In fact, it has been demonstrated that radiotherapy reduce cancer cell proliferation, through different mechanisms. For instance, in squamous cell carcinoma, radiation inhibited cell proliferation by arresting the cell cycle in the G2/M phase [84]. Furthermore, radiotherapy can decrease the Jumonji domain-containing protein 2B levels in gastric cancer, which inhibit the expression of cyclin A1 [85] and activate the protein tyrosine phosphatase non-receptor type 14 in pancreatic cancer [86], leading to inhibition of tumor cell proliferation.

On the other hand, in MDA-MB-231 spheroids, a decrease in cell viability and an increase in apoptosis was clearly observed, confirming the anti-tumor effect of radiotherapy, and highlighting the possible role of macrophages on providing TNBC radioresistance. Indeed, TAMs presence had already been associated with a worse prognosis of this breast cancer subtype [52, 53]. These results led us to deduce that this poor prognosis may be associated with tumor cells radioresistance conferred by macrophages. In fact, some studies already demonstrated the ability of macrophages to induce BC radioresistance [54, 58].

Despite this, irradiated macrophages polarized towards a pro-inflammatory phenotype, displaying an increase on CD86 and CD40 pro-inflammatory markers, and a decrease on CD163 and CD206 anti-inflammatory markers expression. These results are in line with previous studies, since the irradiation of macrophage with doses superior to 1 Gy promoted the acquisition of a pro-inflammatory phenotype, through the production of nitric oxide (NO) and of pro-inflammatory cytokines, such as TNF-α and IL-6. The acquisition of this phenotype may occur through the activation of different signaling pathways induced by irradiation, namely NF-κB and p53 [87]. These findings clearly indicate that although acquiring a more pro-inflammatory phenotype after radiotherapy, macrophages did not induce tumor cell death. In fact, our group previously showed that after radiotherapy, macrophages acquire a more pro-inflammatory phenotype; although, in a 2D colorectal cancer model, they were still able to promote the invasion of colorectal tumor cells [20].

These results led us to speculate that cancer cells might be inducing other immune escape mechanisms, as the reduction of MHC-I and CD47 expression, or the modulation of immune checkpoint molecules. When exploiting this question, we observed that ionizing radiation induced the acquisition of a more immunogenic phenotype by cancer cells, through increasing HLA-ABC and decreasing PD-L1 expression. Indeed, it is well established that radiotherapy increases the immunogenicity of tumor cells [88], since it could, for example, induce MHC class I expression [89] and decrease the expression of

CD47 in cancer cells surface [90]. However, in tumor-immune spheroids, irradiated cancer cells became less immunogenic, increasing the immune checkpoint PD-L1 expression. Importantly, these results demonstrated that although radiotherapy drives macrophages towards a more pro-inflammatory phenotype, their presence in the tumor microenvironment may contribute to decrease tumor cell immunogenicity, promoting their survival and even invasion, upon RT exposure. Further, *in vivo* experiments are required to exploit their role in assisting cancer cell immune escape and tumor progression.

Furthermore, in this study, no differences regarding cytokines (IL-6, CCL18 and TGF-β) secretion was observed upon radiotherapy treatment. However, as this therapeutic strategy is known for cytokines levels in the tumor microenvironment [36], more studies regarding cytokines production by mRNA expression, and secretion through an extended multiplex array, are required.

Overall, the effect of radiotherapy on macrophage and tumor cell markers was only significant after exposure to five fractions of radiotherapy, mimicking one week of cancer patients' treatment, while a single fraction of ionizing radiation did not induce a significant effect on the selected markers expression. Furthermore, no major differences were observed between the two radiotherapy schemes. Indeed, the only meaningful difference between the 2.67 and 5.2 Gy doses, after one week of ionizing radiation exposure, was the increased cell death observed in 5.2 Gy irradiated tumor spheroids. The lack of studies comparing the two radiotherapy schemes used in this study emphasize the need to further exploit the effect of different radiotherapy fractions on the immune response. However, a previous study has shown that radiation treatment, in a fractionated regimen (3 fractions of 8 Gy), is more effective than a single fraction (20 Gy) in activating the immune system response, through dendritic cell recruitment and cytotoxic T cells activation [91]. Therefore, this study demonstrates the importance of radiotherapy fractionation to induce the immune response after treatment.

Strikingly, in this study, we successfully established a 3D model co-cultured with TNBC cells and human macrophages. This protocol was based on the liquid overlay technique using agarose micro-molds, an easy, fast and low-cost system. Importantly, we developed a model using human MDA-MB-231, a cell line described as difficult to spontaneously form spheroids without the addition of extracellular matrix components [92]. The introduction of macrophages in this 3D model allowed us to recapitulate several aspects of the breast cancer microenvironment complexity. We envisage that, in the near future, the system can be easily upgraded by adding other elements, such as fibroblasts or T cells. This model can be a crucial tool to study other aspects of the tumor microenvironment, explore the molecular interactions established and exploit new therapeutic approaches, or investigate tumor resistance to other therapies.

Altogether our results also suggest that the combination of radiotherapy with immunotherapy might be successful to TNBC patients treatment, turning cancer cells more immunogenic to improve their recognition and response to irradiation. In fact, FDA already approved two immunotherapies for TNBC: Atezolizumab, an anti-PD-L1 inhibitor, and Pembrolizumab, an anti-PD-1 inhibitor [45], and several studies are now evaluating the effectiveness of other immune targets, such as CD40 [93-95] and CD47 [42, 96, 97], that have a direct impact on macrophage-tumor cell interaction.

The combination of radiotherapy with immunotherapy has been considered a promising anti-cancer therapy. Radiation treatment is essential to increase tumor immunogenicity, by increasing the release of antigens and cytokines into the tumor microenvironment. Furthermore, this treatment also promotes the recruitment of immune cells to the tumor site and induces cytotoxic T cell activation. On the other hand, immunotherapy can turn the immune system more effective in tackling cancer cells, by blocking immune checkpoints [88, 98]. We believe that the 3D model here developed, by mimicking more closely the tumor architecture and by combining cancer and immune cells, may be a powerful tool to exploit the mechanisms underlying the combination of these immunotherapeutic approaches with conventional radiotherapy.

VI. CONCLUSION AND FUTRUE PERSPECTIVES

In this study, we established a 3D model that gathers TNBC cells and human macrophages to mimic, as close as possible, the breast tumor microenvironment to explore its response to radiotherapy.

In summary, our results demonstrated that, after ionizing radiation exposure (5x2.67 Gy or 5x5.2 Gy), macrophages acquire a more pro-inflammatory phenotype exhibiting a significant increase in pro-inflammatory markers (CD86 and CD40) and decrease in anti-inflammatory markers (CD163 and CD206) expression. Nevertheless, the macrophages presence in the TNBC microenvironment allows to significantly protect tumor cells from death after five fractions of radiotherapy exposure. Furthermore, radiotherapy promotes cancer cell immunogenicity. However, and interestingly, the presence of macrophages reduced the TNBC immunogenic phenotype promoted by radiotherapy. The achieved results highlight the need to combine radiotherapy with immunotherapy for TNBC treatment in order to make cancer cells more immunogenic.

Noteworthy, we successfully established a reproducible and high-throughput scalable 3D model, comprised by triple-negative breast tumor cells and human macrophages, which allowed us to study the role of macrophages on TNBC radioresponse. This model can now be used to explore the molecular mechanisms underlying breast cancer radioresistance and to elucidate the role of macrophages or other immune cells, as well as tumor cells resistance to other anti-cancer treatments.

As future perspectives, it would be important to further characterize this model by analyzing the macrophages localization within the tumor-immune spheroids through CD68 staining, and to elucidate how the different macrophages phenotypes are distributed, using specific anti-CD80 and anti-CD163 antibodies. It would be also essential to stain tumor spheroids and tumor-immune spheroids with an anti-Ki67 and an anti-γ-H2AX antibodies to analyze cancer cell proliferative rate and DNA damage status, respectively, as induced by ionizing irradiation and by macrophages co-culture.

Further, it would be extremely interesting to exploit the involvement of some conventional radioresistance signaling pathways previously described as being activated by macrophages or ionizing radiation, such EGFR, NF-κB (p65), Bcl2 and Bcl-xL. Indeed, this was one of our initial goals, but unfortunately, time restrictions imposed by the pandemic situation, impaired us to achieve these aims.

Additionally, it would be also interesting to add complexity to the established tumor-immune spheroids, by gathering other cell populations, such as T cells and fibroblasts. This would certainly increase breast cancer microenvironment understanding, and better mimic the complexity of *in vivo* interactions.

Finally, in the future, we intend to compare the obtained results in this project with those of an MDA-MB-231 radioresistant cell line, to evaluate the role of macrophages in TNBC radioresponse with two cell lines that have different degrees of radio sensibility.

VII. SUPPLEMENTARY FIGURES

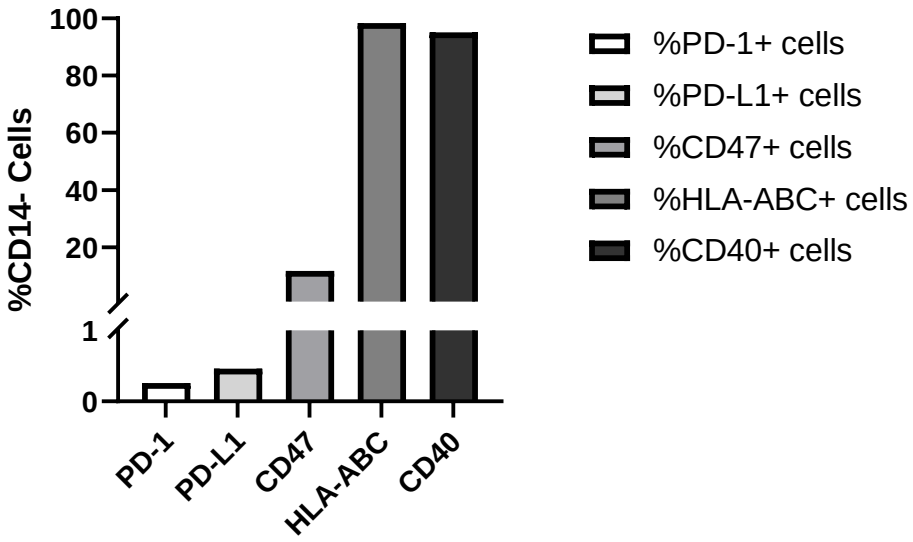

Supplementary Figure 1- M-CSF does not impact MDA-MB-231 cancer cell immunogenicity. Percentage of $CD14^-$ cells expressing PD-1, PD-L1, CD47, HLA-ABC, and CD40 at their surface, as determined by flow cytometry at day 3 (n=1)

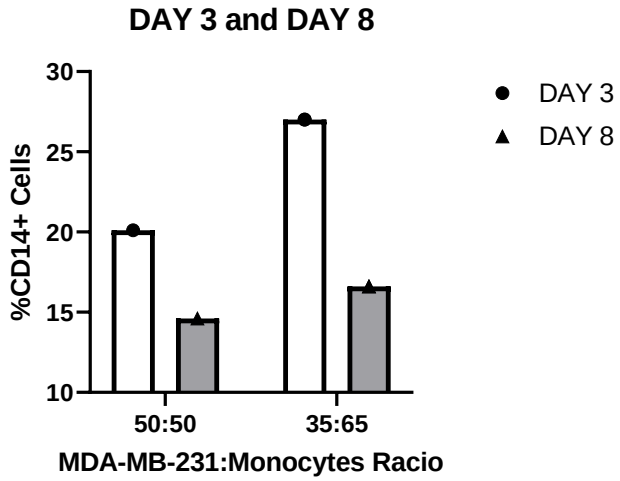

Supplementary Figure 2- Percentage of macrophages on tumor-immune spheroids. The percentage of macrophages ($CD14^+$ cells) on tumor-immune spheroids, comprising in initially to distant MDA-MB-231:monocytes ratios (50:50 and 35:65) was calculated at day 3 and day 8, as evaluated by flow cytometry (n=1).

VIII. REFERENCES

1. Sung, H., et al., *Global cancer statistics 2020: GLOBOCAN estimates of incidence and mortality worldwide for 36 cancers in 185 countries.* CA Cancer J Clin, 2021.
2. Carioli, G., et al., *Trends and predictions to 2020 in breast cancer mortality in Europe.* Breast, 2017. **36**: p. 89-95.
3. Feng, Y., et al., *Breast cancer development and progression: Risk factors, cancer stem cells, signaling pathways, genomics, and molecular pathogenesis.* Genes & Diseases, 2018. **5**(2): p. 77-106.
4. Shah, R., K. Rosso, and S.D. Nathanson, *Pathogenesis, prevention, diagnosis and treatment of breast cancer.* World J Clin Oncol, 2014. **5**(3): p. 283-98.
5. Senkus, E., et al., *Primary breast cancer: ESMO Clinical Practice Guidelines for diagnosis, treatment and follow-up.* Ann Oncol, 2015. **26 Suppl 5**: p. v8-30.
6. Cao, A., L. Huang, and Z. Shao, *The Preventive Intervention of Hereditary Breast Cancer.* Adv Exp Med Biol, 2017. **1026**: p. 41-57.
7. Fernandes, I., et al, *Manual de Oncologia SPO Abordagem e tratamento do cancro da mama*. 1st edition, edit.on.lab.,lda., 2020.
8. Dai, X., et al., *Cancer Hallmarks, Biomarkers and Breast Cancer Molecular Subtypes.* J Cancer, 2016. **7**(10): p. 1281-94.
9. Dawson, S.J., E. Provenzano, and C. Caldas, *Triple negative breast cancers: clinical and prognostic implications.* Eur J Cancer, 2009. **45 Suppl 1**: p. 27-40.
10. Yip, C.H. and A. Rhodes, *Estrogen and progesterone receptors in breast cancer.* Future Oncol, 2014. **10**(14): p. 2293-301.
11. Cardoso, F. *100 perguntas Chave no Cancro da Mama* - 2nd Edition. Permanyer Portugal, 2017.
12. Denkert, C., et al., *Molecular alterations in triple-negative breast cancer-the road to new treatment strategies.* Lancet, 2017. **389**(10087): p. 2430-2442.
13. Saraiva, D.P., et al., *How many diseases is triple negative breast cancer: the protagonism of the immune microenvironment.* ESMO Open, 2017. **2**(4): p. e000208.
14. Li, X., et al., *Triple-negative breast cancer has worse overall survival and cause-specific survival than non-triple-negative breast cancer.* Breast Cancer Research and Treatment, 2016. **161**(2): p. 279-287.
15. The American Cancer Society medical and editorial content team. (2019). *Triple-negative breast cancer*. https://www.cancer.org/cancer/breast-cancer/about/types-of-breast-cancer/triple-negative.html visit on june 2021.
16. The American Cancer Society medical and editorial content team. (2020). *Survival rates for breast cancer.* https://www.cancer.org/cancer/breast-cancer/understanding-a-breast-cancer-diagnosis/breast-cancer-survival-rates.html visit on june 2021.
17. Eifel, P., et al., *National Institutes of Health Consensus Development Conference Statement: adjuvant therapy for breast cancer, November 1-3, 2000.* J Natl Cancer Inst, 2001. **93**(13): p. 979-89.
18. Baskar, R., et al., *Cancer and radiation therapy: current advances and future directions.* Int J Med Sci, 2012. **9**(3): p. 193-9.
19. Langlands, F.E., et al., *Breast cancer subtypes: response to radiotherapy and potential radiosensitisation.* Br J Radiol, 2013. **86**(1023): p. 20120601.
20. Pinto, A.T., et al., *Ionizing radiation modulates human macrophages towards a pro-inflammatory phenotype preserving their pro-invasive and pro-angiogenic capacities.* Sci Rep, 2016. **6**: p. 18765.
21. Boustani, J., et al., *The 6th R of Radiobiology: Reactivation of Anti-Tumor Immune Response.* Cancers, 2019. **11**(6): p. 860.
22. Withers, H.R., *The Four R's of Radiotherapy*, in *Advances in Radiation Biology*, J.T. Lett and H. Adler, Editors. 1975, Elsevier. p. 241-271.
23. Zhou, Z.R., et al., *Building radiation-resistant model in triple-negative breast cancer to screen radioresistance-related molecular markers.* Ann Transl Med, 2020. **8**(4): p. 108.

24. Brunt, A.M., et al., *Five-fraction Radiotherapy for Breast Cancer: FAST-Forward to Implementation.* Clin Oncol (R Coll Radiol), 2021. **33**(7): p. 430-439.
25. Murray Brunt, A., et al., *Hypofractionated breast radiotherapy for 1 week versus 3 weeks (FAST-Forward): 5-year efficacy and late normal tissue effects results from a multicentre, non-inferiority, randomised, phase 3 trial.* Lancet, 2020. **395**(10237): p. 1613-1626.
26. T-SWu, et al., *National Taiwan Un Radio Resistance Mechanisms of Cancers: An Overview and Future Perspectives.* Biol Med S2, 2015. **002**.
27. White, J. and E. Mamounas, *Locoregional radiotherapy in patients with breast cancer responding to neoadjuvant chemotherapy: a paradigm for treatment individualization.* J Clin Oncol, 2014. **32**(6): p. 494-5.
28. Bian, L., et al., *ATM Expression Is Elevated in Established Radiation-Resistant Breast Cancer Cells and Improves DNA Repair Efficiency.* Int J Biol Sci, 2020. **16**(7): p. 1096-1106.
29. Zhang, P., et al., *ATM-mediated stabilization of ZEB1 promotes DNA damage response and radioresistance through CHK1.* Nat Cell Biol, 2014. **16**(9): p. 864-75.
30. Horsman, M.R. and J. Overgaard, *The impact of hypoxia and its modification of the outcome of radiotherapy.* J Radiat Res, 2016. **57 Suppl 1**(Suppl 1): p. i90-i98.
31. He, M.Y., et al., *Radiotherapy in triple-negative breast cancer: Current situation and upcoming strategies.* Crit Rev Oncol Hematol, 2018. **131**: p. 96-101.
32. Lee, J.M. and A. Bernstein, *p53 mutations increase resistance to ionizing radiation.* Proc Natl Acad Sci U S A, 1993. **90**(12): p. 5742-6.
33. Huang, X., et al., *miRNA-95 mediates radioresistance in tumors by targeting the sphingolipid phosphatase SGPP1.* Cancer Res, 2013. **73**(23): p. 6972-86.
34. Barker, H.E., et al., *The tumour microenvironment after radiotherapy: mechanisms of resistance and recurrence.* Nat Rev Cancer, 2015. **15**(7): p. 409-25.
35. Mareel, M., M.J. Oliveira, and I. Madani, *Cancer invasion and metastasis: interacting ecosystems.* Virchows Arch, 2009. **454**(6): p. 599-622.
36. Lumniczky, K., et al., *Editorial: Radiation and the Immune System: Current Knowledge and Future Perspectives.* Front Immunol, 2017. **8**: p. 1933.
37. Shiao, S.L. and L.M. Coussens, *The tumor-immune microenvironment and response to radiation therapy.* J Mammary Gland Biol Neoplasia, 2010. **15**(4): p. 411-21.
38. Rahat, M.A. and B. Hemmerlein, *Macrophage-tumor cell interactions regulate the function of nitric oxide.* Frontiers in physiology, 2013. **4**: p. 144-144.
39. Hanahan, D. and R.A. Weinberg, *Hallmarks of cancer: the next generation.* Cell, 2011. **144**(5): p. 646-74.
40. Denkert, C., *The immunogenicity of breast cancer--molecular subtypes matter.* Ann Oncol, 2014. **25**(8): p. 1453-5.
41. Chabanon, R.M., et al., *Mutational Landscape and Sensitivity to Immune Checkpoint Blockers.* Clin Cancer Res, 2016. **22**(17): p. 4309-21.
42. Candas-Green, D., et al., *Dual blockade of CD47 and HER2 eliminates radioresistant breast cancer cells.* Nat Commun, 2020. **11**(1): p. 4591.
43. Kim, H., et al., *Direct Interaction of CD40 on Tumor Cells with CD40L on T Cells Increases the Proliferation of Tumor Cells by Enhancing TGF-β Production and Th17 Differentiation.* PLoS One, 2015. **10**(5): p. e0125742.
44. Chen, D.S. and I. Mellman, *Oncology meets immunology: the cancer-immunity cycle.* Immunity, 2013. **39**(1): p. 1-10.
45. Howard, F.M., et al., *The emerging role of immune checkpoint inhibitors for the treatment of breast cancer.* Expert Opin Investig Drugs, 2021: p. 1-18.
46. Solinas, G., et al., *Tumor-associated macrophages (TAM) as major players of the cancer-related inflammation.* J Leukoc Biol, 2009. **86**(5): p. 1065-73.
47. Mosser, D.M. and J.P. Edwards, *Exploring the full spectrum of macrophage activation.* Nat Rev Immunol, 2008. **8**(12): p. 958-69.

48. Mantovani, A., et al., *Macrophage polarization: tumor-associated macrophages as a paradigm for polarized M2 mononuclear phagocytes.* Trends in Immunology, 2002. **23**(11): p. 549-555.
49. Viola, A., et al., *The Metabolic Signature of Macrophage Responses.* Frontiers in Immunology, 2019. **10**(1462).
50. Lu, D., et al., *Beyond T Cells: Understanding the Role of PD-1/PD-L1 in Tumor-Associated Macrophages.* Journal of Immunology Research, 2019. **2019**: p. 1919082.
51. Owen, J. and M. Mohamadzadeh, *Macrophages and chemokines as mediators of angiogenesis.* 2013. **4**(159).
52. Santoni, M., et al., *Triple negative breast cancer: Key role of Tumor-Associated Macrophages in regulating the activity of anti-PD-1/PD-L1 agents.* Biochim Biophys Acta Rev Cancer, 2018. **1869**(1): p. 78-84.
53. Laoui, D., et al., *Tumor-associated macrophages in breast cancer: distinct subsets, distinct functions.* Int J Dev Biol, 2011. **55**(7-9): p. 861-7.
54. Meng, Y., et al., *Blockade of tumor necrosis factor alpha signaling in tumor-associated macrophages as a radiosensitizing strategy.* Cancer Res, 2010. **70**(4): p. 1534-43.
55. Genard, G., S. Lucas, and C. Michiels, *Reprogramming of Tumor-Associated Macrophages with Anticancer Therapies: Radiotherapy versus Chemo- and Immunotherapies.* Front Immunol, 2017. **8**: p. 828.
56. Pinto, A.T., et al., *Intricate Macrophage-Colorectal Cancer Cell Communication in Response to Radiation.* PLoS One, 2016. **11**(8): p. e0160891.
57. Chen, X., et al., *IL-6 induced M1 type macrophage polarization increases radiosensitivity in HPV positive head and neck cancer.* Cancer Lett, 2019. **456**: p. 69-79.
58. Rahal, O.M., et al., *Blocking Interleukin (IL)4- and IL13-Mediated Phosphorylation of STAT6 (Tyr641) Decreases M2 Polarization of Macrophages and Protects Against Macrophage-Mediated Radioresistance of Inflammatory Breast Cancer.* Int J Radiat Oncol Biol Phys, 2018. **100**(4): p. 1034-1043.
59. Lindström, A., et al., *Fusion between M2-macrophages and cancer cells results in a subpopulation of radioresistant cells with enhanced DNA-repair capacity.* Oncotarget, 2017. **8**(31): p. 51370-51386.
60. Chaicharoenaudomrung, N., P. Kunhorm, and P. Noisa, *Three-dimensional cell culture systems as an in vitro platform for cancer and stem cell modeling.* World J Stem Cells, 2019. **11**(12): p. 1065-1083.
61. Franchi-Mendes, T., et al., *3D Cancer Models: Depicting Cellular Crosstalk within the Tumour Microenvironment.* Cancers (Basel), 2021. **13**(18).
62. Wiesner, C., et al., *Podosomes in space: macrophage migration and matrix degradation in 2D and 3D settings.* Cell Adh Migr, 2014. **8**(3): p. 179-91.
63. Huang, Z., P. Yu, and J. Tang, *Characterization of Triple-Negative Breast Cancer MDA-MB-231 Cell Spheroid Model.* Onco Targets Ther, 2020. **13**: p. 5395-5405.
64. Espinoza-Sánchez, N.A., G.K. Chimal-Ramírez, and E.M. Fuentes-Pananá, *Analyzing the Communication Between Monocytes and Primary Breast Cancer Cells in an Extracellular Matrix Extract (ECME)-based Three-dimensional System.* J Vis Exp, 2018(131).
65. Espinoza-Sánchez, N.A., et al., *IL-1β, IL-8, and Matrix Metalloproteinases-1, -2, and -10 Are Enriched upon Monocyte-Breast Cancer Cell Cocultivation in a Matrigel-Based Three-Dimensional System.* Front Immunol, 2017. **8**: p. 205.
66. Heaster, T.M., et al., *Autofluorescence Imaging of 3D Tumor-Macrophage Microscale Cultures Resolves Spatial and Temporal Dynamics of Macrophage Metabolism.* Cancer Res, 2020. **80**(23): p. 5408-5423.
67. Tevis, K.M., et al., *Mimicking the tumor microenvironment to regulate macrophage phenotype and assessing chemotherapeutic efficacy in embedded cancer cell/macrophage spheroid models.* Acta Biomater, 2017. **50**: p. 271-279.

68. Bengsch, F., et al., *Cell type-dependent pathogenic functions of overexpressed human cathepsin B in murine breast cancer progression.* Oncogene, 2014. **33**(36): p. 4474-84.
69. Carter, K.P., et al., *Macrophages enhance 3D invasion in a breast cancer cell line by induction of tumor cell tunneling nanotubes.* Cancer Rep (Hoboken), 2019. **2**(6): p. e1213.
70. Ören, B., et al., *Tumour stroma-derived lipocalin-2 promotes breast cancer metastasis.* J Pathol, 2016. **239**(3): p. 274-85.
71. Huang, C.P., et al., *Engineering microscale cellular niches for three-dimensional multicellular co-cultures.* Lab Chip, 2009. **9**(12): p. 1740-8.
72. Fang, W.B., et al., *Targeted gene silencing of CCL2 inhibits triple negative breast cancer progression by blocking cancer stem cell renewal and M2 macrophage recruitment.* Oncotarget, 2016. **7**(31): p. 49349-49367.
73. Leonard, F., et al., *Macrophage Polarization Contributes to the Anti-Tumoral Efficacy of Mesoporous Nanovectors Loaded with Albumin-Bound Paclitaxel.* Front Immunol, 2017. **8**: p. 693.
74. Emami, F., et al., *Photoimmunotherapy with cetuximab-conjugated gold nanorods reduces drug resistance in triple negative breast cancer spheroids with enhanced infiltration of tumor-associated macrophages.* J Control Release, 2020.
75. Chan, R., et al., *Investigating the Radioresistant Properties of Lung Cancer Stem Cells in the Context of the Tumor Microenvironment.* Radiat Res, 2016. **185**(2): p. 169-81.
76. Steer, A., et al., *Impact of Cancer-Associated Fibroblast on the Radiation-Response of Solid Xenograft Tumors.* Front Mol Biosci, 2019. **6**: p. 70.
77. Oliveira, M.I., et al., *Chitosan drives anti-inflammatory macrophage polarisation and pro-inflammatory dendritic cell stimulation.* Eur Cell Mater, 2012. **24**: p. 136-153.
78. Saraiva, D.P., et al., *Establishment of a 3D Co-culture With MDA-MB-231 Breast Cancer Cell Line and Patient-Derived Immune Cells for Application in the Development of Immunotherapies.* Front Oncol, 2020. **10**: p. 1543.
79. Bauleth-Ramos, T., et al., *Colorectal cancer triple co-culture spheroid model to assess the biocompatibility and anticancer properties of polymeric nanoparticles.* Journal of Controlled Release, 2020. **323**: p. 398-411.
80. Mokhtari, R.B., et al., *3D Multicellular Stem-Like Human Breast Tumor Spheroids Enhance Tumorigenicity of Orthotopic Xenografts in Athymic Nude Rat Model.* Cancers (Basel), 2021. **13**(11).
81. Toufexis, A.G., N.C. Reddy, and R.W. O'Donnell, *The Effect of a Histone Deacetylase Inhibitor on PD-L1, HLA-ABC, HLA-E, and HLA-G on Human Breast Cancer Cell Lines.* The FASEB Journal, 2020. **34**(S1): p. 1-1.
82. Grubczak, K., et al., *Differential Response of MDA-MB-231 and MCF-7 Breast Cancer Cells to In Vitro Inhibition with CTLA-4 and PD-1 through Cancer-Immune Cells Modified Interactions.* Cells, 2021. **10**(8).
83. Panda AK, et al., *Intratumoral Immune Landscape: Immunogenicity to Tolerogenicity.* Austin J Clin Immunol, 2015. **2(1):1025**.
84. Geraldo, J.M., et al., *HDR brachytherapy decreases proliferation rate and cellular progression of a radioresistant human squamous cell carcinoma in vitro.* Int J Radiat Biol, 2017. **93**(9): p. 958-966.
85. Kim, J.G., et al., *Histone demethylase JMJD2B-mediated cell proliferation regulated by hypoxia and radiation in gastric cancer cell.* Biochim Biophys Acta, 2012. **1819**(11-12): p. 1200-7.
86. Mello, S.S., et al., *A p53 Super-tumor Suppressor Reveals a Tumor Suppressive p53-Ptpn14-Yap Axis in Pancreatic Cancer.* Cancer Cell, 2017. **32**(4): p. 460-473.e6.
87. Wu, Q., et al., *Macrophage biology plays a central role during ionizing radiation-elicited tumor response.* Biomed J, 2017. **40**(4): p. 200-211.

88. Tsoutsou, P.G., et al., *Emerging Opportunities of Radiotherapy Combined With Immunotherapy in the Era of Breast Cancer Heterogeneity.* Frontiers in Oncology, 2018. **8**(609).
89. Reits, E.A., et al., *Radiation modulates the peptide repertoire, enhances MHC class I expression, and induces successful antitumor immunotherapy.* J Exp Med, 2006. **203**(5): p. 1259-71.
90. Vermeer, D.W., et al., *Radiation-induced loss of cell surface CD47 enhances immune-mediated clearance of human papillomavirus-positive cancer.* Int J Cancer, 2013. **133**(1): p. 120-9.
91. Vanpouille-Box, C., et al., *DNA exonuclease Trex1 regulates radiotherapy-induced tumour immunogenicity.* Nat Commun, 2017. **8**: p. 15618.
92. Froehlich, K., et al., *Generation of Multicellular Breast Cancer Tumor Spheroids: Comparison of Different Protocols.* J Mammary Gland Biol Neoplasia, 2016. **21**(3-4): p. 89-98.
93. Li, D.K. and W. Wang, *Characteristics and clinical trial results of agonistic anti-CD40 antibodies in the treatment of malignancies.* Oncol Lett, 2020. **20**(5): p. 176.
94. Richards, D.M., et al., *Concepts for agonistic targeting of CD40 in immuno-oncology.* Hum Vaccin Immunother, 2020. **16**(2): p. 377-387.
95. Yasmin-Karim, S., et al., *Radiation and Local Anti-CD40 Generate an Effective in situ Vaccine in Preclinical Models of Pancreatic Cancer.* Frontiers in Immunology, 2018. **9**(2030).
96. Cao, X., et al., *Effect of cabazitaxel on macrophages improves CD47-targeted immunotherapy for triple-negative breast cancer.* Journal for ImmunoTherapy of Cancer, 2021. **9**(3): p. e002022.
97. Zhang, W., et al., *Advances in Anti-Tumor Treatments Targeting the CD47/SIRPα Axis.* Front Immunol, 2020. **11**: p. 18.
98. Wang, Y., et al., *Combining Immunotherapy and Radiotherapy for Cancer Treatment: Current Challenges and Future Directions.* Front Pharmacol, 2018. **9**: p. 185.